THE FIRST- AND SECOND-ORDER TRANSIENT FREE-SURFACE WAVE RADIATION PROBLEMS

by
F. Thomas Korsmeyer

B. A., English
The University of Michigan, 1973

B. S. E., Naval Architecture and Marine Engineering
The University of Michigan, 1979

M. S. E., Naval Architecture and Marine Engineering
The University of Michigan, 1980

SUBMITTED IN PARTIAL FULFILLMENT
OF THE REQUIREMENTS FOR THE
DEGREE OF

DOCTOR OF PHILOSOPHY

at the

MASSACHUSETTS INSTITUTE OF TECHNOLOGY

January 1988

Signature of Author _____
Department of Ocean Engineering
January 1988

Certified by _____
Paul D. Sclavounos
Associate Professor of Naval Architecture
Thesis Supervisor

Accepted by _____
A. Douglas Carmichael
Professor of Power Engineering
Chairman, Department Committee on Graduate Students

THE FIRST- AND SECOND-ORDER TRANSIENT FREE-SURFACE WAVE RADIATION PROBLEMS

by
F. Thomas Korsmeyer

Submitted to the Department of Ocean Engineering
of the Massachusetts Institute of Technology
in partial fulfillment of the requirements for the degree of
Doctor of Philosophy

ABSTRACT

The first- and second-order transient, free-surface wave radiation problems are posed as initial-boundary-value problems. They are then recast in the form of Fredholm-Volterra integral equations by the use of Green's second identity.

In the case of the first-order problem, the integral equation is solved in discrete form by a panel method. Numerical solutions are presented for simple and complicated (multiple large-volume elements) bodies. It is shown that these solutions exhibit behavior which may be associated with the irregular frequency phenomenon of the analogous frequency-domain solutions. A method is presented for the elimination of this behavior through the use of the large-time asymptotic approximation for the impulse response function. Its efficacy is demonstrated for simple bodies.

In the case of the second-order problem, a method is derived for determining the unsteady force due to the second-order potential without solving for the second-order potential itself. The calculation of this unsteady force, on a heaving, right-circular cylinder, is used as a model problem for the investigation of numerical difficulties in second-order transient problems, in general. The method retains much of the numerical complexity of the equation to be solved for the second-order potential, but reduces the computational effort. The primary numerical difficulty is that of evaluating first-order quantities on the free surface in proximity to the body. The limitations of the discretized Green-formulation for this task are demonstrated by comparison of results with those of an alternate method which is ideally suited to the body under study.

Science is a first-rate piece of furniture for a man's upper chamber, if he has common sense on the ground floor.

—OLIVER WENDEL HOLMES

ACKNOWLEDGMENTS

This work is dedicated to Terry Lea Curl. She has always supported my endeavors and encouraged my dreams. In these past several years spent in pursuit of the Ph. D. degree, her sacrifices for me leave debts I can only hope to repay.

I have been able to pursue this research with enjoyment because of the working environment provided by the Ocean Engineering Department hydrodynamics group. The cooperation and mutual encouragement in this group facilitates and enlivens a research effort. In spite of their disparate backgrounds, the students of this group strive to find a common understanding in matters scientific, cultural, and humanitarian. Professors Newman, Sclavounos and Yue are leaders in research who can speak to motivate, as well as listen to approve or perhaps correct.

Special thanks go to Paul Sclavounos, who has that rare ability to guide research without controlling it. In addition, he has been a steady reference point for an uneven temperament. The Thesis Committee has been a source of valuable advice for which I am grateful. Also thanks to Susan Walsh for her help in the preparation of the manuscript, and more importantly for the upbeat spirit she brings to the office.

This research is supported by The Office of Naval Research (ONR) (Contract N00014-82-k-0198) and The National Science Foundation (NSF) (Grant 8514919). Computations were made on a VAX-11/750 at the Computational Hydrodynamics Facility which is supported by NSF and MIT; on a Cray XM-P/48 at the Pittsburg Supercomputer Center which is supported by NSF; and on a Cyber 205 at the John von Neumann Center which is also supported by NSF.

CONTENTS

LIST OF FIGURES

1. INTRODUCTION

Hydrodynamicists in the fields of Ocean Engineering and Naval Architecture have a considerable interest in studying the fluid flow which results from the interaction of free-surface waves and restrained or floating bodies. Assumptions leading to the representation of the flow field by a scalar potential are usually made, and the problems may be posed as initial-boundary-value problems to be solved for this potential. These problems are non-linear due to the free-surface, and in some cases the body, boundary conditions and may be attacked directly, or through perturbation expansion in some small parameter. Computational resources have limited the former approach to a few special cases, and so the latter approach has received most of the attention. In this method, a series of linear problems are generated, each at an order of the small parameter. This allows Fourier decomposition of the original transient or 'time-domain' problem, into a problem which is usually solved at discrete frequencies as a time-harmonic problem in the 'frequency domain.' A further decomposition, based on physical arguments and justified by John (1950), splits the first-order problem into two problems which are coupled through the equations of motion: the generation of waves due to the unsteady motion of the body, 'the radiation problem;' and the scattering of ambient waves by the stationary body, 'the diffraction problem.' A more elaborate procedure is required at higher orders. There is a further complication if the body is undergoing steady translation as well, giving rise to 'the unsteady forward speed problem.' The frequency-domain analysis of wave-body interactions has been extensive at first-order and has enjoyed some success at second-order [for reviews see Ogilvie (1983) and Kim (1988)]. The perturbation approach in the time domain has been formulated for some time, but only recently have results been reported in the literature.

Cummins (1962) and Ogilvie (1964) derive first-order, time-domain equations of motion for a ship, including forward speed effects in the latter reference. These equations are used by Ogilvie as a framework in which to better understand the frequency domain formulation, and the relationships between time- and frequency-domain quantities are discussed. For instance, that the added-mass and damping coefficients are Fourier cosine and sine transforms of the impulse response function, leads directly to the Kramers-Kronig relations. The equations of motion provide a context for the time-domain radiation and diffraction problems.

Stoker (1957) and Wehausen (1971) discuss the mathematical aspects of the Fredholm-Volterra integral equation which they derive via Green's second identity from the initial-boundary-value problems for first-order radiation or diffraction. The former provides a proof of uniqueness for the general, first-order, transient, wave-body problem in an unbounded domain, based on the work of Finkelstein (1953). The latter relates the frequency- and time-domain problems, and provides an extensive bibliography of the important early references for work in both domains. While Stoker and Wehausen both provide mathematical discussion, they do not contain computational results. It is not until Yeung (1982), for two-dimensional flow, and Newman (1985a), for axisymmetric flow, that transient results from the solution of the Fredholm-Volterra integral equation are reported. Both of these references provide time histories of forces on bodies which are freely floating and in forced motion. Yeung provides the relation between the unit initial-displacement response and the unit initial-velocity response. Newman matches the computed impulse response function to a two term, large-time, asymptotic approximation, and by Fourier transform recovers the familiar frequency-domain hydrodynamic coefficients: added-mass and damping.

Liapis (1986) employs the integral equation for body displacement which is Heaviside like. In this work, solutions of the radiation problem by the source distribution method as well as the potential formulation are explored and compared. The objective of Liapis (1986) is the formulation and solution of the forward-speed radiation problem in the time-domain. This is accomplished, and through the use of the Fourier transform, the

frequency-domain, forward-speed, hydrodynamic coefficients are presented for a Series-60 ship in the heave and pitch modes. Continuing this effort, King (1987) investigates the forward-speed diffraction problem. As in the above cited work of Liapis, there are some important zero-speed results presented as well. Of primary interest is the investigation of initiating transient problems with broad-band but non-impulsive inputs. Through the use of the Fourier transform, King (1987) presents frequency-domain, forward-speed, exciting force coefficients for the Wigley hull in the heave and pitch modes. Both of these authors claim computational advantages over the frequency-domain approach to the unsteady forward-speed problem, and point out that only in the time-domain can the problem of unsteady motion of a ship in a maneuver be considered.

Extension to second-order, of the transient problem without forward speed, is the subject of the thesis of Wang (1987). Wang solves the second-order diffraction problem for a vertical right-circular cylinder of infinite depth, and derives the second-order Green functions for radiation and diffraction. This latter achievement may make the second-order problem more tractable, but considerable numerical analysis remains before this result may be computationally applied.

The present work considers the transient radiation problem at both first and second orders. At first order, the general, three-dimensional-body problem is formulated and solved. At second order, an analogous problem is formulated. A formulation for the calculation of the second-order unsteady force due to the second-order potential is derived, and for an axisymmetric case is used to investigate the properties of panel methods in second-order transient problems. Interest in first-order transient problems at zero speed is motivated by:

1) possible computational efficiencies in finding hydrodynamic quantities traditionally computed in the frequency domain;

2) the need of the impulse response function in the calculation of arbitrary transient responses at first order;

3) the need to provide first-order outer solutions for matching to non-linear solutions near a body;

4) the requirement for time-domain solutions in quasi-non-linear approaches where the body-boundary condition is treated non-linearly for large excursions, while the free-surface boundary condition is approximated at first-order.

Interest in second-order transient problems at zero speed is motivated by:

1) the possibility of using a second-order impulse response function to find sum and difference frequency quantities in the frequency domain;

2) to provide second-order outer solutions for matching to non-linear solutions near a body;

3) investigation of forced motion problems which may not require a fully non-linear treatment.

The Thesis motivates the perturbation approach to the radiation problem, and then investigates the first- and second-order problems. In Section 2, the exact initial-boundary-value problem for the fluid velocity potential is posed and expanded in powers of a small parameter. The emphasis here is on the justification for the proper initial conditions. In the Appendix, the canonical initial-boundary-value problem, which may be written at any order is recast as a Fredholm-Volterra integral equation to be solved for the unknown potential on the surface of the body. This integral equation is derived through the use of the first-order, transient, free-surface, Green function but is applicable to any order. It is specialized to a particular order upon substitution of the appropriate right-hand sides of the free-surface and body boundary conditions. This equation contains an integral to be computed over the free surface at second-order and above, and this aspect is responsible for the difficulty of these higher-order problems.

In Section 3, the first-order transient radiation problem is discussed and its relation to the more familiar frequency-domain formulation is detailed. The discrete form of the integral equation is presented; and in Section 4, the numerical aspects of its solution are discussed. This introduces the subject of irregular-frequency effects which show

up at large time in the impulse response function. Irregular-frequency effects are well documented in the frequency domain, and are shown to be present in the time domain as well by Adachi and Ohmatsu (1979). Newman (1985a) uses a two-term, large-time, asymptotic representation of the impulse response function to mitgate these effects. This was derived from the low-frequency approximation of the exciting force through the use of the Fourier transform. In Section 5, this idea is developed further and connected to the low frequency asymptotic representations of the added-mass or damping coefficients developed by Simon and Hulme (1985). Impulse response functions for the hemisphere with asymptotic corrections are presented in Section 6. There is also a numerical investigation of irregular-frequency effects. The impulse response function for a Tension Leg Platform is shown and its Fourier transform is compared to frequency-domain results. The benefit of parallel time- and frequency-domain analysis for complicated structures becomes evident here.

The second-order transient problem is discussed in Section 7. The problem of determining the second-order velocity potential is not solved. Rather, in Section 8, a quadrature formulation for determining the second-order unsteady force on a harmonically oscillated body which is started impulsively is derived. Computationally, this exercise retains much of the numerical difficulty of determining the potentail itself, and so it is a good model problem at second-order. The numerical difficulties at second-order are substantial. Temporal and spatial derivatives of the first-order potential must be found and integrated over the free-surface. The extent of the free surface involved in the computation is small due to the rapid spatial decay of the integrand, but close to the body, the evaluation of quantities by panel methods is difficult. In fact, very close to the body, panel methods (at least those with constant-strength panels), are not useful for the computation of fluid velocities, a fact also observed in the frequency domain [Kim (1988)]. Section 10, explores the deficiency of the panel method by using a different method, particularly applicable to the right-circular cylinder, to determine more accurately the first-order potential and its derivatives very close to the body. Section 11 contains a discussion of the thesis topics, conclusions and recomendations.

There is no separate listing of nomenclature, because it is defined in context. In Section 2., where the exact problem is posed, the equations are dimensional as that helps to convey the physical aspects of the problem. The rest of the thesis is consistently normalized by setting the acceleration due to gravity, the fluid density, and a representative body dimension equal to one, with the exception of the hydrodynamic coefficients for the hemisphere which are non-dimensionalized by the displaced fluid mass. The following conventions apply throughout the thesis:

1) Vector quantities are indicated by an arrow, as in $\vec{x}$.

2) Subscripts indicate partial differentiation with respect to the subscript variable.

3) Superscript numerals, when not in parentheses, are exponents.

4) Superscript numerals, when in parentheses, indicate the order in the small parameter to which the quantity or function belongs, as in $\phi^{(1)}$, a *first-order* potential.

5) Superscript letters indicate the type of problem to which a function belongs, as in $\phi^{(1)I}$, the first-order *impulsive* potential.

The equations for the velocity potentials at first and second order and the unsteady forces at second order are presented in their most general form, and hence apply to a general three-dimensional body in arbitrary motion unless clearly indicated otherwise. In the sections on numerical considerations, equations are specialized to the particular problem under consideration.

Figures for each section are located after the last page of text of the particular section.

2. PERTURBATION EXPANSION OF THE RADIATION PROBLEM

We consider the problem of determining the flow which results when a body is forced to move in a semi-infinite fluid with a free surface. The problem is idealized by the assumptions of an irrotational flow and an incompressible, inviscid fluid. These assumptions allow us to describe the velocity field as the gradient of a scalar potential, and conservation of mass requires that this potential satisfies the Laplace equation. In addition we simplify the free-surface boundary condition by neglecting surface tension. For generality we consider the case of a surface-piercing body. The inertial coordinate system and the labeling of the fluid boundaries are shown in Figure 2-1.

For a semi-infinite fluid, with the pressure equal to zero on the free surface, we have the following problem formulation (where arguments have been omitted if there is no ambiguity): $\phi(\vec{x},t)$ must satisfy:

$$\nabla^2\phi(\vec{x},t) = 0 \qquad \text{in the fluid domain,} \tag{2.1}$$

$$\vec{\nabla}\phi\cdot\vec{n}(\vec{x},t) = \vec{U}(\vec{x},t)\cdot\vec{n} \qquad \text{on the exact body boundary,} \tag{2.2}$$

where $\vec{U}(\vec{x},t)$ is the body velocity and $\vec{n}(\vec{x},t)$ is the inward directed, unit-vector, normal to the body surface,

$$g\zeta + \phi_t + \frac{1}{2}(\phi_x^2 + \phi_y^2 + \phi_z^2) = 0 \qquad \text{on the exact free surface,} \tag{2.3}$$

$$\phi_x\zeta_x + \phi_y\zeta_y + \zeta_t = \phi_z \qquad \text{also on the exact free surface,} \tag{2.4}$$

and

$$\phi,\ \vec{\nabla}\phi,\ \phi_t, \quad \text{are uniformly bounded as } |\vec{x}| \to \infty \text{ for finite time.} \tag{2.5}$$

In (2.3) and (2.4), $\varsigma(x,y,t)$ is the free-surface elevation. As in any transient problem, we must specify initial conditions. That is, we must specify the position and velocity of every fluid particle at $t = 0^+$. Since $\phi(\vec{x},t)$ is a harmonic function, this reduces to a specification of the boundary positions and the value of $\phi(\vec{x},t)$ or $\phi_n(\vec{x},t)$ on those boundaries at $t = 0^+$. In the radiation problem, the location of all surfaces except the free surface is prescribed for all time, and the body boundary condition (2.2) and the conditions far from the body (2.5) prescribe the potential or its normal derivative for all time, so initial conditions on the free surface are all that remain to be specified. From causality, for a body starting from rest at $t = 0$, all fluid particles are at rest, and the free surface has zero elevation for times $t < 0$. In the present treatment of the problem, the body velocity will be initiated in a Heaviside manner in time. It is necessary in the ensuing derivation of initial conditions that we assume this to be the most singular velocity anywhere in the fluid at time $t = 0$. As fluid particle displacement is the integral in time of fluid particle velocity, the free surface elevation must be bounded at $t = 0^+$. With these two points in mind, we formally integrate the free-surface conditions (2.3) and (2.4) from $t = 0$ to $t = \tau$. Letting $\tau \to 0^+$, eliminates those terms with finite integrands, and the causality condition eliminates contributions at the lower integration limit, leaving only:

$$\varsigma(x,y,0^+) = 0 \tag{2.6}$$

from equation (2.4), and

$$\phi(\vec{x},0^+) = 0 \qquad \text{on } z = 0, \text{ the position of the quiescent free surface} \tag{2.7}$$

from equation (2.3).

We assume that for all time the elevation of the free surface has small slope. This

formally justifies the expansion of the potential and the free-surface elevation in terms of a small parameter. Then, following Stoker (1957) we write:

$$\phi(\vec{x},t) = \epsilon\phi^{(1)} + \epsilon^2\phi^{(2)} + \epsilon^3\phi^{(3)} + ... \tag{2.8}$$

and,

$$\varsigma(x,y,t) = \varsigma^{(0)} + \epsilon\varsigma^{(1)} + \epsilon^2\varsigma^{(2)} + ... \tag{2.9}$$

It is further assumed that since the displacement of any of the boundaries is small, quantities may be represented by Taylor expansions about the initial positions of the body and free surfaces, S_B and S_F, respectively. In addition, the right-hand side of the body boundary condition, which is known exactly, must be expanded as well. This expansion arises from a decomposition of $\vec{U}(\vec{x},t)$ into contributions at each order, as well as terms which relate the normal vector in the inertial frame to the more convenient representation in a body-fixed frame. This expansion is provided in its most general form in Ogilvie (1983), and so will not be presented until specific instances of body motion are investigated.

To formulate problems at different orders, the technique is to insert the expansions (2.8) and (2.9) into the field equation, the boundary conditions and the initial conditions; and separate the resulting expressions in powers of ϵ. The result is a series of *linear* problems, one at each order. It is easy to show $\varsigma^{(0)}$ vanishes for all time. So we are interested in the first two non-trivial problems at $O(\epsilon)$ and $O(\epsilon^2)$, which are examined in detail in the remainder of the thesis, with each problem formulation presented in Sections 3 and 7, respectively.

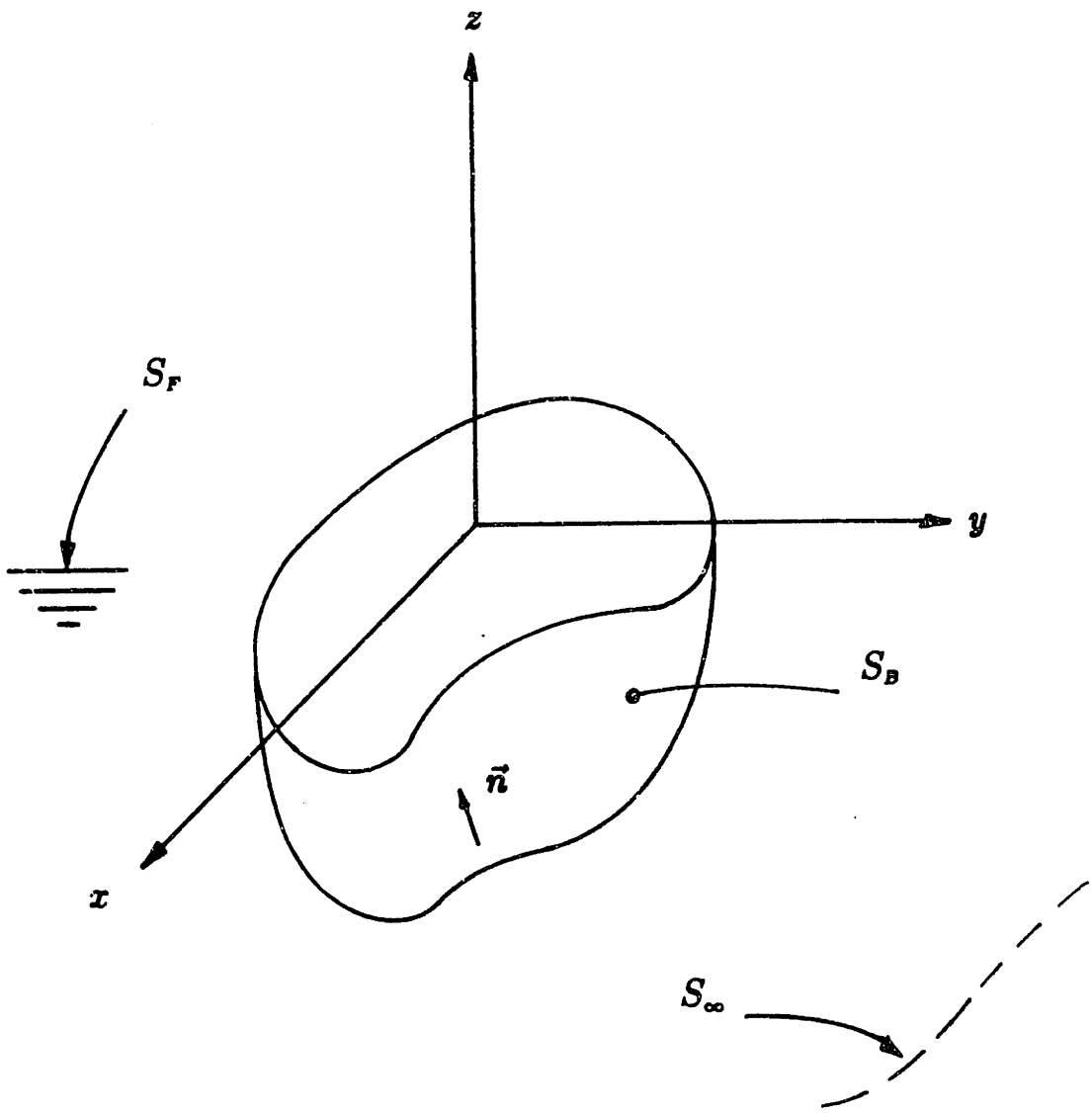

Figure 2-1. The coordinate system for the transient radiation problem. Surface identifications apply to the initial positions of the surfaces as understood in the first- and second-order problems.

3. THE FIRST-ORDER RADIATION PROBLEM

To generate the first-order radiation problem, the expansions for $\phi(\vec{x},t)$, $\varsigma(x,y,t)$, and the right-hand side of the body boundary condition, equations (2.8), (2.9), and (2.10) respectively, are inserted in the exact problem statement, equations (2.1) through (2.7). Boundary conditions are now to be satisfied on the initial body position S_B , and the quiescent free surface S_F . The problem has been normalized by setting the acceleration due to gravity, the fluid density, and a body dimension equal to one. We will consider the radiation of surface waves by a body velocity which is initiated in a Heaviside manner at $t = 0$. The subsequent body velocity may in principle be arbitrary, but we will be interested in two particular cases. One is impulsive motion: the body velocity takes a small constant value at $t = 0^+$. The other is harmonic motion: the velocity begins a small-amplitude cosine variation in time at $t = 0^+$, with frequency ω. In both cases the motion is in a single mode. The problem may also be formulated for a body with displacement, not velocity, which is a Heaviside function (Beck and Liapis 1987).

Without restriction on the nature of the body velocity, provided that it is initiated in a Heaviside manner, the $O(\epsilon)$ problem statement is that $\phi^{(1)}(\vec{x},t)$ must satisfy:

$$\nabla^2\phi^{(1)}(\vec{x},t) = 0 \qquad \text{in fluid domain} \tag{3.1}$$

$$\varsigma^{(1)} + \phi_t^{(1)} = 0 \qquad \text{on the quiescent free surface, } S_F \tag{3.2}$$

$$\varsigma_t^{(1)} - \phi_z^{(1)} = 0 \qquad \text{on the quiescent free surface, } S_F \tag{3.3}$$

The two equations on the free surface may be combined to give a single free-surface condition containing the second derivative of the potential with respect to time:

$$\phi_{tt}^{(1)} + \phi_z^{(1)} = 0 \qquad \text{on the free surface, } S_F \tag{3.4}$$

$$\phi_n^{(1)} = \mathcal{B}^{(1)}(\vec{x},t) \quad t > 0 \qquad \text{on the body surface, } S_B \tag{3.5}$$

$$\phi^{(1)},\ \vec{\nabla}\phi^{(1)},\ \phi_t^{(1)}, \quad \text{are uniformly bounded on } S_\infty, \text{ for } t \text{ finite.} \tag{3.6}$$

The right-hand side of the body boundary condition, $\mathcal{B}^{(1)}$, is defined for specific cases in equations (3.10) and (3.11), below. The exact initial condition, equation (2.7) by itself; and use of the $O(\epsilon)$ dynamic free-surface condition, equation (3.2), with the exact initial condition, equation (2.6), gives the initial conditions for the first-order problem:

$$\phi^{(1)}(x,y,0,0^+) = 0, \tag{3.7}$$

and

$$\phi_t^{(1)}(x,y,0,0^+) = 0. \tag{3.8}$$

Following Stoker (1957) or Wehausen (1971), we may recast this initial-boundary-value problem as an integral equation to be solved for the value of the potential on the body surface. For this, we require the transient free-surface Green function $G(\vec{x};\vec{\xi},t)$ as derived by Wehausen and Laitone (1960), equation (A.7). We apply Green's second identity to $\phi_\tau^{(1)}(\vec{x},\tau)$ and $G(\vec{x};\vec{\xi},t-\tau)$, and with some manipulation, the surface integrals on the free surface and at infinity vanish, leaving only an integral on the body surface. After the usual treatment of the spatial singularity and integration of the equation in time, we have a Fredholm-Volterra equation for the unknown potential on the body surface. The definition of the Green function, its decomposition into Rankine and wave parts, and the details of the derivation are found in the Appendix. The result, which we find by specializing equation (A.16) for the $O(\epsilon)$ problem is:

$$2\pi\phi^{(1)}(\vec{x},t) + \iint_{S_B} d\vec{\xi}\,\phi^{(1)}(\vec{\xi},t)G^{(0)}_{n_\xi}(\vec{x};\vec{\xi}) + \int_{0^+}^{t} d\tau \iint_{S_B} d\vec{\xi}\,\phi^{(1)}(\vec{\xi},\tau)G^{(F)}_{n_\xi t}(\vec{x};\vec{\xi},t-\tau)$$
$$= \int_{0^+}^{t} d\tau \iint_{S_B} d\vec{\xi}\,\mathcal{B}^{(1)}(\vec{\xi},\tau)G^{(F)}_{t}(\vec{x};\vec{\xi},t-\tau)$$
$$+ \iint_{S_B} d\vec{\xi}\,\mathcal{B}^{(1)}(\vec{\xi},t)G^{(0)}(\vec{x};\vec{\xi}), \tag{3.9}$$

where the 0^+ integration limit acknowledges the Heaviside time dependence of $\mathcal{B}^{(1)}(\vec{x},t)$. In the case of unit harmonic motion in a single non-rotative mode, with body-normal component n, and at frequency ω,

$$\mathcal{B}^{(1)}(\vec{x},t) = n\,\cos\omega t \qquad t > 0. \tag{3.10}$$

In the case of unit impulsive motion, again in a single, non-rotative mode with body-normal component n,

$$\mathcal{B}^{(1)}(\vec{x}) = n \qquad t > 0, \tag{3.11}$$

and equation (3.9) simplifies to:

$$2\pi\phi^{(1)}(\vec{x},t) + \iint_{S_B} d\vec{\xi}\,\phi^{(1)}(\vec{\xi},t)G^{(0)}_{n_\xi}(\vec{x};\vec{\xi}) + \int_{0^+}^{t} d\tau \iint_{S_B} d\vec{\xi}\,\phi^{(1)}(\vec{\xi},\tau)G^{(F)}_{n_\xi t}(\vec{x};\vec{\xi},t-\tau)$$
$$= \iint_{S_B} d\vec{\xi}\,n(\vec{\xi})\left[G^{(0)}(\vec{x};\vec{\xi}) + G^{(F)}(\vec{x};\vec{\xi},t)\right] \tag{3.12}$$

This impulsive problem formulation may be thought of as the Fourier transform of the usual frequency-domain radiation problem formulation [given in Section 5] and has small- and large-time limit solutions which are related to the low- and high-frequency limits found in the frequency domain. A figure from Newman (1977) which explains the frequency-domain limits may be extended to include the time domain limits and this idea is demonstrated in Figures 3-1 and 3-2.

As will be described in detail in Section 4, we solve discrete approximations to equations (3.9) and (3.12). This discretization is made in both space and time. The body is approximated by N, plane, quadrilateral panels upon which $\phi^{(1)}(\vec{x},t)$ is assumed to be constant. The convolution integral is computed by the trapezoidal rule. The discrete version of equation (3.9), which must be solved at each time-step, M, up to the last time-step M_T, is:

$$\begin{aligned} 2\pi\phi^{(1)}_{i,M} + \sum_{j=1}^{N} \phi^{(1)}_{j,M} \iint_{S_j} d\vec{\xi}\, G^{(0)}_{n_\xi}(\vec{x};\vec{\xi}) = &- \sum_{m=0}^{M-1}{}' \Delta t \sum_{j=1}^{N} \phi^{(1)}_{j,m} \iint_{S_j} d\vec{\xi}\, G^{(F)}_{n_\xi t}(\vec{x};\vec{\xi},t_{M-m}) \\ &+ \sum_{m=0}^{M}{}' \Delta t \sum_{j=1}^{N} \mathcal{B}^{(1)}_j(t_m) \iint_{S_j} d\vec{\xi}\, G^{(F)}_t(\vec{x},\vec{\xi},t_{M-m}) \\ &+ \sum_{j=1}^{N} \mathcal{B}^{(1)}_j(t_M) \iint_{S_j} d\vec{\xi}\, G^{(0)}(\vec{x};\vec{\xi}) \\ &i = 1,2...N \qquad M = 0,1...M_T\ , \end{aligned} \tag{3.13}$$

where S_j is the surface of the j^{th} panel and the prime on the summation in time indicates a weight of one-half is applied when $m = 0$. There are two points which are too important to be left until the section on numerics: one, the Fredholm kernel is independent of time, and two, $G^{(F)}_{nt}(\vec{x};\vec{\xi},t) = 0$ at $t = 0$, so that the current value of the unknown $\phi^{(1)}(\vec{x},t)$ does not appear inside the discretized Volterra integral. The discrete form of (3.12) is:

$$\begin{aligned} 2\pi\phi^{(1)}_{i,M} + \sum_{j=1}^{N} \phi^{(1)}_{j,M} \iint_{S_j} d\vec{\xi}\, G^{(0)}_{n_\xi}(\vec{x};\vec{\xi}) = &- \sum_{m=0}^{M-1}{}' \Delta t \sum_{j=1}^{N} \phi^{(1)}_{j,m} \iint_{S_j} d\vec{\xi}\, G^{(F)}_{n_\xi t}(\vec{x};\vec{\xi},t_{M-m}) \\ &+ \sum_{j=1}^{N} n_j \iint_{S_j} d\vec{\xi}\, \left[G^{(0)}(\vec{x};\vec{\xi}) + G^{(F)}(\vec{x};\vec{\xi},t)\right] \\ &i = 1,2...N \qquad M = 0,1...M_T\ , \end{aligned} \tag{3.14}$$

The time-dependent potential resulting from the solution of (3.14) may be integrated over the body to determine the transient added-mass

$$M(t) = \iint_{S_B} d\vec{x}\, \phi^{(1)}(\vec{x},t)\phi_n^{(1)}(\vec{x}), \tag{3.15}$$

which can be differentiated in time to provide the impulse response function

$$L(t) = \iint_{S_B} d\vec{x}\, \phi_t^{(1)}(\vec{x},t)\phi_n^{(1)}(\vec{x}). \tag{3.16}$$

The impulse response function is related to the added mass and damping coefficients of the linear, frequency-domain, radiation problem through the Fourier cosine and sine transforms

$$a(\omega) = a(\infty) + \int_0^\infty dt\; L(t)\cos\omega t, \tag{3.17}$$

and,

$$\frac{b(\omega)}{\omega} = \int_0^\infty dt\; L(t)\sin\omega t. \tag{3.18}$$

In practice, we numerically transform a truncated, rather than infinite, impulse response function, and this will lead to inaccuracies which are discussed in Section 6. In an effort to provide an infinite record in the time domain, and to reduce these inaccuracies in the frequency domain, we would like to provide an asymptotic continuation to the truncated time-domain record found from the solution of (3.14). The derivation of the large-time asymptotic expansion for $L(t)$, and its effects on the Fourier transform, are discussed in Section 5.

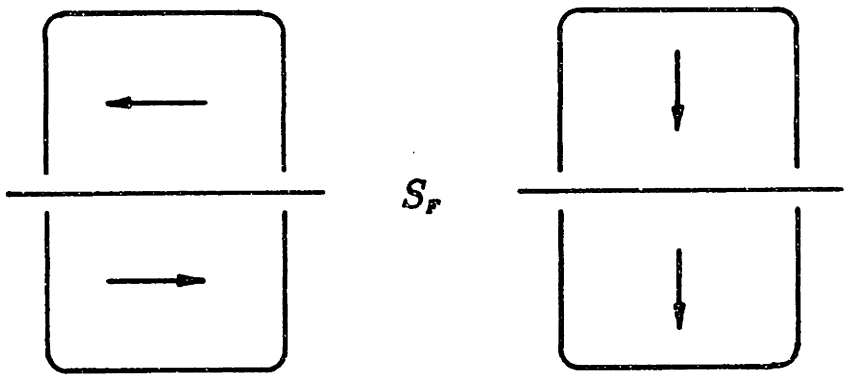

Figure 3-1. When $t \to 0$, $G(\vec{x};\vec{\xi},t) \to \frac{1}{R} - \frac{1}{R'}$. In this limit, $\phi^{(1)}(\vec{x},t) = 0$ on the free surface, as in the frequency-domain limit of $\omega \to \infty$. The potential is anti-symmetric with respect to the free surface. This limit defines the 'pressure-release' problem. For heave, pitch, and roll this is also the infinite-fluid problem.

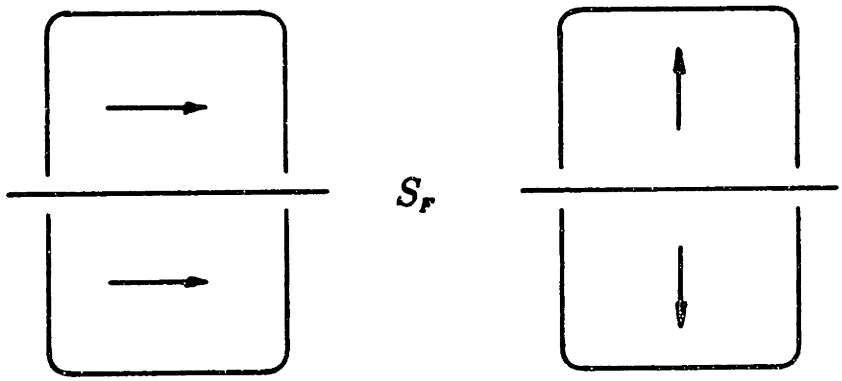

Figure 3-2. When $t \to \infty$, $G(\vec{x};\vec{\xi},t) \to \frac{1}{R} + \frac{1}{R'}$. In this limit, $\phi_s^{(1)}(\vec{x},t) = 0$ on the free surface, as in the frequency-domain limit of $\omega \to 0$. The potential is symmetric with respect to the free surface. This limit defines the 'rigid-lid' problem. For surge, sway, and yaw this is also the infinite-fluid problem.

4. NUMERICAL TECHNIQUES IN THE FIRST-ORDER PROBLEM

A FORTRAN computer code TIMIT (TIme domain, Massachusetts Institute of Technology) has been written which solves equation (3.13) by a panel method. The name 'panel' refers to the fact that the body is described by a finite set of facets. The panel-method approach to the solution of boundary integral equations is attributable to Hess and Smith (1964), and was used in their solution of infinite-fluid aerodynamic problems. Since that time, there has been wide use of this technique in the solution of boundary-integral equation formulations of free-surface problems; primarily in the solution of first-order, frequency-domain radiation and diffraction problems. Unlike the time-domain formulation for wave-body interactions, the frequency-domain approach is often considered to be thoroughly investigated. However, Eatock Taylor and Jefferys (1986) and Jefferys (1987) indicate that at least for complicated bodies (that is multiple large volume elements which may be connected physically and interact hydrodynamically) there can be large discrepancies between results from different panel codes. These references present various investigator's solutions for the frequency-domain hydrodynamic coefficients for two different Tension Leg Platforms (TLP). In the former reference, results are widely scattered, with 50 percent differences commonplace. In the latter reference, results differ by as much as 20 percent over the frequency range of interest. Either these results are not convergent results for each program or else complicated structures impose difficulties for panel-method programs which are not revealed by the usual testing with simple bodies. In any case these results are disquieting; and unfortunately, cast undeserved doubt on the validity of panel methods in general.

Apparently, it is one thing to write a panel-method computer code which produces acceptable results for simple bodies if sufficient computer resources are available; and

quite another to write a computer code which produces efficient and accurate results for simple bodies, and accurate results for complicated bodies as well. Provided that there are no basic flaws in the aforementioned panel codes, then a likely source of the discrepancies could be the care with which the Rankine and wave parts of the Green function are calculated. During the last ten years of panel program development in the hydrodynamics group of the Ocean Engineering Department at MIT, a major effort has been directed towards this problem for both the frequency- and time-domain, free-surface Green functions. The resulting subroutines for Green function evaluation have been designed for efficient computation to an accuracy of six or seven significant digits: RPAN, for the Rankine part; FINGREEN, for the wave part of the frequency-domain Green function; and TGREEN, for the wave part of the transient Green function [Newman (1986), Newman (1985b)]. TGREEN shares the accuracy of its frequency-domain counterpart FINGREEN, but has not undergone extensive optimization. The other tasks common to both time- and frequency-domain panel codes are the description of the body geometry, and the solution of linear systems. The former is performed by a subroutine GEOM, which was originally written for frequency-domain work, and the latter by routines from the LINPAC library. This history of panel-method research has made it possible to construct a time-domain radiation code by employing these well-tested subroutines and thereby reducing the uncertainty in the quality of the results.

The computer code which solves the discretized integral equation has been written for a general 3-D body, with impulsive or harmonic motion in any mode. The body is approximated by N_P, plane, quadrilateral panels. Each panel has four vertices although two vertices may coalesce so that the quadrilateral becomes a triangle. The program can take advantage of one or more planes of body symmetry. In the following discussion we use N_U to refer to the number of unknowns, and this will be a fraction of N_P if the body symmetry allows it. That is, if N_P panels are required to accurately model the body, the number of unknowns in the problem will be $N_U = N_P$ if there is no symmetry, and $N_U = N_P/(2\,N_S)$, if there are N_S planes of symmetry. The potential is assumed to be constant over each panel, and the convolution is approximated by the trapezoid

rule, which has an error proportional to $O(\Delta t^2)$ (where Δt is the time-step). The linear system implied by equation (3.13), or the impulsive version (3.14), is established by collocation at the panel centroids. The input consists of control parameters for the number of panels, the extent of symmetry, the frequency and mode of motion, the number and size of the time-steps, and a listing of the panel vertices.

Before time-stepping through M_T increments of time can begin, there are several tasks to be accomplished. The first of these is that the complete geometric description of the body and the panels must be calculated. GEOM is called, and this routine finds panel geometric properties such as centroid, area, moments of area, side lengths, and direction cosines for its local coordinate system relative to the global system. Then the $t = 0^+$ problem is set-up. This requires calls to RPAN to compute the Rankine coefficients $G_n^{(0)}(\vec{x};\vec{\xi})$, which constitute the left-hand side matrix, and $G^{(0)}(\vec{x};\vec{\xi})$, which are part of the $t = 0^+$ right-hand side. This left-hand side is LU factored *once* and for *all* subsequent time-steps by a LINPAC routine which performs Gauss elimination with partial pivoting, and the factored matrix is stored in the memory location previously occupied by the original matrix elements. Now the $t = 0^+$ problem is solved by back substitution. As was mentioned in Section 3 this is the infinite fluid problem for vertical modes and so for simple bodies its solution can provide a check of the body discretization and geometry calculations before the computational effort is invested in advancing the solution in time. This advancement requires evaluation of the wave part of the time-domain Green function $G^{(F)}(\vec{x};\vec{\xi},t)$ as defined in (A.19), and convolution with previous solutions to provide new right-hand sides. TGREEN evaluates $G^{(F)}(\vec{x};\vec{\xi},t)$, and its spatial and temporal derivatives, for a particular time and pair of panel centroids. The algorithms for these calculations are described in detail in Newman (1985b), and consist of an ascending series representation when t^2/R' is small; and a five term asymptotic representation when t^2/R' is large. A plot of $G^{(F)}(\vec{x};\vec{\xi},t)$ is provided in Figure 4-1. At each time-step, the N_U^2 values of $G_{nt}^{(F)}(\vec{x};\vec{\xi},t)$ and $G_t^{(F)}(\vec{x};\vec{\xi},t)$ calculated by TGREEN are stored in a scratch file to avoid recomputation as they are required in all subsequent convolutions. Then convolution of $G_{nt}^{(F)}(\vec{x};\vec{\xi},t)$ with pre-

vious values of $\phi^{(1)}(\vec{x},t)$ plus the convolution of $G_t^{(F)}(\vec{x};\vec{\xi},t)$ with $\phi_n^{(1)}(\vec{x},t)$ provides the right-hand side. For most machines, random access memory (RAM) will not be sufficiently large to store the $2 \times M_T \times N^2$ coefficients, so these must be written to an auxiliary memory device. On the VAX 11/750, where the I/O is from and to a disk; and on the Cray X-MP/48, where the I/O is from and to a solid-state device, this technique is an order of magnitude faster than recomputation during convolution. Also, convolution requires that either the coefficients or the solution vectors $\phi^{(1)}(\vec{x},t)$ must be retrieved in the reverse order from which they were calculated. Since $\phi^{(1)}(\vec{x},t)$ requires far less storage than the coefficients, only $N_U \times M_T$, it can be stored in RAM where it is just as convenient and nearly as efficient to read 'backwards.'

The output from T[MIT consists of $\phi^{(1)}(\vec{x},t)$ at each panel centroid, $M(t)$ and $L(t)$ (where $L(t)$ is the impulse response function if the motion is impulsive), all as discrete functions of time up to the maximum time of the calculation, $M_T \times \Delta t$. A post-processor is used to Fourier transform the impulse response function, $L(t)$, to obtain the frequency-domain hydrodynamic coefficients, as in equations (3.17) and (3.18). Filon quadrature (Abramowitz and Stegun (1964)) is used for this task because it is more robust than the Fast Fourier Transform (FFT) although the latter may be faster. Also, Filon quadrature allows the order of the polynomial approximating the function to be adjusted as required, and has no requirement for 2^k input points as does the FFT. For slowly varying functions, such as the typical $L(t)$, quadratic approximation is sufficient.

The accuracy of the impulse response function is affected only by the discrete geometric model of the body and the size of the time-step, up to the limit of about six or seven significant digits, which is the precision of the computation of the Green function influence coefficients. The obvious inaccuracy in the computed impulse response function is the spurious oscillation at large time, mentioned in Section 3. This is the effect of irregular frequencies manifested in the time domain. In addition, we find differences over the entire time history as the temporal and spatial discretization is refined. The functional form of the oscillatory behavior is discussed in Section 6, but here we have

an interest in quantifying the inaccuracy and relating it to the level of discretization.

In Figure 4-2, it is clear that the time domain solution is like its frequency-domain counterpart in that the effect of irregular frequencies may be mitigated by improving the accuracy of the spatial discretization of the body. Empirical evidence suggests that for hydrodynamic coefficients computed from the *frequency-domain* formulation for the potential, the *bandwidth* of the inaccurate region centered on an irregular frequency may be narrowed by a more accurate body model. In the time domain, the *amplitude* of the oscillatory behavior may be reduced by a more accurate body model. Extremely fine discretizations of the body may render the oscillations undetectable over a time history like that shown in Figure 4-2, but they will show up eventually, as seen in Figure 6-7 where there are results for a 4608-panel hemisphere.

The effect of reducing the time-step is less clear. In Figure 4-3, it is evident that the effect of reducing the time-step from $\Delta t = 0.5$ to $\Delta t = 0.3$, is a reduction in the amplitude of the oscillations, and some change in the results in the earlier-time, non-oscillatory portion of the record. However, the reduction to a time-step of $\Delta t = 0.05$ has increased the oscillatory amplitude and shifted the location of the maxima on the time axis. As discussed below, however, the accuracy over the entire time-history of the computation with $\Delta t = 0.05$, is superior to those with larger time-steps.

Quantification of the accuracy of solutions at various levels of discretization has been done by comparison to a very finely discretized model: $N_P = 4608$, $\Delta t = 0.05$. In Figure 4-4, the mean-square error relative to this fine model, for a matrix of different panelizations and time-steps, is presented. Although we cannot make a general statement about the reduction in the amplitude of the oscillatory behavior as the time-step is reduced, the mean-square error for any particular body model decreases approximately as a function of $(\Delta t)^2$, as may be expected for trapazoid rule convolution. Refering to Figure 4-2, the reduction in the mean-square error for each body model, is largely a consequence of the reduction in the amplitude of the irregular frequency effect.

The plot of the Green function in Figure 4-1 indicates that we may expect panels near

the free surface to have a greater effect on the solution than panels at greater depth, at least at large times. Consequently the idea of cosine spacing the vertical distribution of panels as the free surface is approached may be justified. The mean-square errors for several such body models are plotted in Figure 4-4, and indeed, for exactly the same numerical effort as the regularly distributed panel models, the cosine distribution of panels slightly improves the results. The impulse response function for a cosine distributed body model is presented in Figure 6-8, and it may be seen that this panel distribution has an effect on the oscillatory behavior when compared to the regularly spaced results of Figure 4-2. In general, changing panel aspect ratios, without changing the number of panels, affects results unless the discretization is very fine. This fact makes it imperative that panel aspect ratios be preserved when convergence studies are undertaken. In summary, Figure 4-4 suggests that the maximum accuracy for any particular amount of computational effort may be had by a cosine distribution of the least required number of panels. It is inefficient to obtain this accuracy by a larger number of panels combined with larger time-steps because the computational effort is quadratic in the number of unknowns and linear in the number of time-steps.

Numerical stability has not been a concern in these computations. For temporal and spatial discretizations which were expected to produce usefully accurate results for simple bodies there has never been any evidence that the solution might break down; Figures 6-1 and 6-2 should be ample evidence of this, as they represent 500 time-steps for the swaying and heaving hemisphere respectively.

The computational effort in time-domain calculations can be formidable; but not for the reason which seems to be the prevailing notion. It is not convolution, with all of its fetches from RAM and files on the auxiliary memory device which consumes the central processing unit (CPU) time. It clearly is not the reduction of the $N_U \times N_U$, real, linear system, which must be done just once. It is the calculation of $N_U \times N_U \times 2 \times N_S \times M_T$ values of the wave part of the Green function and its derivatives which requires all of the effort. By comparison, a frequency-domain radiation program makes $N_U \times N_U \times 2 \times N_S \times K$ (where K is the number of frequencies) equivalent computations,

and solves K, $N_U \times N_U$, complex, linear systems. While T[MIT has been written with efficiency in mind; that is, short loops have been unrolled, indices are ordered as well as possible, *etc.*, it has not received any special optimization efforts, and so timing information should be construed as a starting point which can only improve. As written, on the VAX 11/750, T[MIT spends approximately 90 percent of its running time in the subroutine TGREEN. The TGREEN ascending series calculation in double precision is partly responsible for this; but not entirely, because the VAX has hardware which performs a double precision flop (floating point operation) in less than double the time required for a single precision flop. On the Cray X-MP/48, the 90 percent is roughly preserved because the speed increase of the now vectorized convolution, is offset by the fact that the double precision requirement of the ascending series approximation is met by the standard, full precision of the Cray. On the Cray X-MP/48, T[MIT typically runs 60 times faster than on the VAX 11/750, and approximate running times for the Cray may be calculated as $N_U \times N_U \times 2 \times N_S \times M_T \times 5 \times 10^{-5}$ CPU seconds.

The subject of timing for transient codes invites comparison to frequency-domain codes. Comparitive times are available in Korsmeyer, Lee, Newman and Sclavounos (1988). This reference indicates that the effort per time-step in the transient approach is of the same order as that per frequency in the frequency-domain approach, if the number of unknowns is comparable. This should not be surprising because iterative methods of linear system solution for frequency domain codes, and fast (vectorized, perhaps) I/O and convolution techniques for time-domain codes, have shifted most of the effort to the calculation of the influence coefficients and there are the same number of these evaluations at one frequency as there are at one time-step. So overall, the frequency domain approach appears to consume less effort if we are satisfied with results at only 20 to 30 frequencies, because in the time domain 200 or more time-steps may have to be evaluated before the response function has decayed sufficiently to allow an accurate transform.

In the following section, a method is presented which may be used to reduce computational effort in time-domain calculations. In this section, the large-time, asymptotic

representation of $L(t)$ is derived from the frequency-domain, convergent series representations of the hydrodynamic coefficients. This asymptotic result may be used to reduce computational effort for simple bodies because patching of a computed $L(t)$ to the asymptotic $L(t)$ eliminates the oscillatory behavior. This allows both coarser spatial discretization in the body model, and shorter time histories to be calculated.

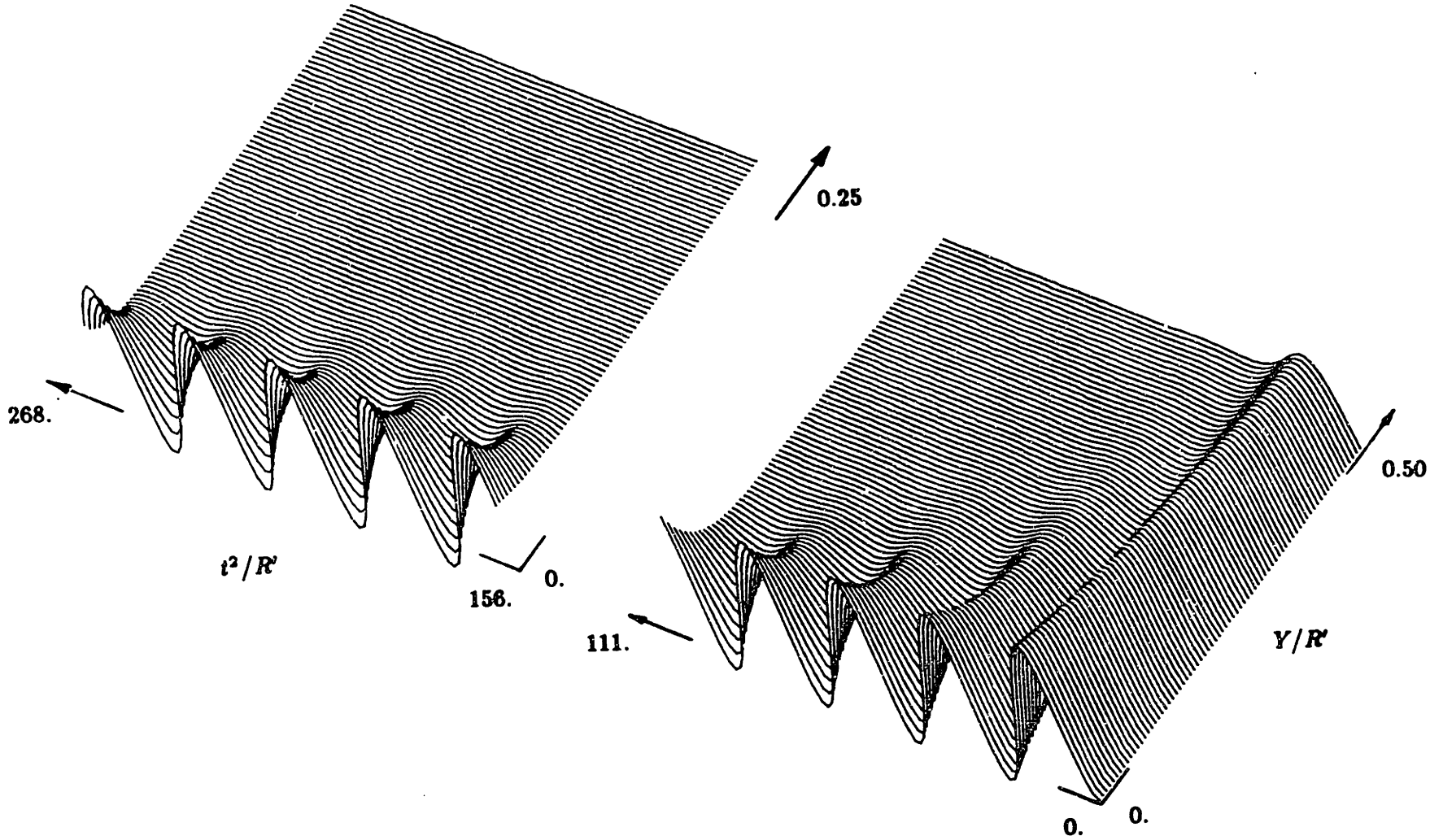

Figure 4-1. The wave part of the transient free-surface Green function. The function plotted is $R'\,G^{(F)}$. The coordinates are as defined after (A.7).

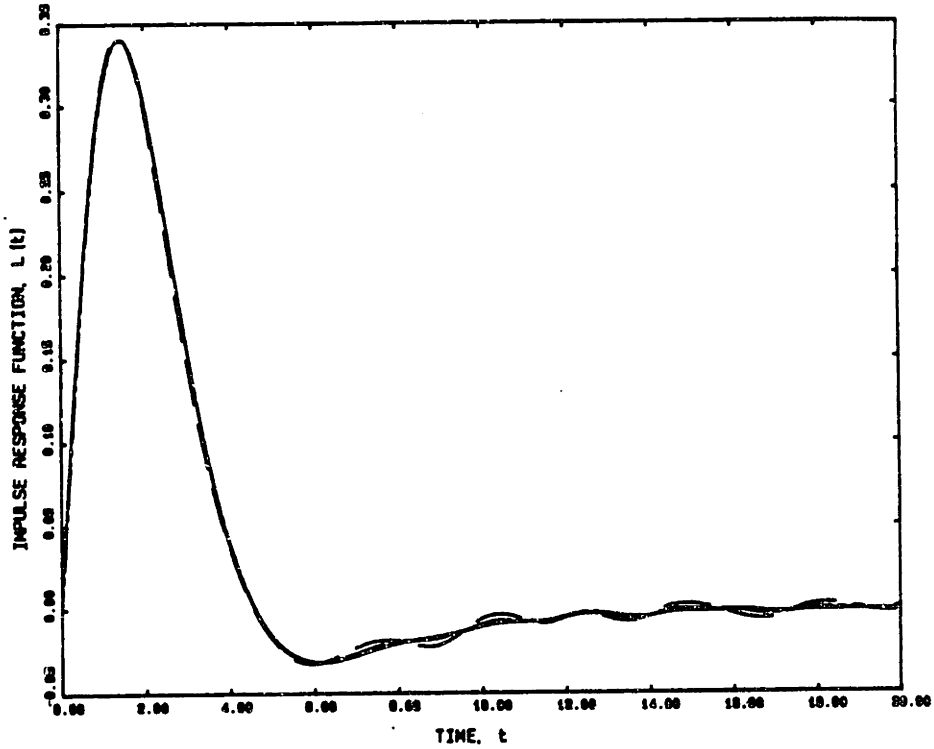

Figure 4-2. Heaving hemisphere; $\Delta t = 0.1$; 64 panels — —, 144 panels — - —, 256 panels ——— .

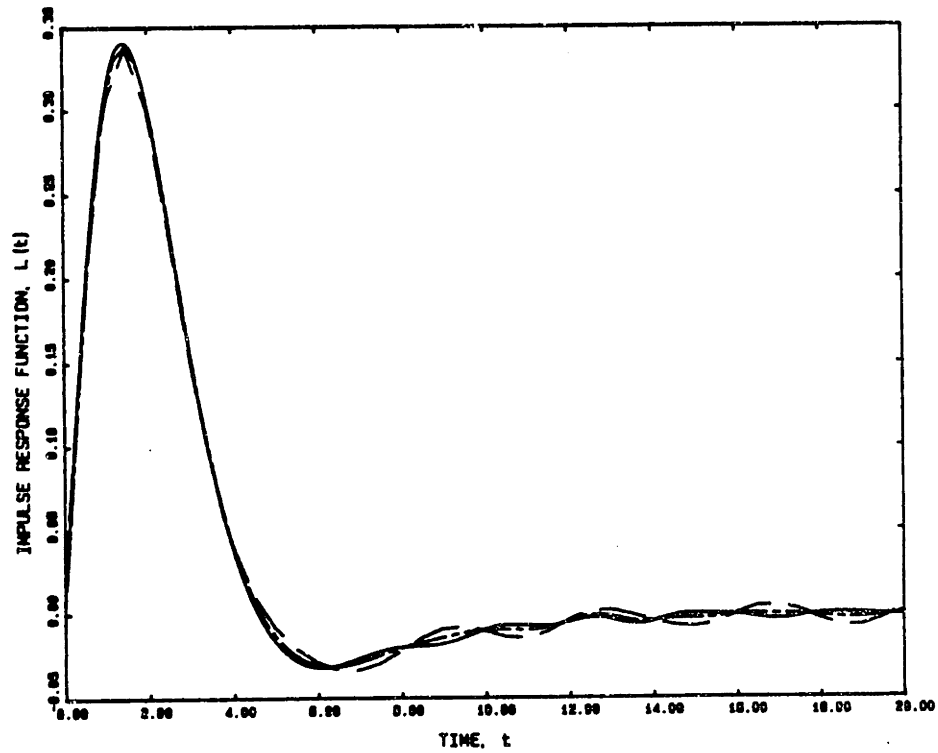

Figure 4-3. Heaving hemisphere; 144 panels; $\Delta t = 0.5$ — —, $\Delta t = 0.3$ — - —, $\Delta t = 0.05$ ——— .

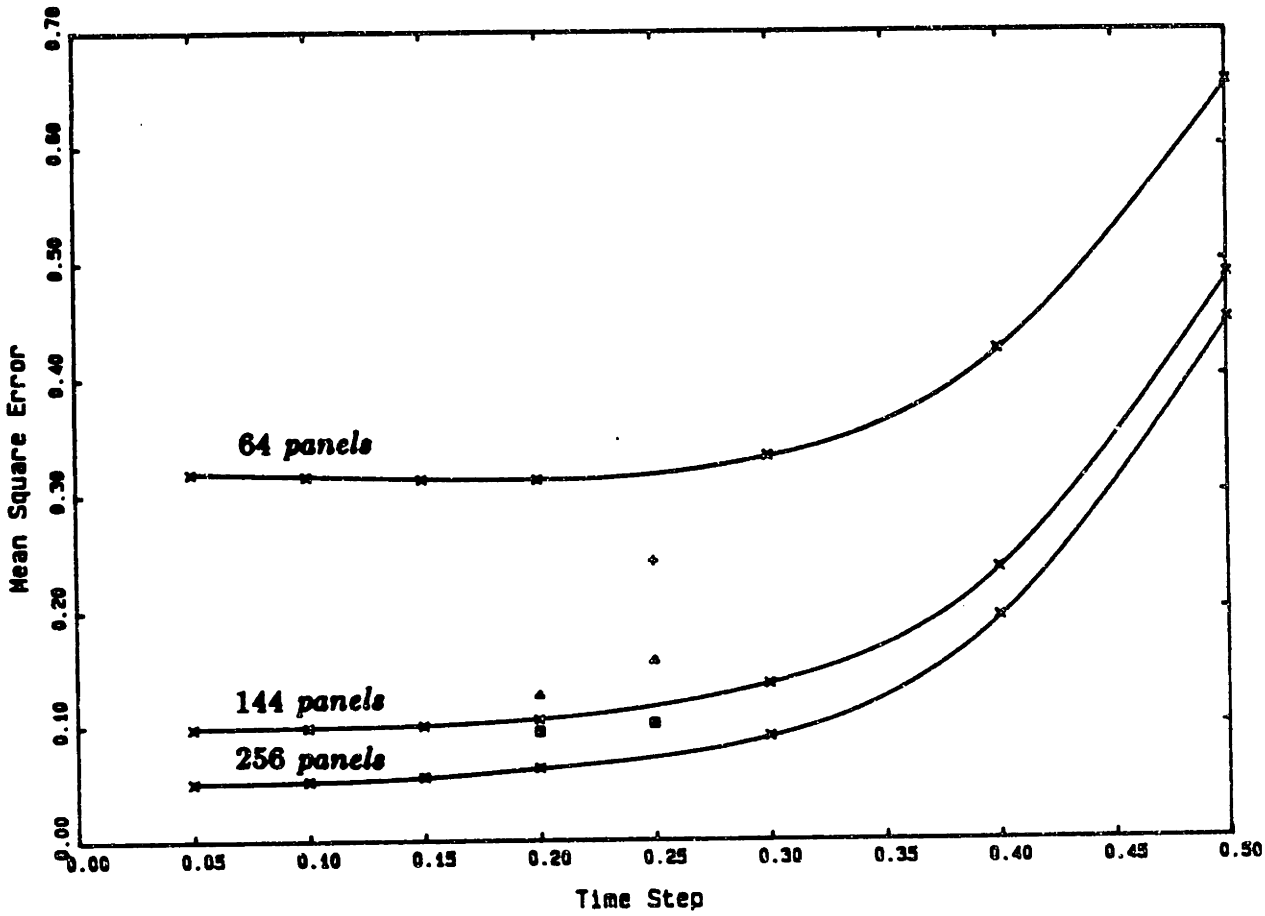

Figure 4-4. Heaving hemisphere. Mean square error in the impulse response function (compared to a 4608-panel model with $\Delta t = 0.05$). Solid lines are splines through the marked data-points for regularly distributed panel models. Cosine distributed panel models are marked: 64 panels ✦ , 100 panels ▲ , 144 panels ▫ .

5. THE LARGE-TIME ASYMPTOTIC EXPANSION OF THE IMPULSE RESPONSE FUNCTION

OVERVIEW

All of the authors cited in Section 1, who have contributed to the time-domain literature, point out that irregular frequency effects are encountered in the time domain as well as in the frequency domain. These effects result from the fact that the boundary-value problem is re-cast in Fredholm integral equation form, and this technique is common to both domains. Adachi and Ohmatsu (1979) state that in the time domain the effect of irregular frequencies is manifested in an oscillation of the impulse response function at large time. If the impulse response function is Fourier transformed to obtain the added-mass and damping coefficient curves in the frequency domain, these large-time oscillations transform to an irregular behaviour in the vicinity of the irregular frequencies. In the frequency-domain potential formulation of the radiation problem, accurate solutions may be computed by panel methods at frequencies which are increasingly close to an irregular frequency by increasing the accuracy of the body discretization. The analogous situation in the time domain, as discussed in the previous section, is that the amplitude of the oscillatory behavior in the impulse response function may be reduced by increasing the accuracy of the body discretization. Newman (1985) suggests that impulse response results may be improved by matching a suitably accurate numerical solution to a large-time asymptotic solution.

The large-time asymptotic representation of the impulse response function may be obtained from the low-frequency, convergent series form of either the added-mass or damping coefficient functions through the Fourier transform. One or two terms of the low-frequency expansion for the damping coefficient function are readily available from

the Haskind relations applied to well-known, one-or two-term approximations of the exciting force. Simon and Hulme (1985) however, show that the velocity potential, and therefore the hydrodynamic coefficients, may be expanded to *any* order in the wavenumber through the direct expansion of the Green formulation of the radiation problem in the frequency domain.

In this Section, the frequency-domain Green formulation for the velocity potential in the radiation problem is expanded directly for low frequencies by using an ascending series representation for the Green function. This provides a hierarchy of problems at each order of the wavenumber for the coefficients of the velocity potential expansion. The coefficients in the added-mass and damping expansions up to orders $k \log k$ and k^2 respectively, are analytically shown to agree with values derived independently by using a low-frequency exciting force expansion in the Haskind relations. Computed coefficients of the heave damping coefficient expansion for a hemisphere up to order k^5, are Fourier transformed and used in the time domain to remove the oscillatory behavior in the impulse response function. On transformation back to the frequency domain, we find that the effects of the irregular frequencies are removed. The technique presented is applicable to arbitrary three dimensional bodies in any mode of motion.

THE RADIATION PROBLEM IN THE FREQUENCY DOMAIN

We consider the first order problem of Section 3, but now with harmonic body motion which exists *for all time* . This is the familiar frequency-domain radiation problem with implied time dependence of $\phi^{(1)}(\vec{x},t) = \varphi(\vec{x},k)e^{i\omega t}$, with only the real part understood to have physical significance. Recall that the problem is normalized by setting the acceleration due to gravity, the fluid density, and a representative body length equal to one. If the body velocity in a particular mode is $e^{i\omega t}$ and n is the component of the body normal vector in this mode, then the problem formulation for $\varphi(\vec{x},k)$ in this case is:

$$\nabla^2\varphi(\vec{x},k) = 0 \qquad \text{in the fluid domain} \tag{5.1}$$

$$-\omega^2\varphi + \varphi_z = 0 \qquad \text{on } S_F \tag{5.2}$$

$$\varphi_n = n \qquad \text{on } S_B \tag{5.3}$$

$$\varphi e^{i\omega t} \propto \frac{1}{\sqrt{\hat{R}}} e^{-i(\hat{R}-\omega t)} \qquad \hat{R} \to \infty, \quad \hat{R}^2 = x^2 + y^2. \tag{5.4}$$

In the usual manner, Green's second identity with $\varphi(\vec{x},k)$ and $G(\vec{x};\vec{\xi},k)$ leads to

$$2\pi\varphi(\vec{x},k) + \iint_{S_B} d\vec{\xi}\,\varphi(\vec{\xi},k)G_{n_\xi}(\vec{x};\vec{\xi},k) = \iint_{S_B} d\vec{\xi}\,n(\vec{\xi})G(\vec{x};\vec{\xi},k), \tag{5.5}$$

where the Green function is defined by Wehausen and Laitone (1960) to be:

$$G(\vec{x};\vec{\xi},k) = \frac{1}{R} + \frac{1}{R'} + 2k\int_0^\infty \frac{1}{K-k} J_0(KX)e^{-KY}\,dK \tag{5.6}$$

with R, R', X and Y defined as in the time-domain Green function, following equation (A.7), and $k = \omega^2$. The contour over the real $k-$axis is indented above the pole at $K = k$ in order to enforce the radiation condition (5.4).

This Green function has been shown by Hulme (1982) to possess the convergent ascending series expansion, which through $O(k^2)$ is:

$$\begin{aligned} G(\vec{x};\vec{\xi},k) = \frac{1}{R} + \frac{1}{R'} - 2k\log k - 2\big[[\log(R'+Y) - \log 2 + \gamma] + \pi i\big]k \\ + 2Yk^2\log k + 2\big[[\log(R'+Y) - \log 2 + \gamma]Y - R' + \pi Y i\big]k^2 + O(k^3\log k). \end{aligned} \tag{5.7}$$

where γ is Euler's constant. Insertion of this series in equation (5.5) suggests a similar series expansion for $\varphi(\vec{x},k)$. In a method demonstrated by Simon and Hulme, (1985) (a reference we were not aware of when we developed this approach) a series representation for $\varphi(\vec{x},k)$ is assumed and both sides of equation (5.5) are expanded, to produce a hierarchy of problems for the unknown coefficients of the series for $\varphi(\vec{x},k)$. This

series, unlike that for $G(\vec{x};\vec{\xi},k)$, will contain powers of $\log k$. Using the convenient nomenclature, where for instance, G appears as

$$G(\vec{x};\vec{\xi},k) = g_{00} + g_{11}k\log k + g_{10}k + g_{21}k^2\log k + g_{20}k^2 + ..., \tag{5.8}$$

$\varphi(\vec{x},k)$ has the expansion

$$\varphi \sim \sum_{n=0}^{\infty} k^n \sum_{m=0}^{M(n)} p_{nm}\log^m k, \tag{5.9}$$

where $M(n) = (n+1)/2$, when n is odd, $M(n) = n/2$, when n is even, and $M = 0$ when $n = 0$. This pattern for the introduction of logarithmic terms in $\varphi(\vec{x},k)$ is a result of the fact that the normal derivative of $G(\vec{x};\vec{\xi},k)$ has no term at $O(k\log k)$. The resulting problems for the complex coefficients of the radiation potential are:

$$2\pi p_{00} + \iint_{S_B} d\vec{\xi}\, p_{00}\frac{\partial}{\partial n}(g_{00}) = \iint_{S_B} d\vec{\xi}\, n_3 g_{00} \tag{5.10}$$

$$2\pi p_{11} + \iint_{S_B} d\vec{\xi}\, p_{11}\frac{\partial}{\partial n}(g_{00}) = \iint_{S_B} d\vec{\xi}\, n_3 g_{11} \tag{5.11}$$

$$2\pi p_{10} + \iint_{S_B} d\vec{\xi}\, p_{10}\frac{\partial}{\partial n}(g_{00}) = \iint_{S_B} d\vec{\xi}\left(n_3 g_{10} - p_{00}\frac{\partial}{\partial n}(g_{10})\right) \tag{5.12}$$

$$2\pi p_{21} + \iint_{S_B} d\vec{\xi}\, p_{21} \frac{\partial}{\partial n}(g_{00}) = \iint_{S_B} d\vec{\xi} \left(n_3 g_{21} - p_{00} \frac{\partial}{\partial n}(g_{21}) - p_{11} \frac{\partial}{\partial n}(g_{10}) \right) \quad (5.13)$$

$$2\pi p_{20} + \iint_{S_B} d\vec{\xi}\, p_{20} \frac{\partial}{\partial n}(g_{00}) = \iint_{S_B} d\vec{\xi} \left(n_3 g_{20} - p_{00} \frac{\partial}{\partial n}(g_{20}) - p_{10} \frac{\partial}{\partial n}(g_{10}) \right) \quad (5.14)$$

. . . .
. . . .
. . . .

The infinite set of equations represented by (5.10) through (5.14) may be solved to obtain the coefficients of the expansion for $\varphi(\vec{x}, k)$ to any order. Note that the kernel is the same at all orders, but the right-hand sides are increasingly more complicated combinations of lower order solutions and coefficients from the expansion of $G(\vec{x}; \vec{\xi}, k)$. The coefficients of expansions for the added-mass and damping functions are found by integration over the body surface of the potential coefficients. We can use the hierarchy of integral equations to find, in closed form, the first few coefficients of the expansions for the heave damping and added-mass $a_3(\omega)$ and $b_3(\omega)$; and in particular, we can recover the first two terms of the heave damping expansion derived from the low-frequency approximation for the heave exciting force

$$X_3(\omega) \sim A_w + i\omega b_3 - \omega^2 (a_3(0) + \forall) + \ldots \quad (5.15)$$

where $\forall$ is the body displacement and A_w is the waterplane area. When this expression is inserted into the Haskind relations, the low-frequency expansion for the heave damping function is found to be

$$\frac{b_3(\omega)}{\omega} \sim \frac{A_w^2}{2} k - A_w (a_3(0) + \forall) k^2 . \quad (5.16)$$

The hierarchy of integral equations to order k^2 recovers this result. For the added-mass, we can find in closed form, terms at orders 1, $k \log k$, and $k^2 \log k$. Consider the following definitions

$$\frac{b_3(\omega)}{\omega} \sim \sum_{n=0}^{\infty} k^n \sum_{m=0}^{M(n)} b_{nm} \log^m k \tag{5.17}$$

$$a_3(\omega) \sim \sum_{n=0}^{\infty} k^n \sum_{m=0}^{M(n)} a_{nm} \log^m k. \tag{5.18}$$

Then,

$$b_{nm} = -\iint_{S_B} d\vec{\xi}\, \Im p_{nm}\, n_3, \tag{5.19}$$

and,

$$a_{nm} = \iint_{S_B} d\vec{\xi}\, \Re p_{nm}\, n_3. \tag{5.20}$$

Looking order by order at equations (5.10) through (5.14):

<u>O(1)</u>

This equation is real, so $\Im p_{00} = 0$ and hence $b_{00} = 0$. The equation for p_{00} is

$$2\pi p_{00} + \iint_{S_B} d\vec{\xi}\, \frac{\partial}{\partial n}(g_{00}) p_{00} = \iint_{S_B} d\vec{\xi}\, n_3 g_{00}. \tag{5.21}$$

This is

$$2\pi p_{00} + \iint_{S_B} d\vec{\xi}\, p_{00} \frac{\partial}{\partial n}\left(\frac{1}{R} + \frac{1}{R'}\right) = \iint_{S_B} d\vec{\xi}\, n_3 \left(\frac{1}{R} + \frac{1}{R'}\right), \tag{5.22}$$

the equation for the rigid-lid potential, ψ_{RL} [*i.e.* $\frac{\partial}{\partial n}\psi_{RL} = 0$ on S_F, see Figure 3-2]. Therefore, a_{00} is the infinite-fluid, dilating-body added-mass, a_{RL}.

$\underline{O(k \log k)}$

This equation is also real, so $\Im p_{11} = 0$ and $b_{11} = 0$. The equation for p_{11} is

$$2\pi p_{11} + \iint_{S_B} d\vec{\xi}\, p_{11} \frac{\partial}{\partial n}(g_{00}) = \iint_{S_B} d\vec{\xi}\, n_3 g_{11}. \tag{5.23}$$

Since the right-hand side is a constant, we have a constant solution; and since

$$\iint_{S_B} d\vec{\xi} \frac{\partial}{\partial n}\left(\frac{1}{R} + \frac{1}{R'}\right) = 2\pi \tag{5.24}$$

it follows that

$$p_{11} = -\frac{A_w}{2\pi}, \tag{5.25}$$

and

$$a_{11} = -\frac{A_w^2}{2\pi}. \tag{5.26}$$

$\underline{O(k)}$

This equation is complex. The real part has not yielded to analysis, hence the exact coefficient for $a_3(\omega)$ is not available at this order, although some coefficients at higher orders may still be found in closed form. Taking the imaginary part of the equation we obtain

$$\begin{aligned} 2\pi \Im p_{10} + \iint_{S_B} d\vec{\xi} \frac{\partial}{\partial n}(g_{00}) \Im p_{10} &= \iint_{S_B} d\vec{\xi}\, n_3 \Im g_{10} \\ &= -2\pi A_w. \end{aligned} \tag{5.27}$$

Since the right-hand side is a constant, we have a constant solution

$$\Im p_{10} = \frac{-A_w}{2}, \tag{5.28}$$

thus,

$$b_{10} = \frac{A_w^2}{2}. \tag{5.29}$$

$\underline{O(k^2 \log k)}$

This is another real equation, so $b_{21} = 0$. For p_{21} we have

$$2\pi p_{21} + \iint_{S_B} d\vec{\xi}\, p_{21} \frac{\partial}{\partial n}(g_{00}) = \iint_{S_B} d\vec{\xi} \left[n_3 g_{21} - p_{00} \frac{\partial}{\partial n}(g_{21}) - p_{11} \frac{\partial}{\partial n}(g_{10}) \right]. \tag{5.30}$$

We have found that $p_{00} = \psi_{RL}$, and $p_{11} = -\frac{A_w}{2\pi}$, so we have

$$2\pi p_{21} + \iint_{S_B} d\vec{\xi}\, p_{21} \frac{\partial}{\partial n}(g_{00}) = \iint_{S_B} d\vec{\xi} \left[2n_3(Y + \psi_{RL}) - \frac{A_w}{\pi} \frac{\partial}{\partial n} \log(Y + R') \right]. \tag{5.31}$$

Letting $p_{21} = \hat{p} + \hat{\hat{p}}$, we separate the integral equation (5.31) into the following components

$$2\pi \hat{\hat{p}} + \iint_{S_B} d\vec{\xi}\, \hat{\hat{p}} \frac{\partial}{\partial n}(g_{00}) = \iint_{S_B} d\vec{\xi}\, 2(-\zeta + \psi_{RL}) n_3 \tag{5.32}$$

and

$$2\pi \hat{p} + \iint_{S_B} d\vec{\xi}\, \hat{p} \frac{\partial}{\partial n}(g_{00}) = -\frac{A_w}{\pi} \iint_{S_B} d\vec{\xi} \frac{\partial}{\partial n} \log(Y + R') dS - 2A_w z. \tag{5.33}$$

where the definition $Y = -(z + \zeta)$ has been used. The equation for $\hat{\hat{p}}$ has a right-hand side which is a constant function over the body surface, equal to $2(a_3(0) + \forall)$. Since its kernel is non-singular, it must possess a unique solution. Here, we seek it to be a constant function.

It is easy to verify that

$$\hat{\hat{p}} = \frac{1}{2\pi}(a_3(0) + \forall) \tag{5.34}$$

solves the integral equation (5.32), thus is its unique solution. To solve the equation for $\hat{p}$, we first use the identity

$$-\iint_{S_B} d\vec{\xi}\,\frac{\partial}{\partial n}\log(Y+R') = \iint_{S_W}\frac{1}{R'} = \frac{1}{2}\iint_{S_W}(\frac{1}{R}+\frac{1}{R'}), \tag{5.35}$$

where S_W is the body waterplane surface. Identity (5.35) follows by conserving the mass flux across the closed surface $S_B + S_W$ due to the flow generated by the harmonic function $\log(Y+R')$ which is singular at a point above the free surface. Applying next Green's second identity with the potentials $\varphi_1 = \frac{1}{R} + \frac{1}{R'}$, and $\varphi_2 = \zeta$ in the domain interior to the body surface, we obtain

$$\frac{1}{2}\iint_{S_W}(\frac{1}{R}+\frac{1}{R'}) = \frac{1}{2}\iint_{S_B} d\vec{\xi}\,[(\frac{1}{R}+\frac{1}{R'})n_3 - \zeta\frac{\partial}{\partial n}(\frac{1}{R}+\frac{1}{R'})] + \pi z \tag{5.36}$$

where the term πz on the right-hand-side is the contribution from the hemispherical indentation around the location of the Rankine source $1/R$ on the body surface S_B. Utilizing (5.35) and (5.36) in the right-hand side of the integral equation (5.33) we obtain

$$2\pi\hat{p} + \iint_{S_B} d\vec{\xi}\,\hat{p}\frac{\partial}{\partial n}(g_{00}) = \frac{A_w}{2\pi}\iint_{S_B} d\vec{\xi}\,\left[(\frac{1}{R}+\frac{1}{R'})n_3 - \zeta\frac{\partial}{\partial n}(\frac{1}{R}+\frac{1}{R'})\right] - A_w z. \tag{5.37}$$

The right-hand side of equation (5.37) consists of three terms. The first term is proportional to the right-hand side of the rigid-lid integral equation. The corresponding contribution to the velocity potential $\hat{p}$ is $\frac{A_w}{2\pi}\psi_{RL}$. The last two terms can be obtained if we substitute $-z\frac{A_w}{2\pi}$ for $\hat{p}$ on the left-hand side. Therefore, this is the second component of the solution for the velocity potential $\hat{p}$. Thus, the solution of the integral equation (5.37) is

$$\hat{p} = \frac{A_w}{2\pi}(\psi_{RL} - z). \tag{5.38}$$

Combining (5.34) and (5.38) gives

$$p_{21} = \frac{1}{2\pi}(a_3(0) + \forall) + \frac{A_w}{2\pi}(\psi_{RL} - z). \tag{5.39}$$

Integrating for the term a_{21} in the expansion for the added mass coefficient function, we obtain

$$a_{21} = \frac{A_w}{\pi}(a_3(0) + \forall). \tag{5.40}$$

<u>$O(k^2)$</u>

This equation is complex. The real part has not been solved in closed form. Taking its imaginary part

$$2\pi\Im p_{20} + \iint_{S_B} d\vec{\xi}\,\frac{\partial}{\partial n}(g_{00})\Im p_{20} = \iint_{S_B} d\vec{\xi}\,\left[n_3\Im g_{20} - p_{00}\Im\frac{\partial}{\partial n}(g_{20}) - \Im p_{10}\frac{\partial}{\partial n}(g_{10})\right]. \tag{5.41}$$

We have found that $p_{00} = \psi_{RL}$, and $\Im p_{10} = -\frac{A_w}{2}$, so we have

$$2\pi\Im p_{20} + \iint_{S_B} d\vec{\xi}\,\frac{\partial}{\partial n}(g_{00})\Im p_{20} = \iint_{S_B} d\vec{\xi}\,\left[2\pi n_3(Y + \psi_{RL}) - A_w\frac{\partial}{\partial n}\log(Y + R')\right]. \tag{5.42}$$

However, the right-hand side of (5.41) is just that of (5.31) with the multiplicative factor of π. Therefore

$$\Im p_{20} = \pi p_{21}, \tag{5.43}$$

and so

$$b_{20} = -A_w\,(a_3(0) + \forall) \tag{5.44}$$

recovering the second term in equation (5.16), which was derived from the low-frequency expansion of the exciting force. Summarizing, in closed form we have found the first two terms in the low-frequency expansion for the heave added-mass coefficient function

$$a_3(\omega) = a_{RL} - \frac{A_w^2}{2\pi} k \log k + O(k), \tag{5.45}$$

and the first two terms in the low-frequency expansion for the heave damping coefficient function

$$\frac{b_3(\omega)}{\omega} = \frac{A_w^2}{2} k - A_w\,(a_3(0) + \forall) k^2 + O(k^3 \log k). \tag{5.46}$$

THE FOURIER TRANSFORM

The impulse response function may be determined from the inverse forms of either equation (3.17) or (3.18); or more generally, we may write:

$$L(t) = \frac{1}{\pi} \Re \int_0^\infty e^{i\omega t} \left[W(\omega) - a(\infty) \right] d\omega, \tag{5.47}$$

where $W(\omega) = a(\omega) - i\frac{b(\omega)}{\omega}$ is the complex impedance function. Using low-frequency expansions for $a(\omega)$ and $\frac{b(\omega)}{\omega}$ we consider two methods for the long-time asymptotic evaluation of equation (5.47): in the complex ω-plane by contour integration, and on the positive real ω-axis by Fourier theory involving generalized functions.

Contour integration

For contour integration of $W(\omega) - a(\infty)$ we require knowledge of that function in the complex ω-plane, and particularly on the imaginary ω-axis. The ascending series representation for $G(\vec{x}; \vec{\xi}, k)$ is exact and may be continued for complex k. When

this is done, the hierarchy of integral equations is continued into the complex k-plane and hence so is the associated complex impedance function, $W(\omega)$. Of course we no longer expect that the real and imaginary parts of $W(\omega)$ represent the added-mass and damping functions of the original wave-body problem. When the expansion for $G(\vec{x};\vec{\xi},k)$ is moved into the complex k-plane to just above the cut on the negative real k-axis, that is $k = -|k| + i\epsilon$ as $\epsilon \to 0$, the expansion may be rewritten with coefficients $\tilde{g}_{mn}$ related to the original g_{mn} as follows:

$$\begin{aligned} \tilde{g}_{n0} &= \pm(\Re g_{n0} + i2\Im g_{n0}) \begin{cases} n \text{ even} \\ n \text{ odd} \end{cases} \\ \tilde{g}_{n1} &= \pm g_{n1} \begin{cases} n \text{ even} \\ n \text{ odd,} \end{cases} \end{aligned} \tag{5.48}$$

and at least through $O(k^5)$ the new integral equations have simple relations to those equations on the positive real k-axis. In fact to all orders, the kernel is not changed, although the right-hand sides are. The $W(\omega)$ corresponding to the solution of these equations with this particular complex k will define the complex impedance function on the positive, imaginary ω-axis, where $\omega = i\Omega$ (Ω a positive real number). This $W(\Omega)$ may be written in terms of the coefficients of $W(\omega)$, for real ω; and the imaginary part which we will need in the contour integration is:

$$\begin{aligned} \Im W(\Omega) \sim 2\big[&b_{10}\Omega^2 - b_{20}\Omega^4 + 2b_{31}\Omega^6 \log\Omega + b_{30}\Omega^6 \\ &- 2b_{41}\Omega^8 \log\Omega - b_{40}\Omega^8 + 4b_{52}\Omega^{10}\log^2\Omega \\ &+ 2b_{51}\Omega^{10}\log\Omega + (b_{50} - \pi^2 b_{52})\Omega^{10}\big] \end{aligned} \tag{5.49}$$

Alternatively, substitution of $\omega = i\Omega$ into $W(\omega)$ on the real ω-axis results in $\Im W(\Omega)$:

$$\begin{aligned} \Im W(\Omega) \sim\ &(b_{10} - \pi a_{11})\Omega^2 - (b_{20} - \pi a_{21})\Omega^4 + (2b_{31} - 4\pi a_{32})\Omega^6 \log\Omega \\ &+ (b_{30} - \pi a_{31})\Omega^6 - (2b_{41} - 4\pi a_{42})\Omega^8 \log\Omega - (b_{40} - \pi a_{41})\Omega^8 \\ &+ (4b_{52} - 12\pi a_{53})\Omega^{10}\log^2\Omega + (2b_{51} - 4\pi a_{52})\Omega^{10}\log\Omega \\ &+ (b_{50} - \pi^2 b_{52} + \pi^3 a_{53} - \pi a_{51})\Omega^{10}. \end{aligned} \tag{5.50}$$

If we equate (5.49) and (5.50), we recover the relations between the coefficients of the expansions for $a(\omega)$ and $\frac{b(\omega)}{\omega}$, a concept suggested by the Kramers-Kronig relations, and discussed by Greenhow (1986).

By contour integration in the first quadrant of the complex ω-plane, we can set equation (5.47) equal to a Laplace integral plus some unknown set of residues from poles which may exist in this quadrant. As $t \to \infty$ their contribution decays exponentially so that asymptotically $L(t)$ may be determined from:

$$L(t) \sim \frac{-1}{\pi} \int_0^\infty e^{-\Omega t} \Im W(\Omega) d\Omega. \tag{5.51}$$

Olver (1974) presents an asymptotic analysis of this type of integral if the function $W(\Omega)$ can be represented by a power series which may include powers of logarithms.

Results required for the evaluation of terms through $O(k^5)$ are:

function	Laplace contribution	
Ω^n	$\frac{-1}{\pi} n! \, t^{-(n+1)}$	(5.52)
$\Omega^n \log \Omega$	$\frac{-1}{\pi} n! \, [\psi(n) - \log t] t^{-(n+1)}$	(5.53)
$\Omega^n \log^2 \Omega$	$\frac{-1}{\pi} n! \, [\log^2 t - 2\psi(n) \log t$ $+ (\psi^2(n) + \frac{\pi^2}{6} - \sum_{j=1}^{n} \frac{1}{j^2})] t^{-(n+1)}$	(5.54)

where $\psi(N) = \sum_{n=1}^{N} \frac{1}{n} - \gamma$.

Fourier integration

For this analysis it is more convenient to work with the inverse form of either equation (3.13) or (3.14) than with the general form (5.47). We choose the inverse sine transform of the damping function:

$$L(t) = \frac{2}{\pi} \int_0^\infty \frac{b(\omega)}{\omega} \sin \omega t \, d\omega. \tag{5.55}$$

Evaluation of this transform is facilitated by the theory of generalized functions detailed in Lighthill (1958). Table I of this reference can be used to obtain the following results

function	inverse sine transform	
k^n	$\frac{2}{\pi}(-1)^n(2n)!\,t^{-(2n+1)}$	(5.56)
$k^n \log k$	$\frac{4}{\pi}(-1)^n(2n)!\,[\psi(2n) - \log t]t^{-(2n+1)}$	(5.57)

The term of order $k^5 \log^2 k$ requires additional effort. Using the definition

$$\log \mid x \mid = \lim_{\epsilon \to 0}(1 - \mid x \mid^{-\epsilon})/\epsilon, \tag{5.58}$$

we set

$$\log^2 \mid x \mid = \lim_{\epsilon \to 0} \frac{1}{\epsilon^2}\left[\mid x \mid^{\epsilon} + \mid x \mid^{-\epsilon} - 2\right], \tag{5.59}$$

where the transforms for the right-hand side of (5.59) are available in the above cited Table 1. Since $x^m f(x)$ transforms to $(-2\pi i)^{-m}\frac{d^m}{dy^m}g(y)$, it follows that

function	inverse sine transform	
$k^n \log^2 k$	$\frac{8}{\pi}(-1)^n(2n)!\left[\log^2 t - 2\psi(2n)\log t\right.$	
	$\left.+\left[(\psi(2n))^2 - \sum_{j=1}^{2n}\frac{1}{j^2} - \frac{\pi^2}{12}\right]\right]t^{-(2n+1)}.$	(5.60)

THE IMPULSE RESPONSE FUNCTION

Simon and Hulme (1985) present the following expansion for the damping coefficient function of a heaving hemisphere. This was derived from a subset of the hierarchy of integral equations, with the help of relations between the added-mass, damping and exciting-force functions. Their expression includes all terms to order k^5:

$$\begin{aligned}\frac{b_3}{\omega} \sim \frac{2\pi^2}{3}\{&\frac{3}{4}k - 1.830951k^2 + \frac{3}{4}k^3\log k + 2.542917k^3 - 2.746427k^4\log k \\ &- 2.374082k^4 + \frac{9}{16}k^5\log^2 k + 5.646816k^5\log k - 0.442638k^5\}.\end{aligned} \tag{5.61}$$

Using either equation (5.49) and the Laplace integral results of equations (5.52) through (5.54); or equation (5.19) with the Fourier integral results of equations (5.56), (5.57) and (5.60) gives the same expression for the asymptotic form of the impulse response function up to order t^{-11}. Equations (5.54) and (5.60) appear to imply that the Laplace and Fourier analysis methods produce different time-domain results for terms at orders with squares of logarithms. However this apparent difference in the time domain, here specifically at $O(t^{-11})$, is offset by the difference in the coefficients of the impedance functions at $O(k^5)$ on the real $\omega-$axis and at $O(\Omega^{10})$ on the imaginary ω-axis. We find that:

$$\begin{aligned} L(t) \sim -\frac{2}{\pi}\Bigg[& 2!\,b_{10}t^{-3} - 4!\,b_{20}t^{-5} - 2(6!)b_{31}t^{-7}\log t \\ & + 6!\,(b_{30} + 2\psi(6)b_{31})t^{-7} + 2(8!)b_{41}t^{-9}\log t \\ & - 8!\,(b_{40} + 2\psi(8)b_{41})t^{-9} + 4(10!)b_{52}t^{-11}\log^2 t \\ & - 2(10!)(4\psi(10)b_{52} + b_{51})t^{-11}\log t \\ & + 10!\Bigg[4\Big[\big(\psi(2n)\big)^2 - \sum_{j=1}^{10}\frac{1}{j^2} - \frac{\pi^2}{12}\Big]b_{52} \\ & + 2\psi(10)b_{51} + b_{50}\Bigg]t^{-11}\Bigg]. \end{aligned} \tag{5.62}$$

It is interesting to note that equations (5.49) and (5.50) suggest that the coefficients a_{n0} are superfluous to this analysis. This is supported by the Fourier integration as well. If the inverse cosine transform of the added-mass expansion is used, the a_{n0}'s contribute n^{th} order derivatives of $\delta(t)$ (where $\delta(t)$ is Dirac's delta function) which only affect $L(0)$.

6. RESULTS FOR THE FIRST-ORDER PROBLEM

The time-domain radiation panel-code TIMIT has been run for simple bodies such as the hemisphere and the right-circular cylinder and one complicated body, a Tension Leg Platform (TLP). During the verification phase of the work with TIMIT , it became clear that the irregular frequency effects were one of the most intriguing aspects of the problem. Consequently the relation between the time- and frequency-domain radiation problems receives considerable attention, particularly the asymptotic approach to large-time evaluation of the impulse response function which allows very accurate calculation of the frequency-domain hydrodynamic coefficients through the Fourier transform.

IMPULSE RESPONSE FUNCTIONS AND IRREGULAR FREQUENCY EFFECTS FOR SIMPLE BODIES

The emphasis in this work is not to present impulse response functions for various simple bodies. Rather it is on the interpretation and application of these results. There are impulse response functions presented in various sections of the Thesis in the context of discussions concerning numerical errors, large-time behavior, and first-order input to the second-order problem. The List of Figures may be consulted as a guide to the location of all of the presented impulse response functions. For the impulse response functions for a family of right-circular cylinders in heave, see Newman (1985a); and for additional hemisphere results, see Beck and Liapis (1987). In this sub-section we analyze the oscillatory behavior in the impulse response function at large time.

When the frequency-domain hydrodynamic coefficients are calculated from the impulse response function, the inaccuracies which are present are due to conflicting constraints.

Although the Fourier cosine and sine transforms, equations (3.17) and (3.18), which relate $L(t)$ to $a(\omega)$ and $b(\omega)$ are exact for infinite time histories; in practice, the calculated record is truncated at some large time, usually dictated by computational resources. For simple bodies, the evidence suggests that the impulse response function approaches zero monotonically after one or two oscillations, and it is possible to carry out computations with sufficient panels and to sufficiently large time that $|L(t)|$ is less than, say, 5×10^{-3}. The Fourier transforms of such records may agree with analytical results, or carefully computed frequency-domain results, within a similar tolerance. It is more likely, however, that computing resources will dictate fewer panels and at large time there will be the typical oscillatory behavior with an amplitude which affects the first or second decimal of $L(t)$ and which appears early in the monotonically decaying region. [For instance, see Figure 6-3.] In this case, the conflicting constraints are that if $L(t)$ is truncated at too small a time before transformation, the hydrodynamic coefficients will be inaccurate in the low frequency range, but inclusion in the record of a long sample of the oscillatory behavior will produce inaccuracy in the vicinity of the irregular frequencies.

We would like to know the functional form of the oscillatory behavior. Adachi and Ohmatsu (1979) explore the irregular frequency problem in both the time and frequency domains and address this question. In that work, considerably more is said about the source-distribution form of the integral equation method, than the potential form. This is because of the incorrect conclusion that the Fredholm alternative indicates that there are no irregular frequency effects in the potential form. This is not the case. There *is* a difference in the two approaches, but it is not that indicated by Adachi and Ohmatsu.

As is shown by Adachi and Ohmatsu there is a set of frequencies at which the source formulation has no solution. It is reasoned, then, that at these frequencies, the Fredholm determinant vanishes. Since source and potential integral formulations have transpose kernels they share the set of frequencies at which the Fredholm determinant vanishes. At these eigenfrequencies the Fredholm alternative states that the integral equation has either no solution or an infinity of solutions depending on the orthogonality of the

right-hand side to the eigensolutions. As is demonstrated by the above cited reference, at these frequencies the potential formulation has a right-hand side which is orthogonal to the eigensolutions, but the source formulation, in general, does not. The correct conclusion is that the source form of the integral equation has *no* solutions, and as will be discussed below, is singular at these frequencies, and the potential form of the integral equation has *non-unique* solutions. In either case, irregular frequency effects are present in the continuous form of the equation which we discretize and attempt to solve numerically. Care must be exercised in extending conclusions about the continuous formulation to the discrete formulation, but we can expect numerical difficulties due to poor conditioning of the kernel matrix, in the vicinity of the irregular frequencies, for both potential and source distribution methods.

Adachi and Ohmatsu provide the important result that in the frequency-domain, source-distribution method the singularity in the source strength is of Cauchy type in wave number. That is, like $1/(\omega_i^2 - \omega^2)$ at the irregular frequency ω_i. Liapis (1986) reinforces this conclusion for the source formulation with numerical results in the time domain. These results suggest that the sinusoidal oscillation, with frequency ω_i, seen in the time domain computations, does not decay at large time. This would be expected for a Cauchy-type singularity because $1/(\omega_i^2 - \omega^2)$, in the frequency domain, may be shown by residue calculus to lead to a non-decaying sinusoidal oscillation at frequency ω_i in the time-domain as $t \rightarrow \infty$. However, the time histories presented in Liapis (1986) may not extend to sufficiently large time to warrant the conclusion that there is no decay. In the case of the potential formulation, this conclusion is also stated by Liapis, but the oscillatory effects which are present in the potential formulation calculations in the present work *do* decay at large time, though the decay may be slow in some cases. This provides numerical evidence for a functional difference between irregular frequency effects in the discrete form of the source-distribution method and irregular frequency effects in the discrete form of the potential formulation. The frequency-domain aspects of this question are pursued further by Lee (1988).

It is possible to get a qualitative impression of time-domain, irregular-frequency effects

from Figures 6-1 and 6-3. In these figures it may be seen that the first and most prominent oscillation 'turns-on' at some time, and remains present with very slow (Figure 6-1) or no (Figure 6-3) apparent decay. At a later time, a second oscillation 'turns-on,' but its decay is faster than that of the first oscillation. Each successively higher irregular frequency has an effect on $L(T)$, but the effect is less strong as the frequency increases as is shown by the frequency-domain results for the swaying hemisphere in Figure 6-2. It is not clear how this oscillatory effect is initiated, but its form after it is visible in the figures may be (disregarding phase):

$$E_L(t) = A(N)e^{-\alpha(\omega_i)t}\sin\omega_i t \tag{6.1}$$

where E_L is the oscillatory effect due to a single irregular frequency ω_i superposed on the exact $L(t)$, $A(N)$ is the *primarily* panelling-dependent amplitude, and $\alpha(\omega_i)$ is the decay factor and may be very small. We are interested in knowing how the effect in the frequency domain is dependent on the length of the sample of such an oscillation contained in a time history. This may be examined if we perform the Fourier sine (for example) transformation of the right-hand side of equation (6.1) for a variable range of integration between t_1 and t_2. The result is:

$$\begin{aligned}\mathcal{F}_s E_L = {} & \frac{A(N)}{2}e^{-\alpha t_2}\left\{\frac{(\omega-\omega_i)\sin(\omega-\omega_i)t_2 - \alpha\cos(\omega-\omega_i)t_2}{\alpha^2+(\omega-\omega_i)^2}\right. \\ & \left. - \frac{(\omega+\omega_i)\sin(\omega+\omega_i)t_2 - \alpha\cos(\omega+\omega_i)t_2}{\alpha^2+(\omega+\omega_i)^2}\right\} \\ & - \frac{A(N)}{2}e^{-\alpha t_1}\left\{\frac{(\omega-\omega_i)\sin(\omega-\omega_i)t_1 - \alpha\cos(\omega-\omega_i)t_1}{\alpha^2+(\omega-\omega_i)^2}\right. \\ & \left. - \frac{(\omega+\omega_i)\sin(\omega+\omega_i)t_1 - \alpha\cos(\omega+\omega_i)t_1}{\alpha^2+(\omega+\omega_i)^2}\right\}\end{aligned} \tag{6.2}$$

Equation (6.2) has been computed for varying values of t_2 and for values of $A(N)$ and $\alpha(\omega_i)$ which fit equation (6.1) to the oscillatory behavior in figure 6-3. These functions are plotted in Figure 6-4. For comparison, Figure 6-5 shows the numerical transform of large-time sections of the impulse response function for the heaving hemisphere shown in Figure 6-3. Equation (6.2) does capture the numerical effects of irregular

frequencies in Fourier sine transformed time-domain results, namely a characteristic large oscillation surrounded by decaying small oscillations at the difference frequency $\omega - \omega_i$. Both Figures 6-4 and 6-5 indicate that if the truncation point of the time history of $L(t)$ is increased, the effect on transformation to the frequency domain to define the hydrodynamic coefficients is to: 1) increase the magnitude of the large irregular behavior immediate to the irregular frequency while decreasing its band width, and 2) decrease the magnitude of the small surrounding oscillation while increasing its band width.

In Figure 6-6, the irregular frequency effects are shown in the context of the complete frequency-domain results. The time history of Figure 6-3, from a 64-panel model, has been Fourier transformed with two different truncation points, and the resulting added-mass and damping coefficient curves are plotted along with more accurate results from a model with 256 panels. Again, the form of the irregular behavior in the frequency domain is as predicted by the analysis of the time-domain representation, equation (6.1).

If we examine equation (6.2) in the limit of $t_1 \to 0$ and $t_2 \to \infty$, we obtain what we expect from this numerical argument to be the functional form of irregular frequency effects in the frequency domain. [Admittedly there is some uncertainty concerning the validity of (6.1) as $t_1 \to 0$.] Since we used the Fourier sine transform, we expect to recover the form of the effect in the damping coefficient function. Using these limits, and letting $\omega = \omega_i$ equation (6.2) becomes:

$$\mathcal{F}_s E_L = \frac{-A(N)}{2} \left\{ \frac{1}{\alpha} - \frac{\alpha}{\alpha^2 + 4\omega_i^2} \right\} \tag{6.3}$$

This function is bounded, with the maximum dependent on the decay rate in the time domain. Since we have seen that $\alpha(\omega_i)$ increases as ω_i increases, we expect less effect in the frequency domain from higher irregular frequencies, as seen in Figures 6-2 and 6-6. So from this numerical argument we conclude that the source-distribution and potential formulation methods both suffer from irregular frequency effects in both the

time and frequency domains. However, because (6.3) is bounded, and the transform of the non-decaying behavior in the source formulation solution is a Cauchy singularity, the effects are less severe in the case of the potential form of the integral equation.

REMOVAL OF IRREGULAR FREQUENCY EFFECTS

In Section 5, a method is derived for the removal of irregular-frequency effects from the impulse response function. When the coefficients from the low-frequency asymptotic expansion for the damping function of the heaving hemisphere, which were computed by Simon and Hulme (1985) and are presented in equation (5.61), are inserted in the expression derived in Section 5 for the large-time approximation to the impulse response function, equation (5.62), the result is the specific asymptotic expression for the impulse response function of the heaving hemisphere at large time. This asymptotic result may be used to remove irregular frequency effects in the time domain, and consequently in the Fourier transform results in the frequency domain.

Let l_{nm} have a definition like that of b_{nm} in equation (5.17), and consider the additional definitions

$$L_n(t) = t^{-n} \sum_{m=0}^{M'(n)} l_{nm} \log^m t, \tag{6.4}$$

where $M'(n) = (n-1)/4 - 1/2$ when $(n-1)/2$ is odd, $(n-1)/4 - 1$ when $(n-1)/2$ is even, and $M' = 0$ when $n = 3, 5$; and,

$$\Sigma L_N(t) = \sum_{n=0}^{N} L_n(t). \tag{6.5}$$

$L_n(t)$ is the contribution to $L(t)$ at $O(t^{-n})$ including any logarithmic terms, and ΣL_N is the complete contribution to $L(t)$ up to $O(t^{-N})$. Figure 6-7, is a plot of the ΣL_N for $N = 3, 5, 7, 9, 11$, along with numerical results found by using 1024 panels with a time step of 0.075 and 4608 panels with a time step of 0.05. These numerical results agree to at least four decimals indicating that they are practically convergent. [Note that the

oscillatory behavior which is present is hardly reduced in spite of the increased effort in computation.] There are two important features of the asymptotic results. The first is that ΣL_{11} appears to be inconsistent with the trend in the asymptotic results up to ΣL_9. This may be the first diverging partial sum in the asymptotic series, but it would be necessary to compute at least ΣL_{13} to confirm this. It is more likely that in the time range before the asymptotic results have sufficiently converged, this trend is misleading. A similar behavior is evident in the frequency-domain damping function from which these results were transformed [Cf. Figure 2, Simon and Hulme(1985)]. The second is that these results also share with their frequency-domain counterparts a rather slow convergence; although the most accurate numerical results and the ΣL_9 asymptotic result differ in their prediction of $L(t)$ by only 0.002 beyond $t = 8.0$. For computations for any simple body, there will be a time beyond which the asymptotic representation will be a better estimate of the correct $L(t)$ than the numerical result. The most efficient method for obtaining an accurate impulse response function, then, is to perform the computation with sufficiently fine spatial and temporal discretization to reduce the oscillatory behavior in the time history until the time when the asymptotic representation may be adopted.

In Figure 6-8, this situation is demonstrated. Figure 4-4 was used as a guide in the selection of a model which produces reasonable accuracy for moderate computational effort. This model for the heaving hemisphere consists of 100 panels with a cosine distribution as the free surface is approached, and a time-step of $\Delta t = 0.2$. In Figure 6-8, the numerical results for this model are shown with the asymptotic result to $O(t^{-9})$. In this case, it is apparent that the numerical effort could have been terminated just beyond $t = 8$.

To obtain frequency-domain results for this model, the records were patched at $t = 8.2$ by simply discontinuing the numerical results and picking up the asymptotic approximation. The combined record was then Fourier transformed with a truncation point at $t = 30.0$, where the asymtotic result, $|\Sigma L_9| < 3. \times 10^{-3}$. The results of the transform, added-mass and damping coefficient functions, are presented in Figure 6-9. In

this figure, they are plotted for comparison with the un-patched numerical results, and spherical harmonics results of Hulme (1982). The frequency-domain results from the patched impulse response function contain no visible irregular behavior, and the overall accuracy of this representation of $L(t)$ is sufficient to produce a *maximum* error in the frequency domain of less than 1.5 percent at the peak of the damping curve. In Figure 6-10, the frequency domain results from a less accurate model (64 regularly spaced panels and $\Delta t = 0.2$) are presented. In this case the irregular behavior is also removed, but the overall accuracy of the patched $L(t)$ is less, leading to less accuracy at the maxima of the hydrodynamic coefficient curves.

The choice of the heave mode for demonstration of this method was dictated by the fact that the required coefficients were available. It is expected that generation of coefficients by the solution of the hierarchy of integral equations will be more useful in horizontal modes of motion. There are two reasons for this: one, there is only a leading order term available analytically for the damping function in these modes; and two, irregular frequency effects are more severe in horizontal modes. To find the coefficients, the computer code necessary for the solution of the rigid-lid problem with its right-hand-side forcing as shown in equations (5.10) through (5.14) can be adapted from typical frequency-domain, panel-method codes.

THE IMPULSE RESPONSE FUNTION FOR A TLP

To demonstrate the use of TIMIT for a complicated body, the impulse response function was calculated for a TLP. This body was chosen because there are extensive frequency-domain results available in Korsmeyer, Lee, Newman and Sclavounos (1988), and Jefferys (1987). The latter reference has caused some concern in the offshore community about the accuracy of first-order hydrodynamic coefficient calculations for complicated bodies [see also Section 4]. This is because the multitude of results it reports, which were produced by panel-method approaches to the solution of the boundary integral equation and also a finite-fluid-element method for solving Laplace's equation directly,

are in very poor agreement. Here we will show that this time-domain solution from TIMIT , and the frequency-domain program WAMIT (Dept. of Ocean Eng. 1988) are in excellent agreement. The TLP consists of six vertical columns arranged in a rectangle and connected at their bases by horizontal pontoons. A quadrant of one of the models of the body is shown in Figure 6-11.

The impulse response function for the TLP is shown in Figure 6-12 for two models one of 820 and one of 1652 panels. These results are experimental in that this was the first complicated body analyzed by TIMIT , so there was some doubt as to the number of panels, the size of the time increment, and the total length of time history required. However, experience with simple bodies was used as a guide with good results. The body models were those used for the frequency-domain analysis by WAMIT, and as such were not ideally suited to time-domain analysis. The difference being that for time-domain analysis a cosine spacing (as the free surface is approached) of the cylinder panel size would provide considerably better results for the same numerical effort.

The TLP analysis has demonstrated a shortcoming in the application of large-time asymptotics so useful for simple bodies. The problem is that at large time, the impulse response function of the TLP is not montonically approaching zero, but is oscillating with attenuating amplitude. Presumably some of this oscillation is the effect of irregular frequencies, but it is also due to the complicated interactions of the multiple large volume elements of this structure. Patching of the computed $L(t)$ to the monotonic asymptotic representation of $L(t)$ will eliminate physically relevant information along with the irregular frequency effects. Consequently the only available technique is to transform the record *as computed* to obtain the frequency-domain hydrodynamic coefficients. These are presented in Figure 6-13. Also plotted here are the results from WAMIT for a 1696-panel model. The agreement is excellent over the entire frequency range of interest, although some of the various peaks and troughs differ slightly. It may be argued that this agreement is expected, because the two programs share two important subroutines GEOM and RPAN, and common techniques for exploitation of body symmetries. However both codes can demonstrate excellent agreement to ana-

lytical results using only moderate numbers of panels, thus independently validating these geometry and Green function evaluation techniques, as well as their complimentary routines for the free-surface parts of the Green functions. In light of this, the agreement of the time- and frequency-domain results *for this complicated body* removes doubts that there are subtle errors in either code.

The benefit of the time-domain approach to frequency-domain hydrodynamic coefficients for this body is striking. Initially, the form of the coefficient functions in the frequency domain is unknown, so that the distribution of frequencies at which calculations should be performed cannot be ascertained *a priori* . However, one transient calculation with a coarsely discretized model of the body will efficiently reveal the frequency ranges where high accuracy calculations should be made in the frequency domain.

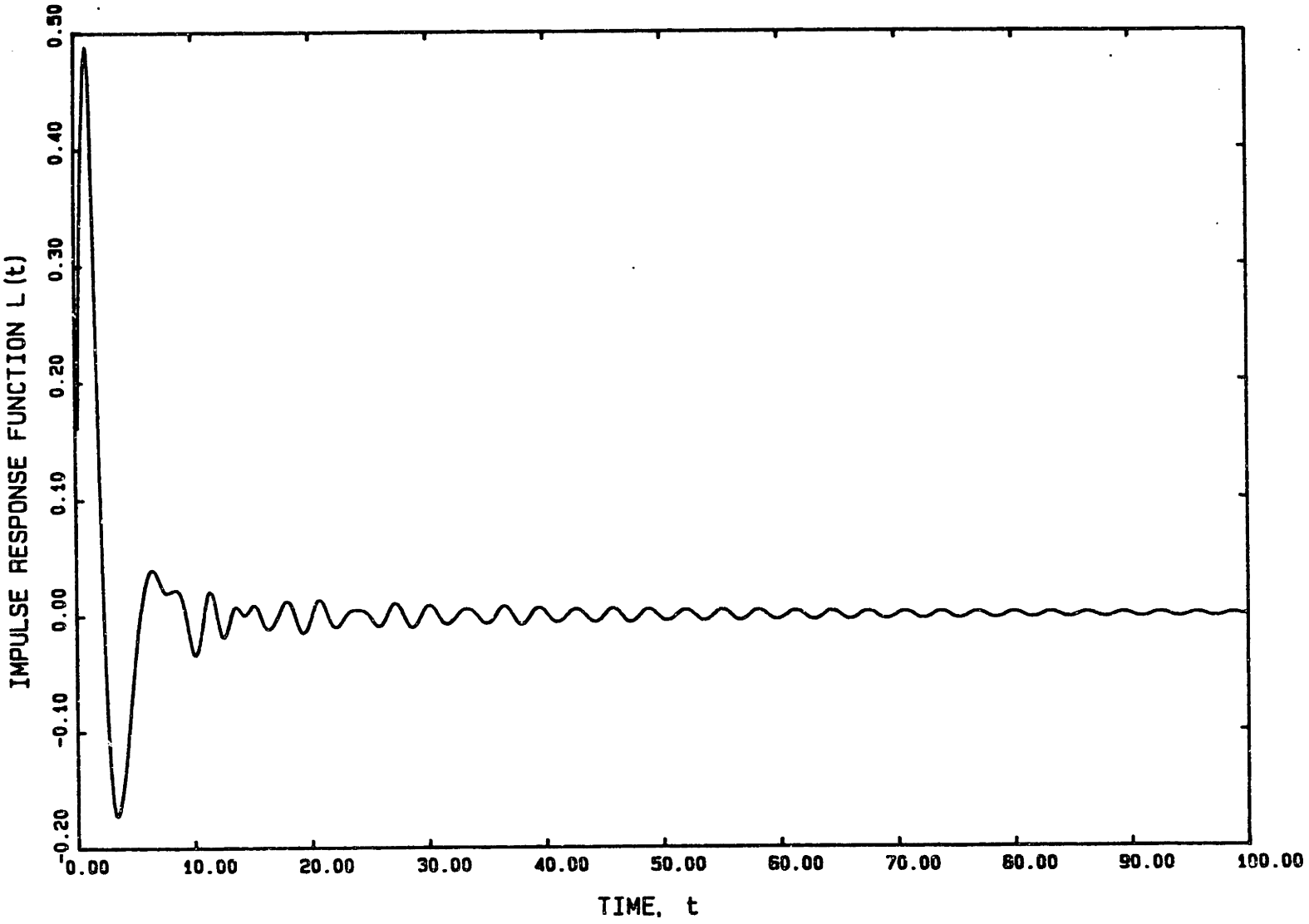

Figure 6-1. Swaying hemisphere; 64 panels, $\Delta t. = 0.2$ ——— .

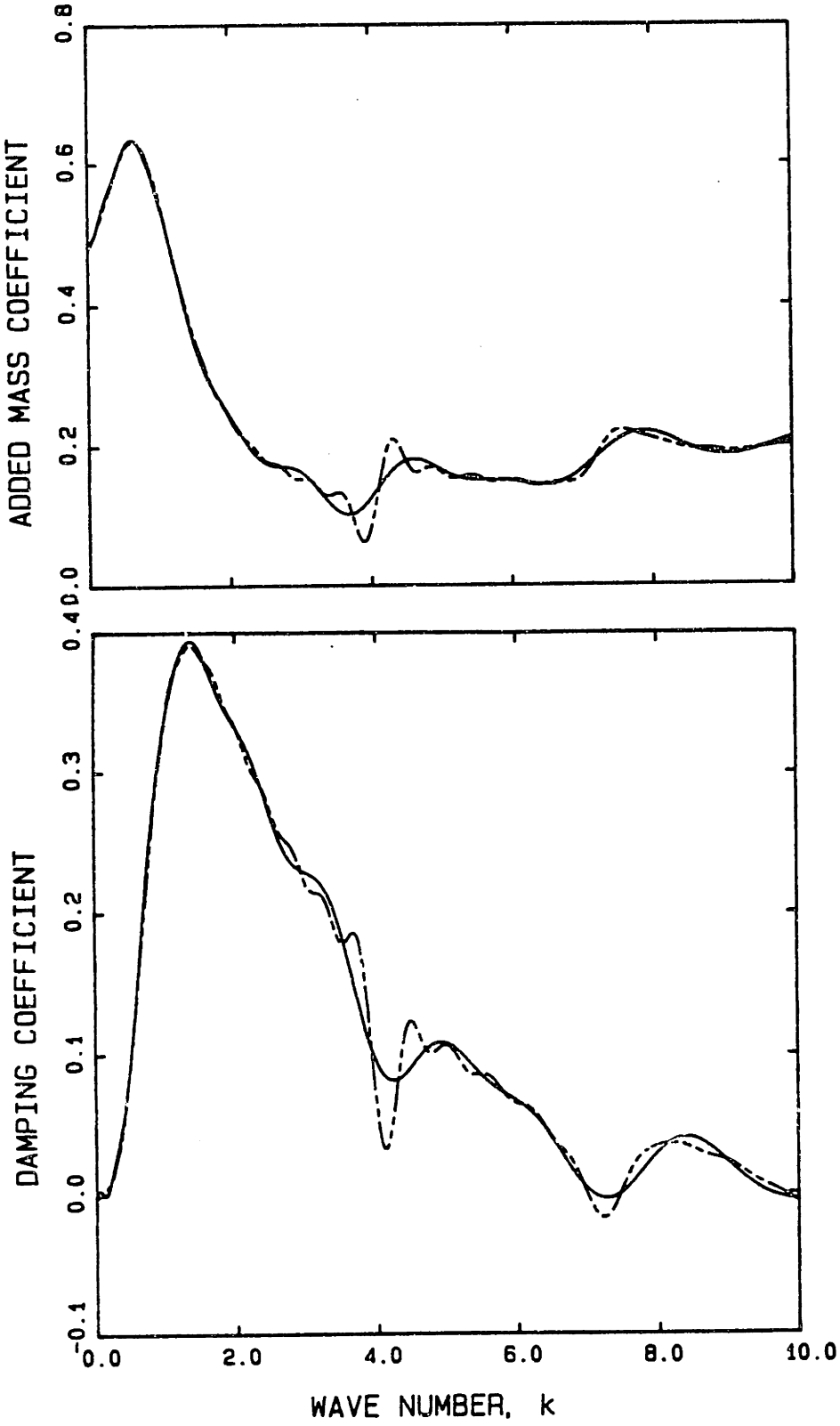

Figure 6-2. Swaying hemisphere; 64 panels, $\Delta t = 0.2$, truncated at $t = 20.$ ———— ; 64 panels, $\Delta t = 0.2$, truncated at $t = 50.$ — - - —. Coefficients are non-dimensionalized by the displaced fluid mass.

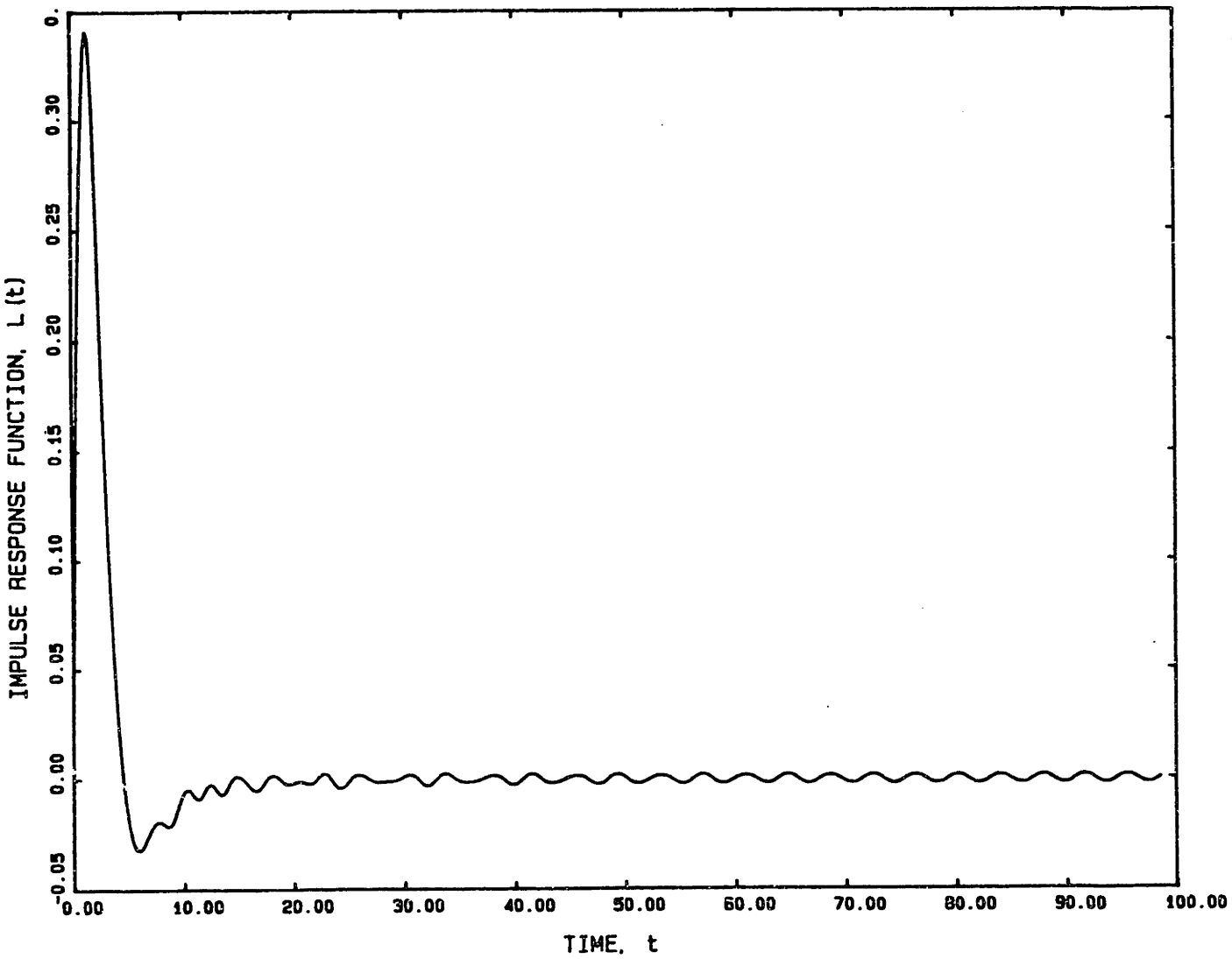

Figure 6-3. Heaving hemisphere; 64 panels, $\Delta t = 0.2$ ——— .

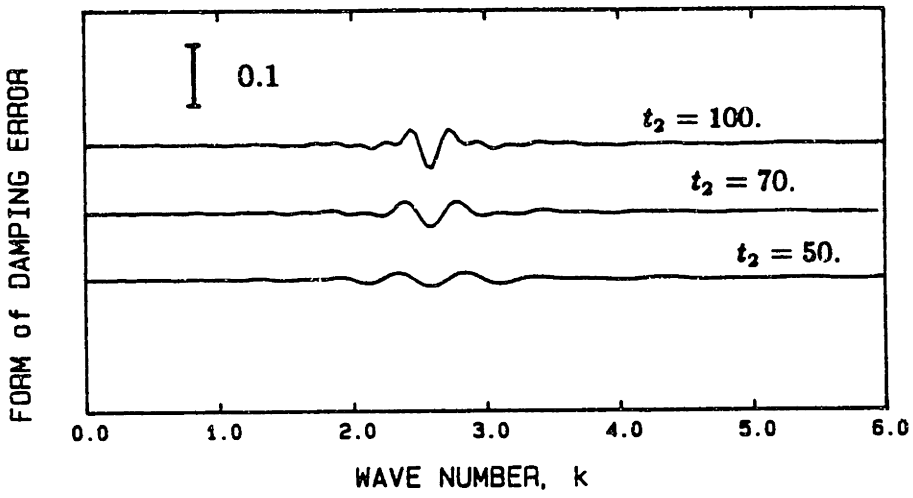

Figure 6-4 Form of the irregular frequency effect in the damping coefficient for the heaving hemisphere predicted by equation (6.2). In all cases, $t_1 = 30.$

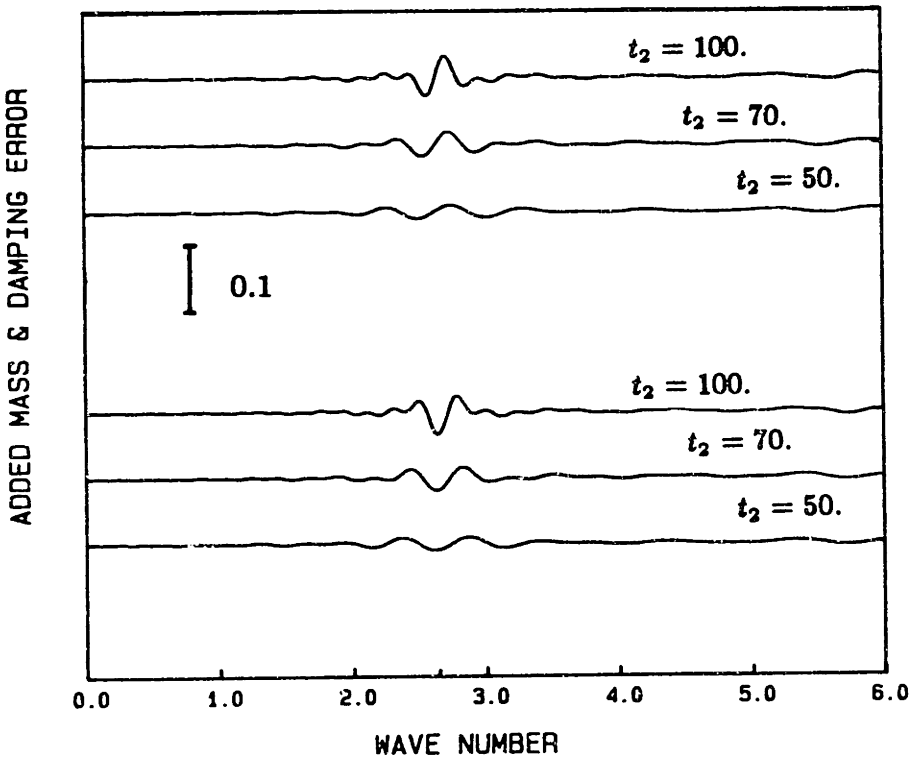

Figure 6-5. Numerical transform of the oscillatory tail from Figure 6-3. In all cases, $t_1 = 30.$

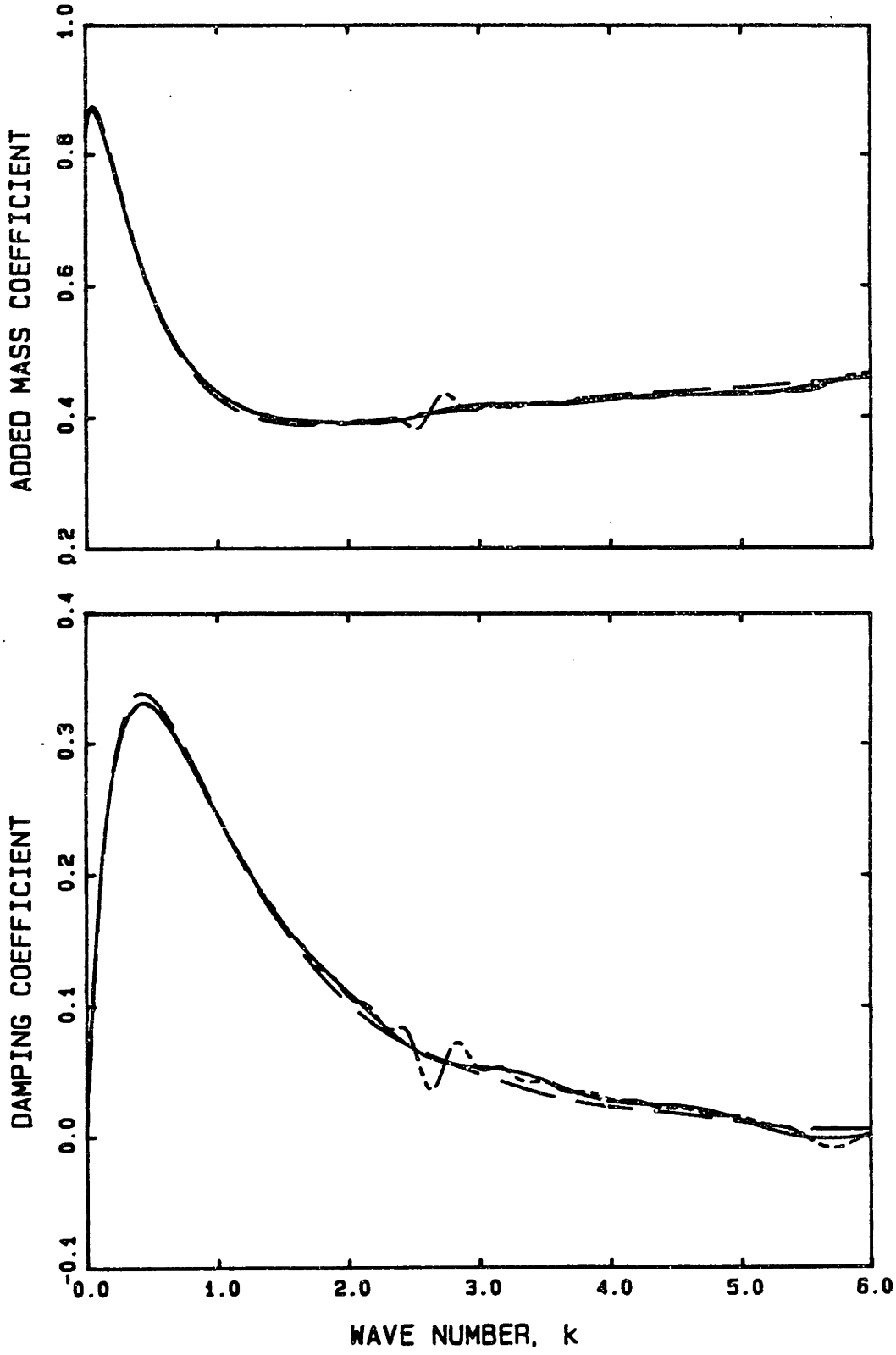

Figure 6-6. Heaving hemisphere; 64 panels, $\Delta t = 0.2$, truncated at $t = 20.$ ——— ; 64 panels, $\Delta t = 0.2$, truncated at $t = 50.$ — - - —; 256 panels, $\Delta t = 0.1$, truncated at $t = 20.$ — — . Coefficients are non-dimensionalized by the displaced fluid mass.

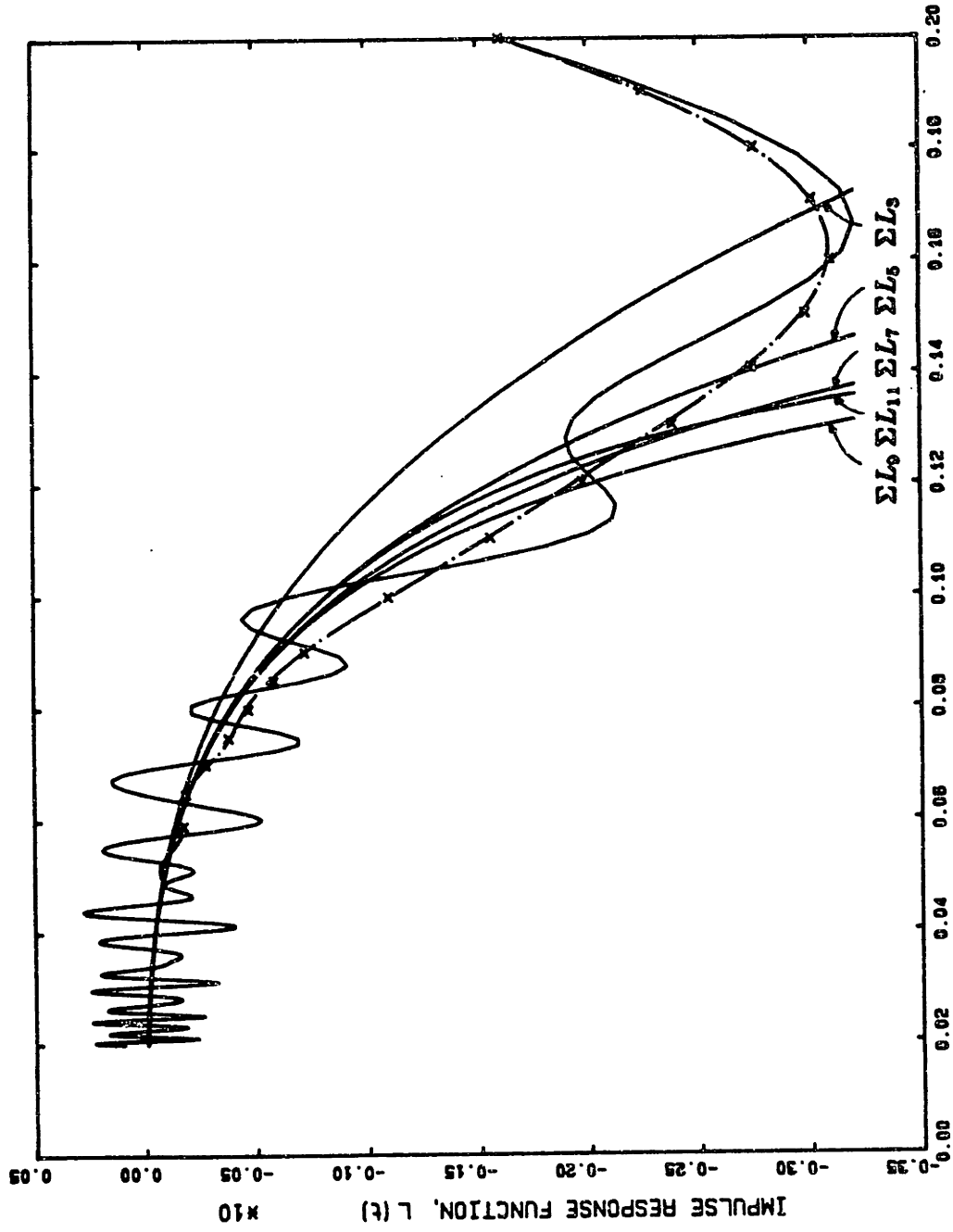

Figure 6-7. Heaving hemisphere; 64 panels, $\Delta t = 0.2$, ——— ; 1024 panels, $\Delta t = 0.075$, — - — ; 4608 panels, $\Delta t = 0.05$, × ; asymptotic results (labeled) to $O(t^{-11})$ ——— .

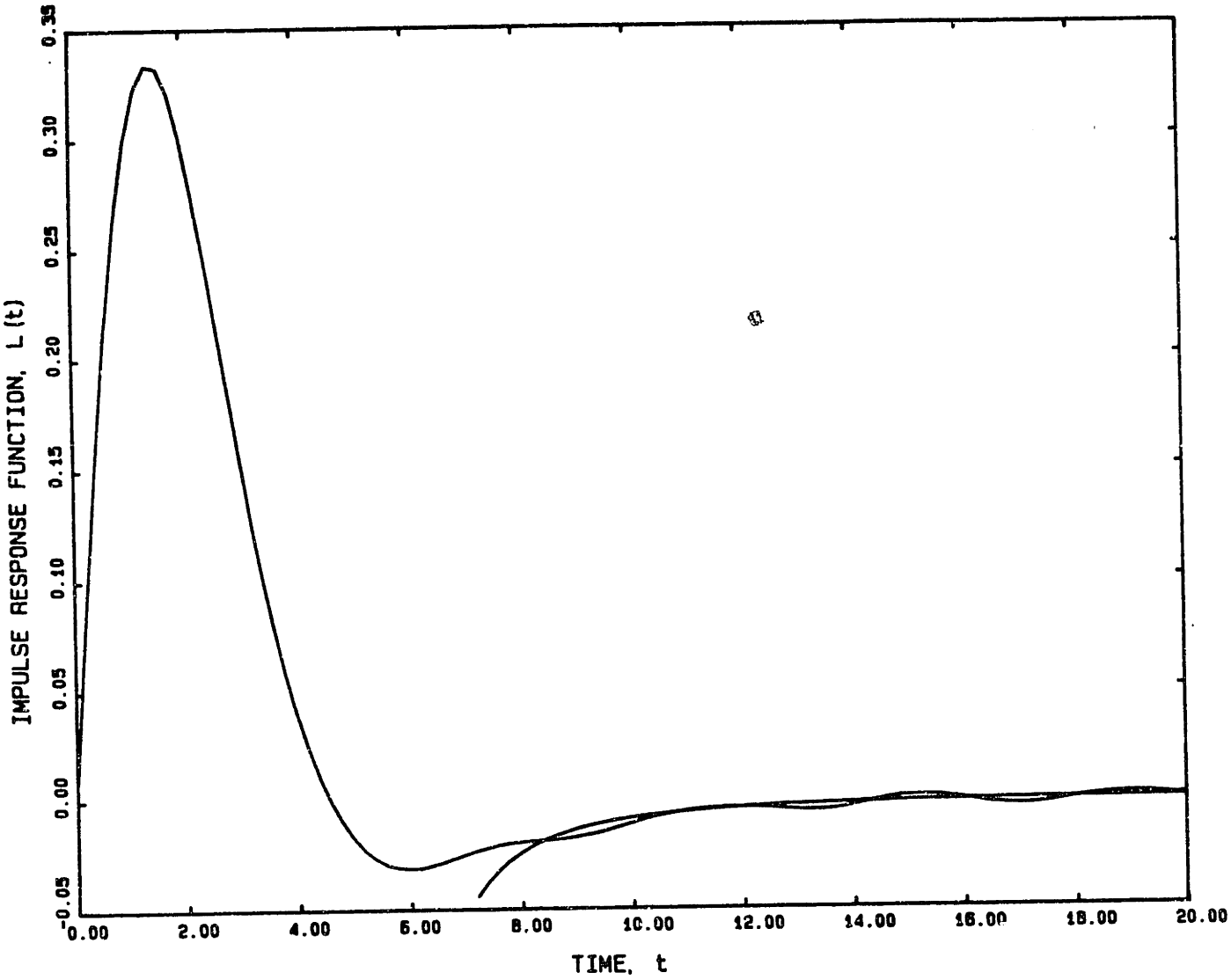

Figure 6-8. Heaving hemisphere; superposition of numerical results for 100 cosine distributed panels, $\Delta t = 0.2$ and the ΣL_o asymptotic result.

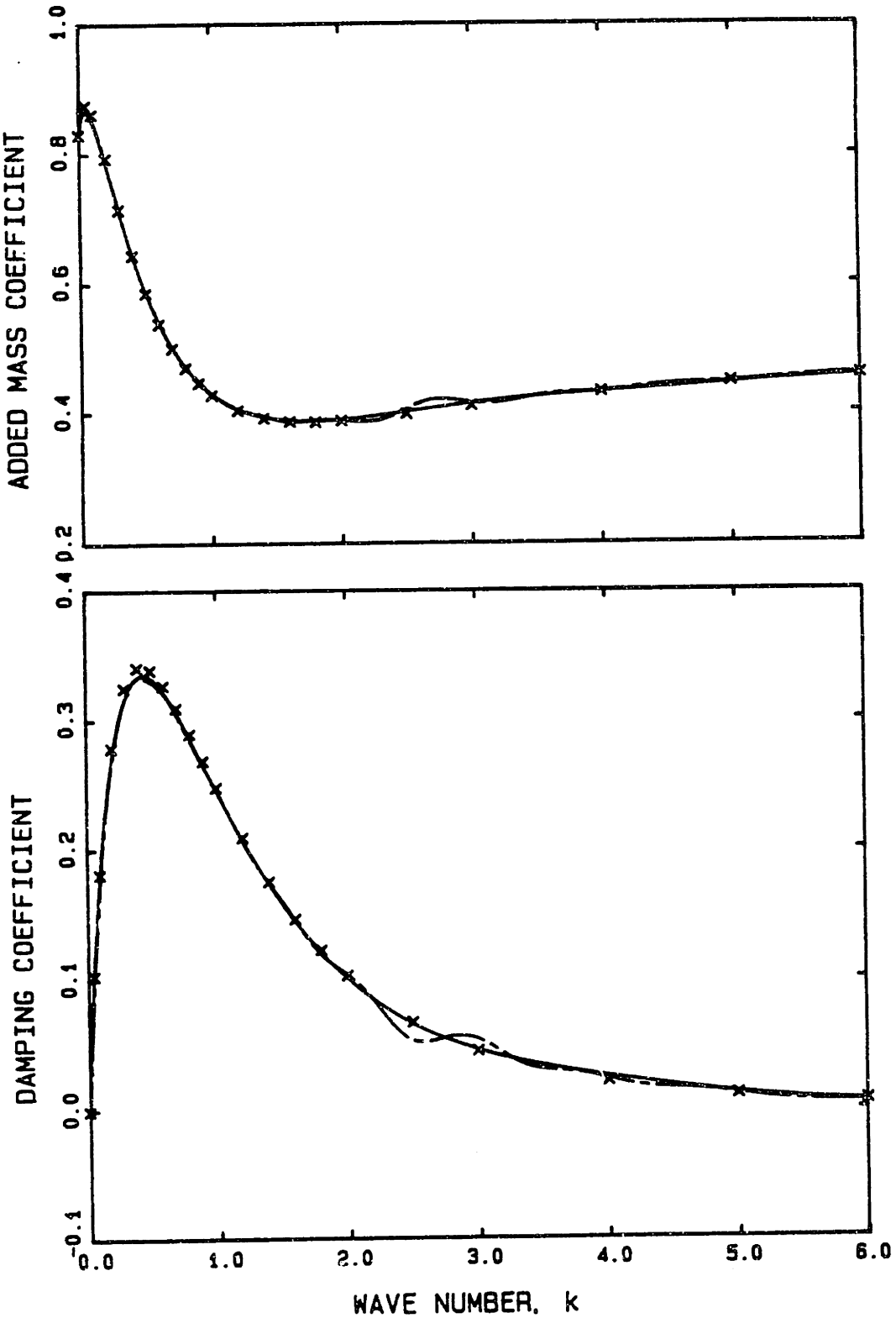

Figure 6-9. Heaving hemisphere. Transform of the patched functions of Figure 7 (numerical portion for 100 cosine distributed panels, $\Delta t = 0.2$) truncated at $t = 30$,——— ; the same model without patching trunctated at $t = 30$,— - —. Results from Hulme (1982) × . Coefficients are non-dimensionalized by the displaced fluid mass.

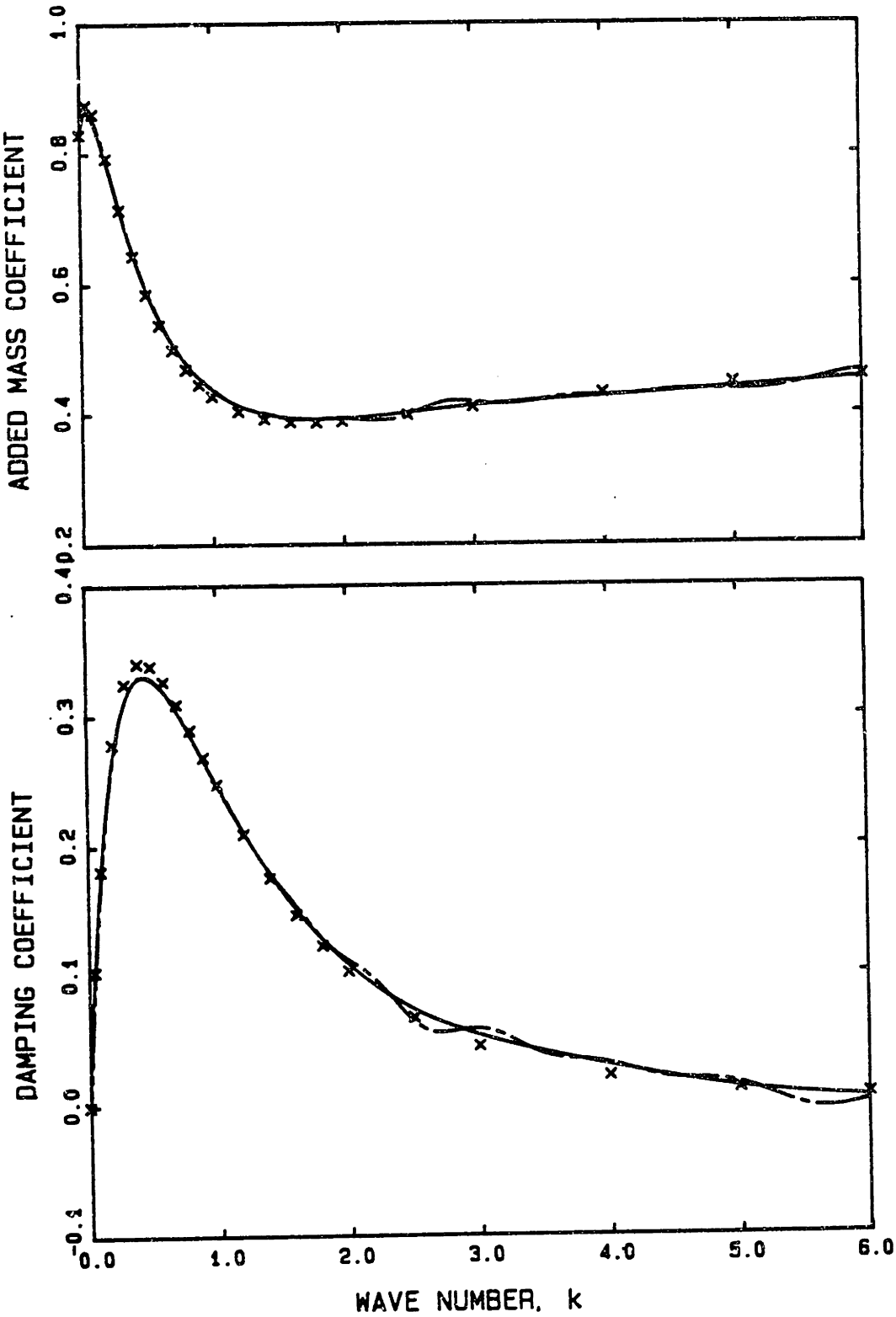

Figure 6-10. Heaving hemisphere. Transform of the patched functions: numerical portion for 64 panels, $\Delta t = 0.2$ truncated at $t = 30$,——— ; the same model without patching truncated at $t = 30$,— - —. Results from Hulme (1982) × . Coefficients are non-dimensionalized by the displaced fluid mass.

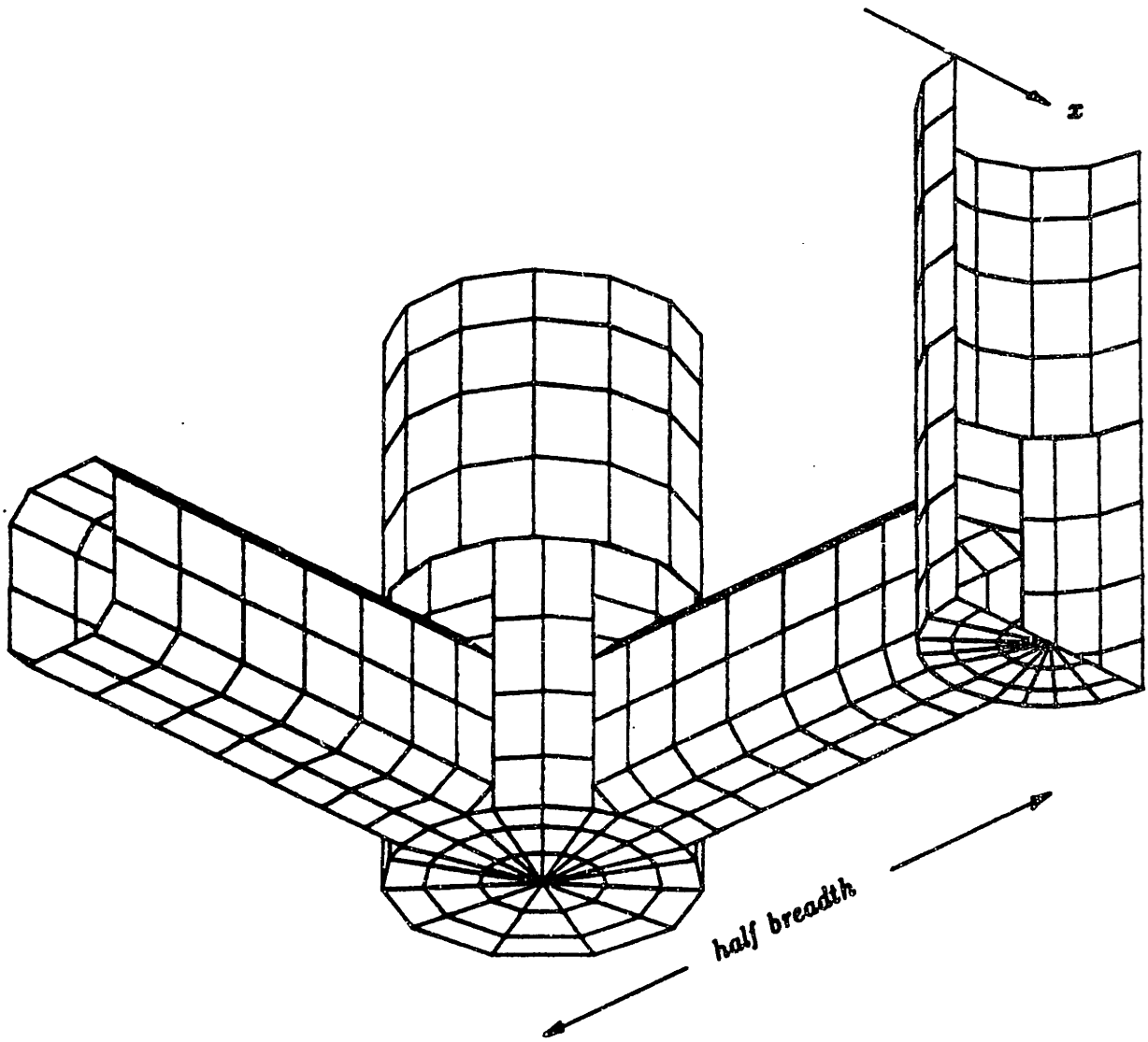

Figure 6-11. One quadrant of the Tension Leg Platform. The number of panels on the entire body is 1652.

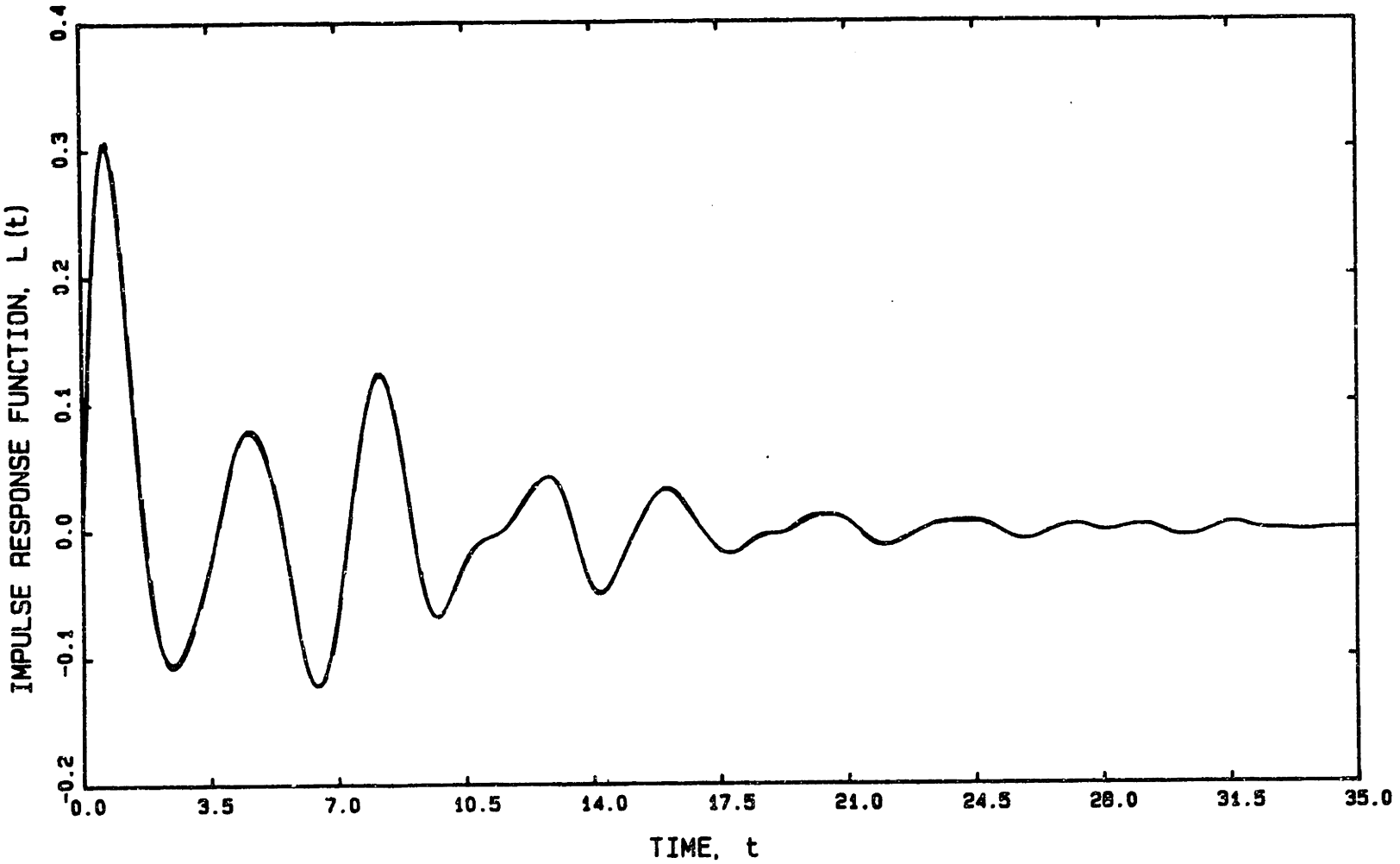

Figure 6-12. The Tension Leg Platform in surge. 820 panels, $\Delta t = 0.1$, ———; 1652 panels, $\Delta t = 0.1$, — — .

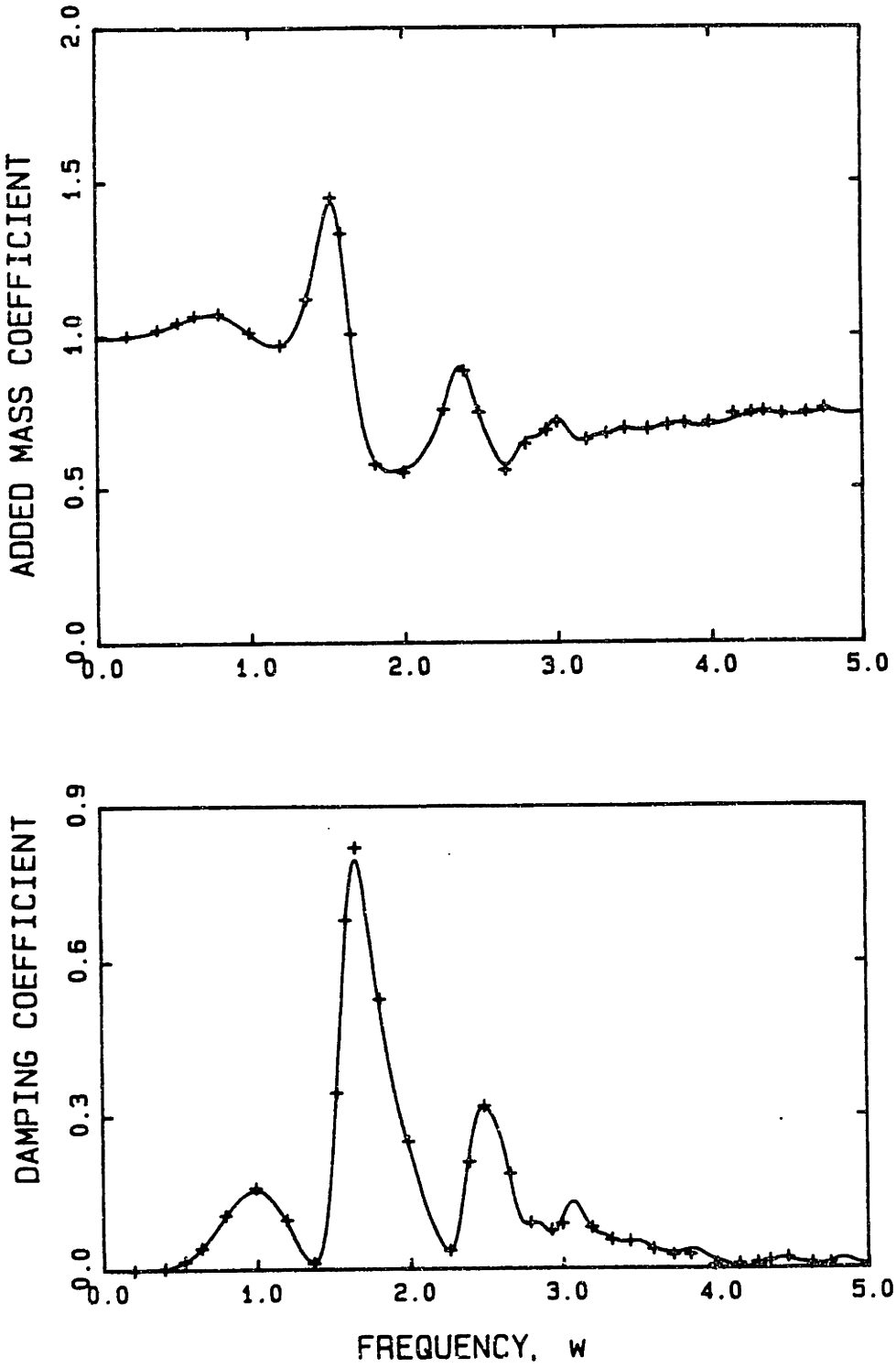

Figure 6-13. The Tension Leg Platform in surge. The Fourier transform of impulse response function of Figure 6-12. 820 panels, $\Delta t = 0.1$, truncated at $t = 35$. ——— ; Frequency domain results from WAMIT, 1696 panels, + . Coefficients are non-dimensionalized by acceleration due to gravity, fluid density and body half-breadth set equal to one.

7. THE SECOND-ORDER RADIATION PROBLEM

In the higher-order radiation problems we expect both analytical and numerical problems which are not encountered in the first-order problem. The field equation is unchanged to any order in ϵ because it is linear. However, complications do arise from the boundary conditions on the free surface and the body. Referring to equations (2.2) through (2.4), these boundary conditions are non-linear, and are to be satisfied on the exact positions of the surfaces. Consequently, their expansions contain terms which are products of the various potential and free-surface elevation derivatives, and terms from the Taylor expansions about the mean surface positions. In particular, at second order, the free-surface condition is no longer homogeneous but contains quadratic, 'forcing' terms from the $O(\epsilon)$ solution, as if there were an applied pressure on the free-surface. Also, the body boundary condition now contains the product of the $O(\epsilon)$ correction to the body normal vector with the gradient of the $O(\epsilon)$ solution.

In principle, the second-order problem may be recast as an integral equation to be solved on the body surface through the use of a Green function and Green's second identity. A second-order transient Green function has been derived by Wang (1987), but its numerical implimentation has not yet been accomplished. As a result, Green's second identity, when employed with the transient Green function for the first-order problem, (A.7), leads to an integral equation to be solved on the body surface, but with a right-hand side which contains an integral to be evaluated over the infinite free surface. This situation is no different from the frequency domain where various investigators have used the Green function for the first-order problem, and then used a combination of analysis and numerical methods to evaluate the free-surface integral. For an example of the method and survey of the progress in the frequency domain, see Kim (1988).

In a method which has been formulated, but not yet applied, Sclavounos (1987) has derived Green functions for second-order frequency-domain problems (both radiation and diffraction). These functions remove the free-surface integral, when used with Green's second identity, and have the desired property of shifting the computational burden of the problem from one which is particular to the body, to one which generally addresses all body geometries. If efficient subroutines are written for the second-order frequency-domain and time-domain Green functions, the second-order problem may be computationally more straightforward than it is now. However, at present, we will have to be content with an integral equation for the $O(\epsilon^2)$ potential which will contain an integral to be evaluated on the free surface.

As was done in Section 3 for the first-order problem, the expansions for $\phi(\vec{x},t)$ and $\varsigma(x,y,t)$, equations (2.8) and (2.9), and the right-hand side of the body boundary condition, are inserted in the exact problem statement, equations (2.1) through (2.7) to allow the separation at $O(\epsilon^2)$ of the linear problem statement for the potential $\phi^{(2)}(\vec{x},t)$. The boundary conditions are to be satisfied on the initial body position, S_B and the quiescent free surface, S_F. Recall that the problem is normalized by setting the acceleration due to gravity, fluid density, and a body dimension equal to one. As usual, in the following equations we will omit functional arguments where the context makes them unnecessary. We consider the same radiation problem as discussed at first-order, that is, the body velocity may be arbitrary so long as it is initiated in a Heaviside manner at $t = 0$. $\phi^{(2)}(\vec{x},t)$ satisfies:

$$\nabla^2\phi^{(2)}(\vec{x},t) = 0 \qquad \text{in the fluid domain,} \tag{7.1}$$

$$\varsigma^{(2)} + \phi_t^{(2)} = \frac{-1}{2}\left[(\phi_x^{(1)})^2 + (\phi_y^{(1)})^2 + (\phi_z^{(1)})^2\right] - \varsigma^{(1)}\phi_{tz}^{(1)} \qquad \text{on } S_F, \tag{7.2}$$

$$\varsigma_t^{(2)} - \phi_z^{(2)} = \varsigma^{(1)}\phi_{zz}^{(1)} - \varsigma_x^{(1)}\phi_x^{(1)} - \varsigma_y^{(1)}\phi_y^{(1)} \qquad \text{on } S_F, \tag{7.3}$$

where the last two equations may be combined to give a single free-surface condition containing the second derivative of the potential with respect to time:

$$\phi_{tt}^{(2)} + \phi_z^{(2)} = \mathcal{H}^{(2)} \qquad \text{on } S_F, \tag{7.4}$$

where the second-order, free-surface inhomogeneity $\mathcal{H}^{(2)}$ is defined as:

$$\mathcal{H}^{(2)}(x,y,0,t) = -\frac{\partial}{\partial t}\left[(\phi_x^{(1)})^2 + (\phi_y^{(1)})^2 + (\phi_z^{(1)})^2\right] + \phi_t^{(1)}\frac{\partial}{\partial z}\left(\phi_{tt}^{(1)} + \phi_z^{(1)}\right). \tag{7.5}$$

$$\phi_n^{(2)} = \mathcal{B}^{(2)} \qquad t > 0 \qquad \text{on } S_B, \tag{7.6}$$

where the second-order body boundary inhomogeneity $\mathcal{B}^{(2)}$ is defined by Ogilvie (1983) for the general body undergoing general motion, and is defined in Section 9 for the specific case we examine.

$$\phi^{(2)}, \vec{\nabla}\phi^{(2)}, \phi_t^{(2)} \quad \text{are uniformly bounded on } S_\infty, \text{ for } t \text{ finite.} \tag{7.7}$$

Equation (2.7) leads directly to an initial condition on $\phi^{(2)}(\vec{x},t)$, and use of the $O(\epsilon^2)$ dynamic free-surface condition (7.2), with the initial condition (2.6), gives the initial condition for $\phi_t^{(2)}(\vec{x},t)$ in terms of quantities known from the solution of the problem at $O(\epsilon)$. We have, then, the two initial conditions:

$$\phi^{(2)}(x,y,0,0^+) = 0, \tag{7.8}$$

and

$$\phi_t^{(2)}(x,y,0,0^+) = \mathcal{I}^{(2)}, \tag{7.9}$$

where the initial condition $\mathcal{I}^{(2)}$ is defined as:

$$\mathcal{I}^{(2)} = \frac{-1}{2}\left(\phi_z^{(1)}(x,y,0,0^+)\right)^2. \tag{7.10}$$

We employ Green's second identity with the time derivative of the unknown potential function $\phi_\tau^{(2)}(\vec{x},\tau)$ and the Green function $G(\vec{x};\vec{\xi},t-\tau)$ of the $O(\epsilon)$ problem defined in equation (A.7). The reason for using the Green function which satisfies the $O(\epsilon)$ free-surface condition is that while it does not eliminate all free-surface integrals, it does eliminate those which contain the unknown $\phi^{(2)}(\vec{x},t)$. If we use the same manipulations in this problem as were used in the first-order problem, and are detailed in the Appendix, the Fredholm-Volterra integral equation to be solved at second order contains a convolution on the free surface which involves the inhomogeniety of the free-surface condition. Specializing equation (A.16) for the second-order problem gives:

$$\begin{aligned}
2\pi\phi^{(2)}(\vec{x},t) + \iint_{S_B} d\vec{\xi}\,\phi^{(2)}(\vec{\xi},t)G_{n_\xi}^{(0)}(\vec{x};\vec{\xi}) \\
&+ \int_{0^+}^{t} d\tau \iint_{S_B} d\vec{\xi}\,\phi^{(2)}(\vec{\xi},\tau)G_{n_\xi t}^{(F)}(\vec{x};\vec{\xi},t-\tau) \\
&= \int_{0^+}^{t} d\tau \iint_{S_B} d\vec{\xi}\,B^{(2)}(\vec{\xi},\tau)G_t^{(F)}(\vec{x};\vec{\xi},t-\tau) \\
&+ \iint_{S_B} d\vec{\xi}\,B^{(2)}(\vec{\xi},t)G^{(0)}(\vec{x};\vec{\xi}) \\
&+ \int_{0^+}^{t} d\tau \iint_{S_F} d\vec{\xi}\,\mathcal{H}^{(2)}(\vec{\xi},\tau)G_t^{(F)}(\vec{x};\vec{\xi},t-\tau) \\
&- \frac{1}{2}\iint_{S_F} d\vec{\xi}\,G_t^{(F)}(\vec{x};\vec{\xi},t)\left(\phi_z^{(1)}(x,y,0,0^+)\right)^2.
\end{aligned} \tag{7.11}$$

As in the first-order problem, the Fredholm kernel is independent of time, and when the equation is discretized, the unknown potential does not appear inside the Volterra integral.

It is convenient to decompose the second-order potential into linearly superposable parts: one satisfiying the inhomgeneous free-surface condition (7.4) with a homgeneous body boundary condition, designated $\phi^{(2)F}$; and one satisfying the inhomogeneous body boundary condition (7.6) with a homogeneous free-surface condition, designated $\phi^{(2)B}$. That is

$$\phi^{(2)}(\vec{x},t) = \phi^{(2)B}(\vec{x},t) + \phi^{(2)F}(\vec{x},t). \tag{7.12}$$

Refering to equation (7.11) it is easy to see that the equation to be solved for $\phi^{(2)B}(\vec{x},t)$ is the same as the equation for $\phi^{(1)}(\vec{x},t)$, but with a more complicated right-hand side. We may expect some numerical difficulties in evaluating the gradients of $\phi^{(1)}(\vec{x},t)$, which are present in $\mathcal{B}^{(2)}$, on the body surface, particularly in the case of a general 3-D body. However the solution of the $\phi^{(2)B}(\vec{x},t)$ problem will still be easier than the solution of the problem for $\phi^{(2)F}(\vec{x},t)$, because in the latter we have the additional computational burden of quadrature on the free surface. This complication motivates the method discussed in the next section, in which it is shown that some of the difficulties associated with the $\phi^{(2)F}(\vec{x},t)$ problem may be mitigated by finding the unsteady second-order force directly. However, gradients of $\phi^{(1)}(\vec{x},t)$, which are present in $\mathcal{H}^{(2)}$, must still be computed, and free surface quadrature must still be performed. The numerical techniques used to solve these problems are discussed in Section 9.

8. THE SECOND-ORDER FORCE

The second-order force on a harmonically oscillated body has both steady and unsteady parts. The steady part, usually referred to as the drift force, is due entirely to quadratic contributions from first-order quantities. The unsteady part is due to both quadratic contributions of first-order quantities and the second-order potential as well. This latter part is the integration of the linear term in Bernoulli's equation over the initial position of the body.

In the frequency domain, there has not yet been a presentation of the complete second-order, three-dimensional, wave-body interaction problem, but in principal the radiation/diffraction decomposition at first order has a second-order analogue and second-order body motions as a result of second-order input may be computed. The state of art, at second order, in the offshore industry has been to use an approximation to the second-order potential which ignores, at least, the contribution from the free-surface integral, or to find the double-frequency exciting force without knowledge of the second-order potential. As explained by Ogilvie (1983), a body held fixed in a bi-chromatic wave field (ω_1, ω_2) experiences both sum- and difference-frequency, unsteady forces and these forces are dependent on both of the frequencies, not just their sum or difference. This implies that a complete solution of the diffraction problem covers all of the ω_1, ω_2-plane. Since this amount of computation has been considered prohibitive for general, three-dimensional bodies, the approximation of Newman (1974) utilizing the steady, time-average force in regular waves, to approximate the slowly-varying second-order force, has been embraced by most frequency-domain investigators.

Similarly in the time domain, we can calculate a second-order impulse response function, which requires two impulsive motions of the body and depends on the time interval

between them. However at present, we wish to investigate the numerical difficulties in the second-order problem in a less ambitious undertaking. We are interested in the portion of the unsteady, second-order force due to the second-order potential, on a body oscillated harmonically with frequency ω. As $t \to \infty$ the amplitude of this force should agree with the 2ω impedence force found in the frequency domain. All of the other parts of the second-force in the radiation problem are calculated from the first-order potential. Recall that the second-order potential has been decomposed into two linearly superposable parts, one forced by the inhomogeneity in the free-surface boundary condition $\phi^{(2)F}(\vec{x},t)$ and one forced by the inhomogeneity in the body boundary condition $\phi^{(2)B}(\vec{x},t)$. The unsteady second-order force $F^{(2)}(t)$, due to the second-order potential, has the decomposition then:

$$F^{(2)}(t) = F^{(2)B}(t) + F^{(2)F}(t), \tag{8.1}$$

We can calculate $F^{(2)}(t)$ without knowledge of the second-order potential $\phi^{(2)}(\vec{x},t)$. This has been demonstrated in the frequency domain by Faltinsen and Løken(1978), Lighthill (1979) and Molin (1979). Claims that the numerical effort is considerably less in these formulations are arguable. The fact is, that in either the second-order force computation or the solution of the second-order potential problem, there remains the task of integrating over the free surface, and both methods require the same number of evaluations of the Green function and its derivatives for field points on the free surface in the integrand. There are distinctions: for instance the second-order potential solution does require the solution of a linear system, but the overall numerical effort in both methods are of the same order. If the force calculation is not *markedly* more straightforward, why be concerned with this method when the second-order potential is a more useful quantity? [For instance, the second order potential allows the calculation of local pressure and wave run-up.] The answer is simply that the second-order force alone is useful, and the numerical procedure required for the determination of the second-order potential is an extension of that required for the calculation of the second-order force. In the time domain, both approaches share the numerical difficulty of the

evaluation of temporal and spatial derivatives of $\phi^{(1)}(\vec{x},t)$ on the free surface near the body.

The derivation of the formula for the transient second-order force, $F^{(2)}(t)$ parallels the analogous derivation in the frequency domain, in that we also use the artifice of an assisting potential. This is a potential which is not related to the physical flow for the body motion under study, but has a body boundary condition which allows the recovery of the definition of the hydrodynamic force from a term resulting from the application of Green's second identity.

The assisting potential is the first-order impulsive motion potential; we restate its definition for completeness:

$$\nabla^2 \phi^{(1)I}(\vec{x},t) = 0 \qquad \text{in } V \tag{8.2}$$

$$\phi^{(1)I} = \mathcal{B}^{(1)} \qquad t > 0 \qquad \text{on } S_B \tag{8.3}$$

where $\mathcal{B}^{(1)}(\vec{x})$ is defined by (3.11) for a non-rotative mode, for example, and is *not* time dependent.

$$\phi_{tt}^{(1)I} + \phi_z^{(1)I} = 0 \qquad \text{on } S_F \tag{8.4}$$

$$\phi^{(1)I}, \vec{\nabla}\phi^{(1)I}, \phi_t^{(1)I} \qquad \text{are uniformly bounded on } S_\infty, \text{ for } t \text{ finite} \tag{8.5}$$

$$\phi^{(1)I}(x,y,0,0^+) = 0 \tag{8.6}$$

$$\phi_t^{(1)I}(x,y,0,0^+) = 0. \tag{8.7}$$

The two second-order potentials, associated with the decomposition of the second-order force in (8.1) may be determined by the solution of the following two problems.

The second-order potential which satisfies the complete second-order free surface condition, but a homogeneous body boundary condition is the solution to:

$$\nabla^2 \phi^{(2)F}(\vec{x},t) = 0 \qquad \text{in } V \tag{8.8}$$

$$\phi^{(2)F} = 0 \qquad t > 0 \qquad \text{on } S_B \tag{8.9}$$

$$\phi_{tt}^{(2)F} + \phi_z^{(2)F} = \mathcal{H}^{(2)} \qquad \text{on } S_F \tag{8.10}$$

$$\phi^{(2)F}, \vec{\nabla}\phi^{(2)F}, \phi_t^{(2)F} \quad \text{are uniformly bounded on } S_\infty, \text{ for } t \text{ finite} \tag{8.11}$$

$$\phi^{(2)F}(x,y,0,0^+) = 0 \tag{8.12}$$

$$\phi_t^{(2)F}(x,y,0,0^+) = \frac{-1}{2}\left(\phi_z^{(1)}(x,y,0,0^+)\right)^2 \qquad \text{on } S_F. \tag{8.13}$$

where $\phi^{(1)}(\vec{x},t)$ is the first-order solution which corresponds to the second-order solution $\phi^{(2)}(\vec{x},t)$ and should not be confused with $\phi^{(1)I}(\vec{x},t)$.

The second-order potential which satisfies the complete second-order body boundary condition, but a homogeneous free-surface condition is the solution to:

$$\nabla^2 \phi^{(2)B}(\vec{x},t) = 0 \qquad \text{in } V \tag{8.14}$$

$$\phi^{(2)B} = \mathcal{B}^{(2)} \qquad t > 0 \qquad \text{on } S_B \tag{8.15}$$

$$\phi_{tt}^{(2)B} + \phi_z^{(2)B} = 0 \qquad \text{on } S_F \tag{8.16}$$

$$\phi^{(2)B}, \vec{\nabla}\phi^{(2)B}, \phi_t^{(2)B}, \quad \text{are uniformly bounded on } S_\infty, \text{ for } t \text{ finite} \tag{8.17}$$

$$\phi^{(2)B}(x,y,0,0^+) = 0 \tag{8.18}$$

$$\phi_t^{(2)B}(x,y,0,0^+) = 0. \tag{8.19}$$

We first derive the expression for $F^{(2)F}(t)$ by application of Green's second identity to $\phi_\tau^{(2)F}(\vec{x},\tau)$ and $\phi^{(1)I}(\vec{x},t-\tau)$. The volume integral vanishes because of equations (8.2) and (8.8); the surface intgral at S_∞ vanishes because of equations (8.5) and (8.11); and one term of the surface integral on S_B vanishes because of equation (8.9). In the remaining term of the integral on S_B, we may exploit the body boundary condition (8.3), and so we may write (with spatial arguments omitted for clarity):

$$\iint_{S_B} d\vec{\xi}\,\phi_\tau^{(2)F}(\tau)B^{(1)} = -\iint_{S_F} d\vec{\xi}\left[\phi_\tau^{(2)F}(\tau)\phi_n^{(1)I}(t-\tau) - \phi_{\tau n}^{(2)F}(\tau)\phi^{(1)I}(t-\tau)\right]. \tag{8.20}$$

From the free-surface condition, equation (8.4) we replace $\phi_n^{(1)I}(t)$ with $-\phi_{tt}^{(1)I}(t)$ and integrate both sides in time from $\tau = 0^+$ to $\tau = t$. Because of the Heaviside manner in which both potentials are initiated, the integration limits must be approached in a limiting sense from inside the range of integration. After integration by parts on the right-hand side we have:

$$\begin{aligned}\int_{0^+}^{t} d\tau \iint_{S_B} d\vec{\xi}\,\phi_\tau^{(2)F}(\tau)\,n = &-\int_{0^+}^{t} d\tau \iint_{S_F} d\vec{\xi}\,\phi_\tau^{(1)I}(t-\tau)[\phi_{\tau\tau}^{(2)F}(\tau) + \phi_n^{(2)F}(\tau)] \\ &- \iint_{S_F} d\vec{\xi}\,[-\phi_t^{(2)F}(0^+)\phi_t^{(1)I}(t) + \phi_n^{(2)F}(0^+)\phi^{(1)I}(t)],\end{aligned} \tag{8.21}$$

where we have used the initial conditions on $\phi^{(1)I}(\vec{x},t)$, (8.6) and (8.7) to eliminate terms. Since we have the left-hand side of the free-surface condition (8.10) in brackets inside the convolution, we may replace these terms which require knowlege of the second-order potential with the right-hand side of this condition which does not. Then

taking the partial derivative of equation (8.21) with respect to time t, we can recover the definition of the hydrodynamic force on the left-hand side:

$$F^{(2)F}(t) = \int_{0^+}^{t} d\tau \iint_{S_F} d\vec{\xi}\, \phi_{\tau t}^{(1)I}(t-\tau)\mathcal{H}^{(2)}(\tau) + \iint_{S_F} d\vec{\xi}\,[-\phi_t^{(2)F}(0^+)\phi_{tt}^{(1)I}(t) + \phi_n^{(2)F}(0^+)\phi_t^{(1)I}(t)]. \tag{8.22}$$

We can show that one of the terms in the second integral makes no contribution. By use of Green's second identity we may equate

$$\iint_{S_F} d\vec{\xi}\, \phi_n^{(2)F}(0^+)\phi_t^{(1)I}(t) = \iint_{S_F} d\vec{\xi}\, \phi^{(2)F}(0^+)\phi_{tn}^{(1)I}(t) + \iint_{S_B} d\vec{\xi}\,[\phi^{(2)F}(0^+)\phi_{tn}^{(1)I}(t) - \phi_n^{(2)F}(0^+)\phi_t^{(1)I}(t)], \tag{8.23}$$

but the right-hand side of this expression vanishes because $\phi^{(2)F}(0^+) = 0$ on S_F by equation (8.12), $\phi_{tn}^{(1)I}(t) = 0$ on S_B by equation (8.3) and $\phi_n^{(2)F}(0^+) = 0$ on S_B by equation (8.9). In the other term in the second integral, $\phi_t^{(2)F}(0^+)$ is specified by equation (8.13). So we have finally:

$$F^{(2)F}(t) = -\int_{0^+}^{t} d\tau \iint_{S_F} d\vec{\xi}\, \phi_{tt}^{(1)I}(t-\tau)\mathcal{H}^{(2)}(\tau) + \frac{1}{2}\iint_{S_F} d\vec{\xi}\, \phi_{tt}^{(1)I}(t)\left(\phi_z^{(1)H}(0^+)\right)^2. \tag{8.24}$$

We can follow a similar procedure to obtain an expression for the force on the body due to the second-order potential $\phi^{(2)B}(\vec{x},t)$. Again we apply Green's second identity, this time to $\phi_\tau^{(2)B}(\vec{x},\tau)$ and $\phi^{(1)I}(\vec{x},t-\tau)$. In this case, both contributions in the body surface integral remain, but because $\phi^{(2)B}(\vec{x},t)$ satisfies the homgeneous free-surface condition, the convolution on the free surface vanishes after the integration by parts [refer to equation (8.21)]. Using similar manipulations as in the derivation of $F^{(2)F}(t)$, we can recover the definition of $F^{(2)B}(t)$ from the integral on the body surface S_B and eliminate integrals on S_F. The final expression for the force due to $\phi^{(2)B}$ is:

$$F^{(2)B}(t) = -\int_{0^+}^{t} d\tau \iint_{S_B} d\vec{\xi}\, \phi_{tt}^{(1)I}(t-\tau) B^{(2)}(\tau) + \iint_{S_B} d\vec{\xi}\, \left[\phi^{(1)I}(0^+) B_t^{(2)}(t) - \phi_t^{(1)I}(0^+) B^{(2)}(t)\right]. \tag{8.25}$$

We expect that for a harmonically excited body, equations (8.24) and (8.25) will recover the equivalent frequency domain formulations as $t \to \infty$. We will demonstrate this for the expression for $F^{(2)F}(t)$, the method for the expression for $F^{(2)B}(t)$ is similar. Consider a body excited in a single mode of motion with frequency ω. In this case,

$$\mathcal{H}^{(2)} \to \Re\{he^{2i\omega_0 t}\} + H \qquad t \to \infty, \tag{8.26}$$

where H and h are not functions of time. As $t \to \infty$, we drop the transient terms, exchange the time and retarded time arguments, and extend the time intgration to $-\infty$, which we may do as $\phi^{(1)I}(t) = 0, t < 0$. Now we can write the force in Fourier convolution form:

$$F(t) = \Re\left\{\iint_{S_F} d\vec{\xi} \int_{-\infty}^{\infty} d\tau\, \phi_{\tau\tau}^{(1)I}(\tau) h e^{2i\omega_0(t-\tau)}\right\}. \tag{8.27}.$$

The Fourier convolution theorem states:

$$\int_{-\infty}^{\infty} d\tau\, f(t-\tau) g(\tau) = \frac{1}{2\pi} \int_{-\infty}^{\infty} d\omega\, e^{-i\omega t} f^*(\omega) g^*(\omega). \tag{8.28}$$

So we require the solution to:

$$h^*(\omega) = h \int_{-\infty}^{\infty} d\tau\, e^{2i\omega_0 t} e^{i\omega t}, \tag{8.29}$$

which is,

$$h^*(\omega) = 2\pi\, h\, \delta(\omega + 2\omega_0), \tag{8.30}$$

where δ signifies the Dirac function. We take the transform of $\phi_{\tau\tau}^{(1)I}$ formally, so that (8.27) may be written:

$$F(t) = \Re\left\{ \iint_{S_F} d\vec{\xi}\, h \int_{-\infty}^{\infty} d\omega\, \delta(\omega + 2\omega_0)\omega^2 \phi^*(\omega) e^{-i\omega t} \right\}. \tag{8.31}$$

The frequency integral is easily solved:

$$F(t) = 4\omega_0^2 \Re\left\{ \iint_{S_F} d\vec{\xi}\, h\phi^*(2\omega_0) e^{2i\omega_0 t} \right\}. \tag{8.32}$$

where $\phi^*(2\omega_0)$ is the solution to the Fourier transformed boundary value problem for $\phi^{(1)I}(t)$. For the real frequency-domain potential $\Phi(2\omega_0)$, $\phi^*(2\omega_0)$ is defined by:

$$\Phi(2\omega_0) = \Re\{\phi^* e^{2i\omega_0 t}\}; \tag{8.33}$$

and $\phi^*(2\omega_0)$ satisfies:

$$\nabla^2 \phi^* = 0 \qquad \text{in the fluid domain,} \tag{8.34}$$

$$\phi_n^*(2\omega_0) = -\frac{i}{2\omega_0} n_i, \tag{8.35}$$

$$\phi_z^*(2\omega_0) - 4\omega_0^2 \phi^*(2\omega_0) = 0 \qquad \text{on } S_F, \tag{8.36}$$

and an appropriate radiation condition. Since we usually write the frequency-domain body boundary condition $\phi(2\omega_0) = n_i$, this more familiar frequency domain potential is related to $\phi^*(2\omega_0)$ by:

$$\phi^*(2\omega_0) = -\frac{i}{2\omega_0} \phi(2\omega_0). \tag{8.37}$$

And finally, the frequency domain expression for the double-frequency hydrodynamic force on a radiating body excited at frequency ω_0 is:

$$f(2\omega_0) = 2i\omega_0 \iint_{S_F} d\vec{\xi}\, h\phi(2\omega_0), \tag{8.38}$$

or for the force as a function of time:

$$F(t) = \Re\{f(2\omega_0)e^{(2i\omega_0 t)}\}. \tag{8.39}$$

So we have recovered the expected frequency-domain expression for the double-frequency force in terms of an assisiting potential, $\phi(2\omega_0)$, and the unsteady portion of the inhomogeneity of the frequency-domain free-surface boundary condition, h.

9. NUMERICAL ASPECTS OF THE SECOND-ORDER PROBLEM

OVERVIEW

To investigate the numerical complexity of the second-order transient problem we would like to compute the second-order unsteady force on a right-circular cylinder heaving at frequency ω. Strictly speaking, the quadratures in the second-order force computations are not panel methods, while the solution of the second-order problem itself is. In the second-order force computation, the panel method effects are entirely contained in the precision of the known, first-order solution, and the quadratures are undertaken in any fashion which is compatible with a specification of this potential at discrete points on the body and free surface. In the second-order potential problem, the panel approximation of the body is present, as at first order, on the left-hand side, in addition to fact that the right-hand side contains the same first-order panel method effects as are present in the force computations. While this is an important distinction, the model problem of computing the second-order force on a heaving axisymmetric cylinder does contain the computation and quadrature of first-order quantities on the free surface, and we anticipate that this is the primary difficulty in either the second-order potential or force problems.

The initial task in solving this axisymmetric problem is the solution of the first-order problem with sufficient accuracy. We expect that the level of accuracy required for first-order solutions, when they are used to determine integrated quantities such as hydrodynamic coefficients, will no longer be sufficient when these solutions are to be used to construct the right-hand sides of either the second-order potential or force problems. This means a possible increase in computational effort at first order if second-order computation is anticipated. Since this model problem is axisymmetric,

the ability of T[MIT to exploit multiple planes of symmetry is used to reduce the computational burden. A wedge of the axisymmetric body is discretized by a strip of panels which is one panel wide, then the influence coefficients are calculated by sufficient reflections of the source or field points to characterize the entire body. This technique tends to retain the general body effect on the accuracy of computations because panels are of finite dimension in two directions.

The codes which evaluate $F^{(2)B}(t)$ and $F^{(2)F}(t)$ use the the first-order potential on the wedge of the body as input. In the case of $F^{(2)B}(t)$, the potential on the body alone is sufficient to evaluate the force, but for $F^{(2)F}(t)$, Green's second identity must be used with the potential on the body to find the potential at field points on the free surface. The first-order potential on the body will be assumed to be piece-wise constant over panels and time-steps, which means that the quadrature follows a mid-point rule in space and the trapazoid rule in time.

Computations are performed in a circular cylindrical coordinate system defined relative to the Cartesian system shown in figure 2-1: the z-axis is coincident with the z-axis of the Cartesian system, r is parallel to the x-y-plane, and angle θ is measured from the positive x portion of the x-z-plane. We examine the numerical details of the computation of $F^{(2)B}(t)$ and $F^{(2)F}(t)$ in the remainder of this section.

THE COMPUTATION OF $F^{(2)B}(t)$

The difficulties associated with the calculation of $F^{(2)B}(t)$ are not well modeled by computations on a right-circular cylinder. We expect that the computation of gradients of the potential may be numerically difficult on a body surface, but for this body in heave, most of the terms in $\mathcal{B}^{(2)}(t)$ vanish, apparently simplifying the computation. However, the submerged corner of this body causes a non-integral singularity in $\mathcal{B}^{(2)}(t)$, so the discussion of numerical aspects of the computation of $F^{(2)B}(t)$ will be limited.

The computation of $F^{(2)B}(t)$ is made by equation (8.25) in which $\mathcal{B}^{(2)}(\vec{r},t)$ may be specialized for a heaving body to:

$$B^{(2)}(\vec{r},t) = \dot{\xi}_3(t)\,\vec{n}(\vec{r}) \cdot \frac{\partial}{\partial z}\vec{\nabla}\phi^{(1)H}(\vec{r},t), \tag{9.1}$$

where $\dot{\xi}(t)$ is the magnitude of the heave velocity. In the case of the right-circular cylinder, with unit heave at frequency ω started impulsively:

$$B^{(2)}(t) = \cos\omega t\ \phi_{zz}^{(1)H} \quad t > 0 \qquad \text{on } S_{BOT}, \tag{9.2}$$

where $\phi^{(1)H}(\vec{r},t)$ is the solution to the first-order problem of impulsively-started oscillation at frequency ω, and S_{BOT} is the initial position of the bottom surface of the cylinder. The discrete form of equation (8.25) is:

$$\begin{aligned} F_M^{(2)B} = &- \sum_{m=0}^{M}{}' \Delta t \sum_{j=1}^{N_{BOT}} S_j (\phi_{tt}^{(1)I})_{j,m} B_{j,M-m}^{(2)} \\ &+ \sum_{j=1}^{N_{BOT}} S_j \left[\phi_{j,0}^{(1)I} (B_t^{(2)})_{j,M} - (\phi_t^{(1)I})_{j,0} B_{j,M}^{(2)}\right] \\ &M = 0, 1 \ldots M_T, \end{aligned} \tag{9.3}$$

where S_j is the area of the j^{th} body-panel, N_{BOT} is the number of panels on the bottom of the cylinder, and the prime indicates that weights of one-half apply when $m = 0$ or $m = M$. So equation (9.3) is merely a convolution and quadrature over the bottom of the cylinder of a second derivative of a first-order quantity. In the case of a body with a corner, such as the right-circular cylinder we are studying, or the TLP discussed in Section 6 (Figure 6-11), $\phi_{zz}^{(1)H}$ has a non-integrable singularity at the intersection of the bottom and side. This may be appreciated by examination of the analytic solution for two-dimensional flow around a corner with included angle of $3\pi/2$ (see equation (10.11) *et seq*). For bodies without such a discontinuity of slope, we do not expect difficulties in evaluating $B^{(2)}(t)$. In Figure 9-1, the value of the potential accros the bottom of the cylinder is presented for a few representative times. The assisting and harmonic potentials are shown, and in both cases, the results for several

discretizations are indistinguishable indicating that convergence for the potential do... not require excessive numerical effort on deeply submerged portions of the body. These functions are well behaved, monotonic in fact, and amenable to finite difference. As will be shown in the next sub-section, difficulties arise in the evaluation of first-order quantities for field points close to the edge of a panel or close to the free-surface-body intersection. In the computation of $F^{(2)B}(t)$, though, the quadrature is on the body only, and all calculations may be performed at the panel centroids. In addition, for wall-sided bodies in modes of motion for which $\mathcal{B}^{(2)}(t)$ vanishes on panels near the free surface, the free-surface difficulties will not be important either.

THE COMPUTATION OF $F^{(2)F}(t)$

In the computation of $F^{(2)F}(t)$, first-order quantities are required at field points which are not at the panel centroids. In this case, there are computational difficulties in the evaluation of first-order quantities on the free surface close to and at the free-surface-body intersection. The discrete form of equation (8.24) is:

$$\begin{aligned} F_M^{(2)F} &= -\sum_{m=0}^{M-1}{}' \Delta t \sum_{j=1}^{N_F} S_j (\phi_{tt}^{(1)I})_{j,m} \mathcal{H}_{j,M-m}^{(2)} \\ &\quad + \frac{1}{2}\sum_{j=1}^{N_F} S_j (\phi_{tt}^{(1)I})_{j,m} (\phi_z^{(1)H})_{j,0} \\ &\quad M = 0, 1 \ldots M_T , \end{aligned} \tag{9.4}$$

where S_j is the area of the j^{th} body-panel, N_F is the number of quadrature points on the free surface, and the prime indicates that weights of one-half apply when $m = 0$ or $m = M$. For an axisymmetric problem, $\mathcal{H}^{(2)}(t)$ may be written:

$$\mathcal{H}^{(2)}(t) = -\frac{\partial}{\partial t}\left[(\phi_r^{(1)H})^2 + (\phi_z^{(1)H})^2\right] + \phi_t^{(1)H}\frac{\partial}{\partial z}(\phi_{tt}^{(1)H} + \phi_z^{(1)H}). \tag{9.5}$$

The temporal and spatial derivatives of $\phi^{(1)H}(\vec{r},t)$ which constitute $\mathcal{H}^{(2)}(t)$ are computed either by Green's second identity or by finite difference. The potential $\phi^{(1)H}(t)$ and the derivatives of the potentials: $\phi_x^{(1)H}$ and $\phi_x^{(1)I}$ (which are $\phi_{xt}^{(1)H}$ and $\phi_{xt}^{(1)I}$, respectively, on the free surface) are computed by extensions of the Green formulations (3.9) and (3.12). When these expressions are used with the field point *not* on the body, the factor 2π is changed to 4π, as is well understood in potential theory, and the integral equation becomes a method for the computation of the potential at any point in the fluid by quadrature of the known solution and the Green function (and its derivatives) over the body surface. If a temporal or spatial derivative of a first-order potential is required at a field point, then the partial derivative of the integral formulation is taken and this derivative may be calculated directly with knowledge of the potential itself on the body. For instance, in the general body case of finding $\phi_x^{(1)}(\vec{x},t)$ on the free surface, equation (3.9) becomes:

$$4\pi\phi_x^{(1)}(\vec{x},t) + \iint_{S_B} d\vec{\xi}\,\phi^{(1)}(\vec{\xi},t)G_{n_\xi x}^{(0)}(\vec{x};\vec{\xi}) + \int_{0^+}^{t} d\tau \iint_{S_B} d\vec{\xi}\,\phi^{(1)}(\vec{\xi},\tau)G_{n_\xi xt}^{(F)}(\vec{x};\vec{\xi},t-\tau)$$
$$= \int_{0^+}^{t} d\tau \iint_{S_B} d\vec{\xi}\,B^{(1)}(\vec{\xi},\tau)G_{xt}^{(F)}(\vec{x};\vec{\xi},t-\tau)$$
$$+ \iint_{S_B} d\vec{\xi}\,B^{(1)}(\vec{\xi},t)G_x^{(0)}(\vec{x};\vec{\xi}). \tag{9.6}$$

Ideally, the computations for the z-derivatives by this method should be as accurate as computations for the potentials themselves. However, in the extension to TGREEN, added to calculate second spatial derivatives, machine precision could not be maintained within the structure of an ascending series matched to an asymptotic approximation. The precision of $G_{n_\xi xt}^{(F)}$ can be as poor as four significant digits near the matching point.

The remaining terms in $\mathcal{H}^{(2)}(t)$ are found by finite difference. In the particular case of $\phi_{xx}^{(1)H}$, this is found from the finite difference results $\phi_r^{(1)H}$ and $\phi_{rr}^{(1)H}$ through Laplace's equation. The other terms are straightforward.

The extent of the free surface over which the quadrature in (9.4) must be performed is

surprisingly limited. The relevant physical parameter for the transient disturbance is t^2/r, as in the Cauchy-Poisson problem. Therefore analysis of the wave-front at large r for any finite t is equivalent to analysis at finite r as $t \to 0$. At $t = 0$, the flow in the heave mode is like a vertical dipole, hence $\phi_z^{(1)I} \sim 1/r^3$ in the plane $z = 0$. When we convolve the functions $\phi_z^{(1)I}$ and $\mathcal{H}^{(2)}$, the integrand is characterized by the product of this small-time behavior of $\phi_z^{(1)I}$ and the steady-state limit of $\mathcal{H}^{(2)}$. This latter function is quadratic in the potential and so has its radial dependence dictated by conservation of energy to be $1/r$. Therefore the integrand in the free-surface quadrature decays in space like $1/r^4$, ensuring that the effort required for this computation will be quite reasonable.

The Green's second identity approach to free-surface quantities contains some numerical limitations which require discussion in detail. These difficulties limit the computation of an accurate solution more so than any complications due to the finite difference approach. In effect, if the quantities $\phi^{(1)H}$, $\phi_z^{(1)H}$, and $\phi_z^{(1)I}$ on the free surface could be found to arbitrary accuracy simply by refinement of the body model and improvement in the precision of the computation of $G^{(F)}$, then the finite difference results could be found to the requisite accuracy through numerical effort. However, we find that very close to the body there are computational errors which may not be surmountable by numerical effort alone. In the remainder of the section we examine the behavior of the quantities $\phi^{(1)H}$, $\phi_z^{(1)H}$ and $\phi_z^{(1)I}$ in the region close to the free-surface-body intersection.

At the free-surface-body intersection we calculate $\phi^{(1)H}$, $\phi_z^{(1)H}$ and $\phi_z^{(1)I}$ by extrapolating a finite difference calculation up the side of the cylinder. We present these results in Figure 9-2. The evidence indicates that the convergence is slow for these quantities and is more dependent on azimuthal panel dimension than on vertical panel dimension. This is important because a 'ring' Green function method would not reveal effects due to the type of panelling which is required for general bodies. The last part of Figure 9-2 shows $\phi_z^{(1)I}$ tending to a non-zero constant at large time even for the finest azimuthal discretization. This is indicative of the slow convergence, for the potential

must tend to zero on the free surface at large time, because the Green function tends to the rigid-lid Green function as $t \to \infty$. Figure 9-3 shows the values of these functions close to the body as calculated by the Green formulation. As there is no singularity at the intersection point the behavior shown is not expected. Further, the trend of the functions is more sensitive to panel aspect ratio than it is to the fineness of the discretization, leading to the conclusion that this is numerical error. The probable cause is that the field points are too close to the edge of a panel upon which the potential is assumed to be constant. This problem may be surmountable in the present panel method, if it can be shown that we may interpolate through this region using reliable free-surface quantities further from the body and quantities at the free-surface-body intersection found by extrapolation of quantities at the panel centroids.

Because the problems which we solve for $\phi^{(1)I}$ and $\phi^{(1)H}$ are initiated impulsively, all wavelengths are present on the free surface for all time. This is reflected by the fact that $G^{(F)}$ contains increasingly short waves as $t/(R')^{1/2} \to \infty$. This is apparent in Figure 4-1, where the frequency at which $R'\,G^{(F)}$ is oscillating is a constant when plotted on a t^2/R' axis. Since the limit $t/(R')^{1/2} \to \infty$ means either very large time or very small distance, we can expect increasingly short waves close to the free-surface-body intersection as $t \to \infty$. This is irrespective of any singularity which may or may not be present at this point due to a confluence of disparate boundary and initial conditions in the first-order problem. Note that in the case of the heaving cylinder, the body boundary condition at the free-surface-body intersection, $\phi_r^{(1)} = 0$, is compatible with the initial condition, $\phi^{(1)} = 0$, on the free surface. This compatibility is not present in the sway mode.

Outside of this region we find the expected short waves radiating from the body. These are indicated by the plot of $\phi_s^{(1)I}$ at successive time steps in Figure 9-4. These waves may be resolved at shorter and shorter wavelengths by a greater density of field points on the free-surface. In Figure 9-5 we see these short waves in the context of the entire free-surface disturbance. The presence of these short waves with significant amplitude is suspect. Because of exponential decay of wave effects, we expect that panels near the

free surface are important in the accurate computation of the short wave components of the free-surface disturbance. But the plot of $\phi_z^{(1)I}$, found by finite differencing $\phi^{(1)I}$ at the panel centroids, shown in Figure 9-2 suggests that the value of the potential at the centroid of the panel closest to the free surface is not accurately computed. Its effect on an integrated quantity, such as the hydrodynamic coefficients may be negligible, but in providing the forcing for the short wave lengths it is critical. $\phi_z^{(1)I}$ has been used as the function to present these various phenomena because it is indicative of problems with any of the derivatives of $\phi^{(1)H}$, and it explicitly appears in the integrand of equation (9.4) (as $\phi_{zt}^{(1)I}$).

Due to the difficulties in computations close to the body and the lack of a closed form solution to this problem for comparison, we cannot be confident of the accuracy of first-order quantities on the free surface. Before equation (9.4) can be used to compute the unsteady second-order force $F^{(2)F}(t)$, we need to justify interpolation through the region where the method breaks down, and we need to assess the importance of resolving short waves. In pursuit of these goals we take a new approach to free-surface quantities, applicable to the right-circular cylinder, which allows evaluation of free-surface quantities arbitrarily close to the body.

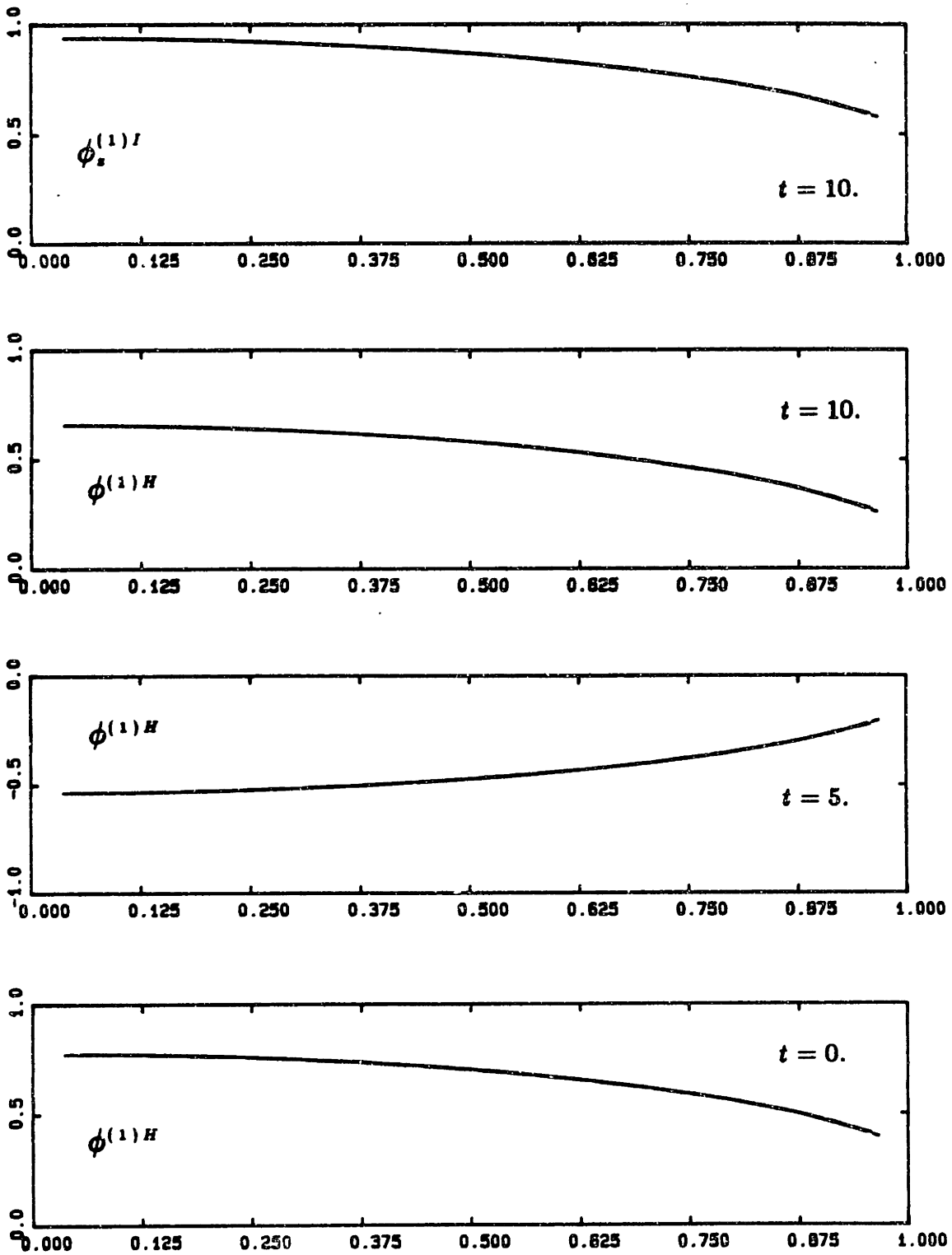

Figure 9-1. The heaving cylinder. $\phi^{(1)H}(\vec{r},t)$ for $\omega = 1.2533$ and $\phi^{(1)I}(\vec{r},t)$ on the cylinder bottom. All results are for $\Delta t = 0.1$. Panelling: 24x36 ——— ; 24x72 — — ; and 36x54 — - — ; (bottom & side x azimuthal).

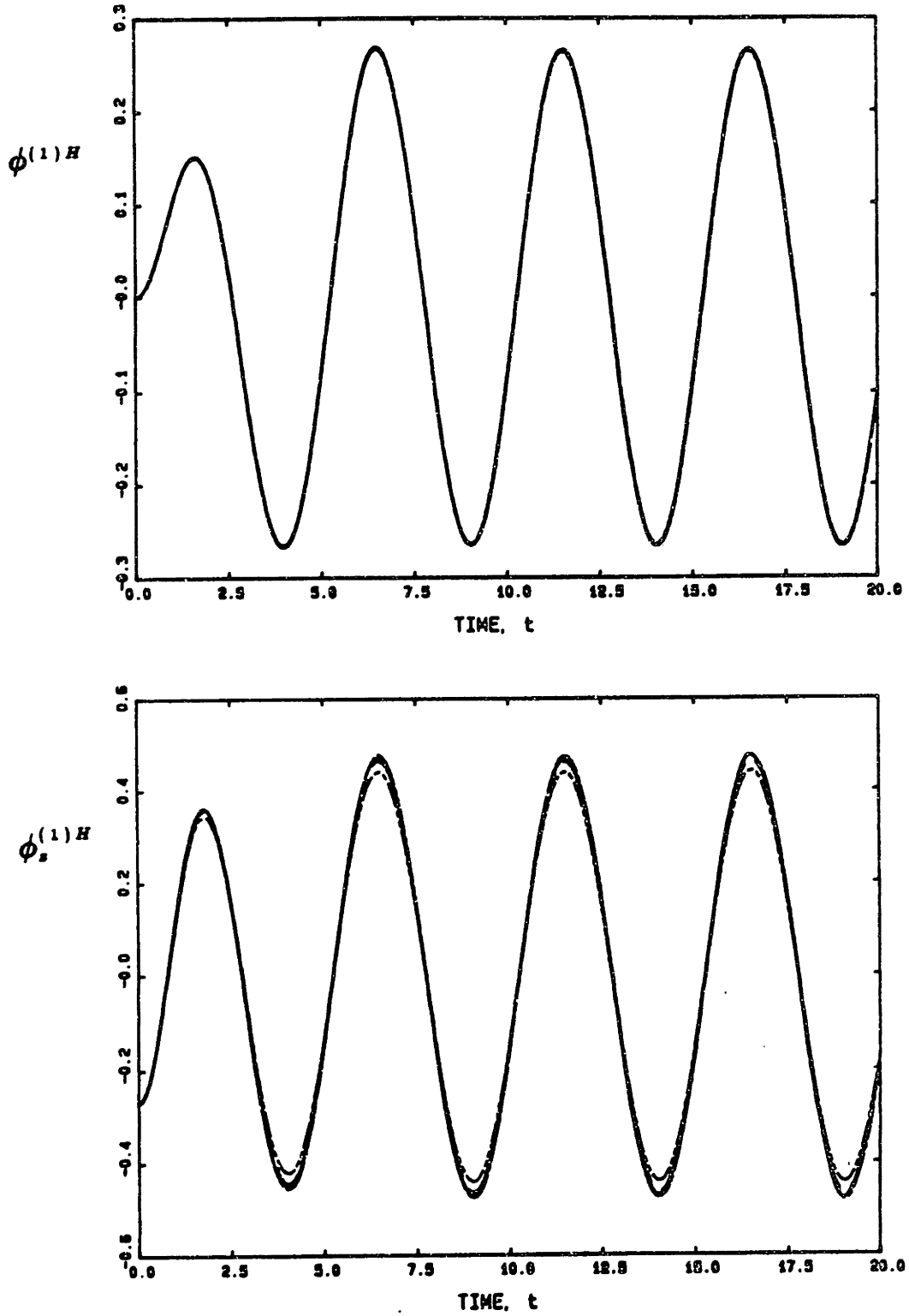

Figure 9-2. The heaving cylinder. $\phi^{(1)H}(\vec{r},t)$ and $\phi_s^{(1)H}(\vec{r},t)$ at the body and free-surface intersection, for $\omega = 1.2533$. All results are for $\Delta t = 0.1$. Panelling: **24x36** ——— ; **24x72** — — ; .**24x144** — · · — ; and **36x54** — · — ; (bottom & side x azimuthal). Continued on next page.

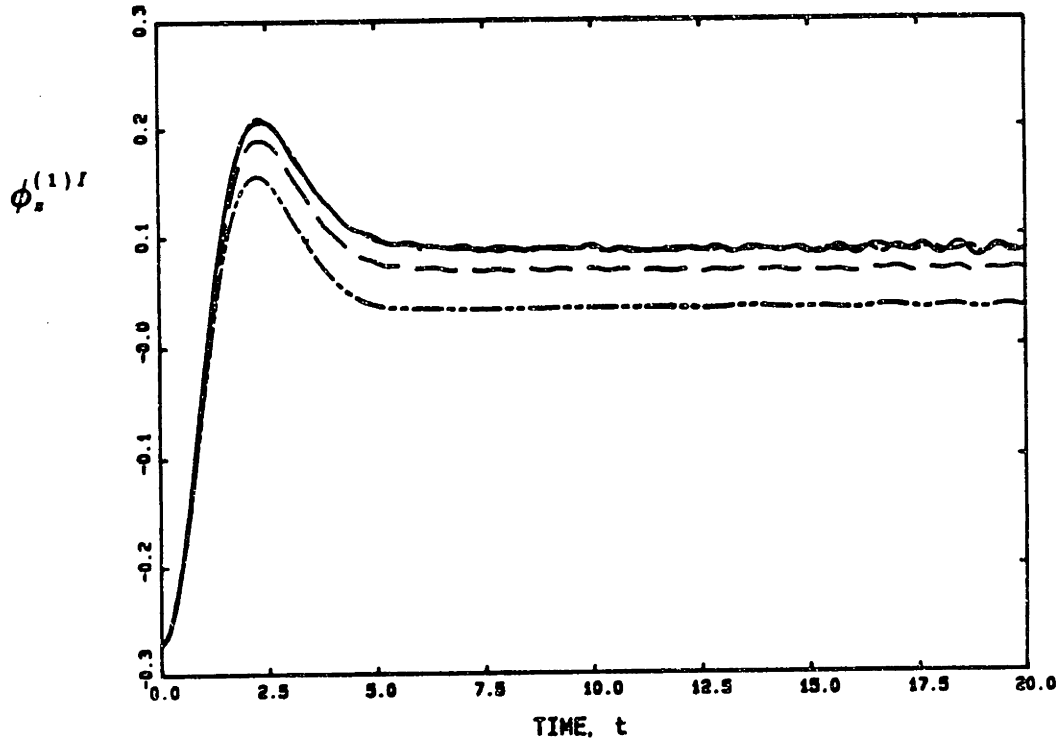

Figure 9-2 cont. The heaving cylinder. $\phi_s^{(1)I}(\vec{r},t)$ at the body and free-surface intersection. All results are for $\Delta t = 0.1$. Panelling: 24x36 ——— ; 24x72 — — ; 24x144 — - - —; and 36x54 — - — ; (bottom & side x azimuthal).

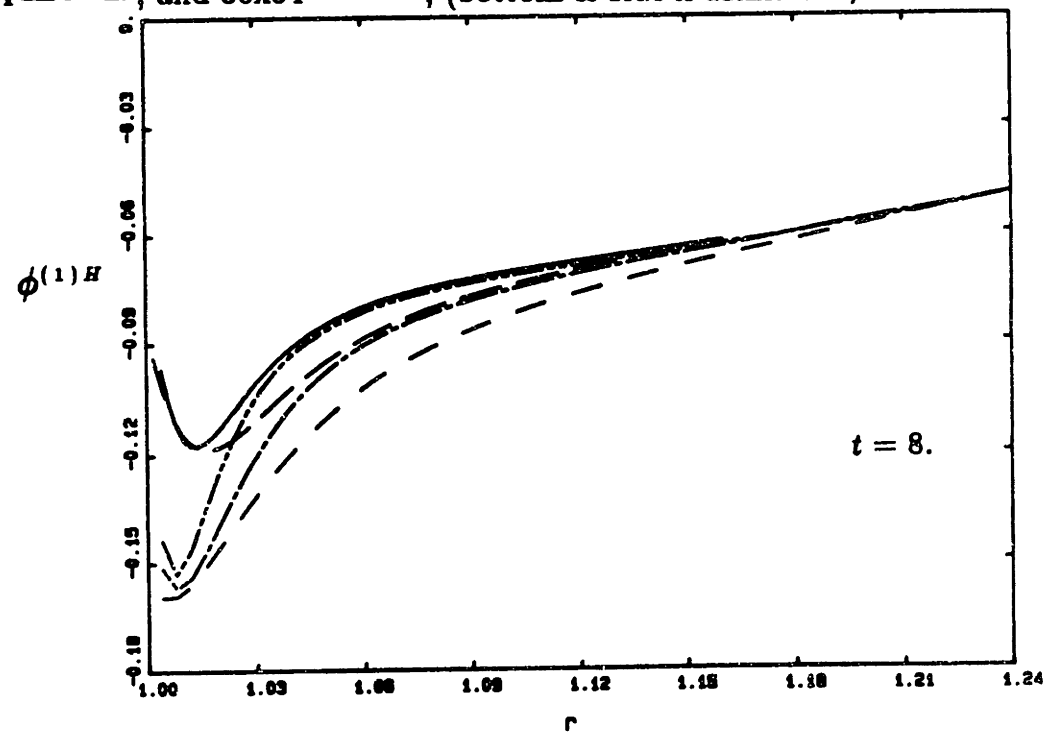

Figure 9-3. The heaving cylinder. $\phi^{(1)H}(\vec{r},t)$ on the free surface close to the body (r=1.0). All results are for $\Delta t = 0.1$. Panelling: 16x16 — — ; 16x24 — — ; 24x24 — - — ; 24x36 ——— ; and 36x36 — - - —; (bottom & side x azimuthal). Continued on next page.

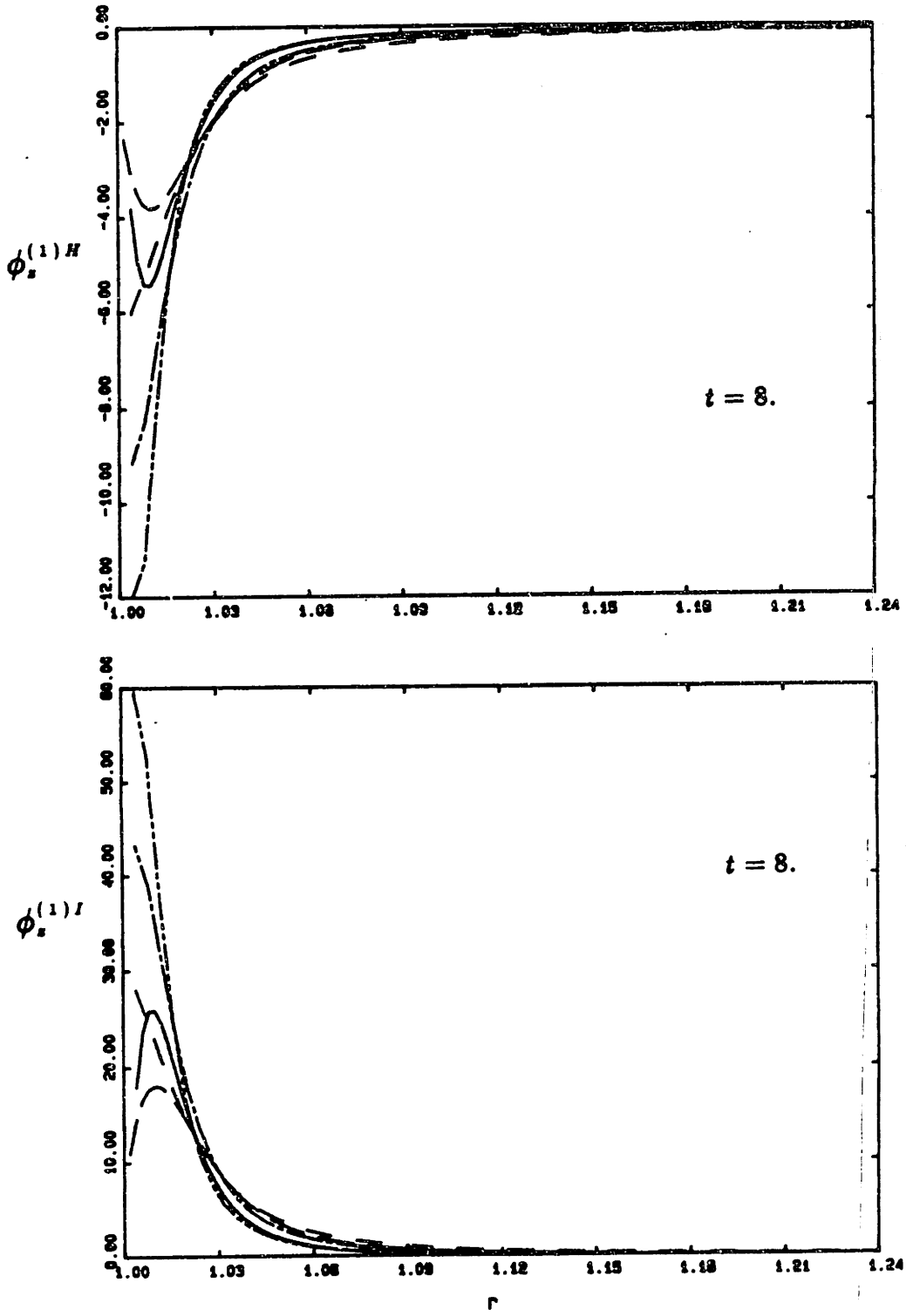

Figure 9-3 cont. The heaving cylinder. $\phi_z^{(1)H}(\vec{r},t)$ and $\phi_z^{(1)I}(\vec{r},t)$ on the free surface close to the body (r=1.0). All results are for $\Delta t = 0.1$. Panelling: 16x16 — — ; 16x24 —— —— ; 24x24 —·- - —; 24x36 ——— ; and 36x36 ——·——; (bottom & side x azimuthal).

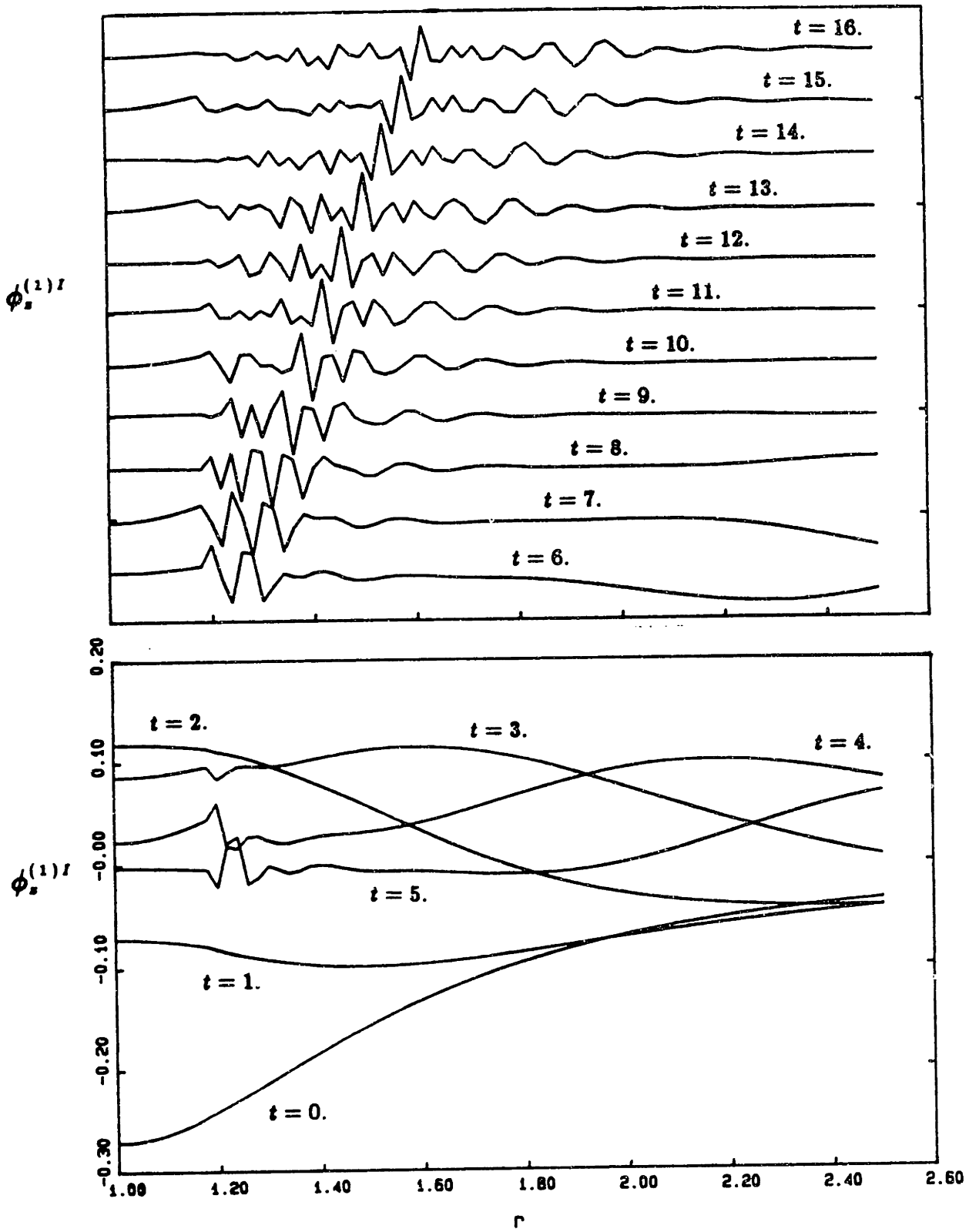

Figure 9-4. The heaving cylinder. $\phi_s^{(1)I}(\vec{r}, t)$ on the free surface in the region of short waves. $\Delta t = 0.1$ panelling: 24x36. The region close to the body (Figure 9-3) has been interpolated through.

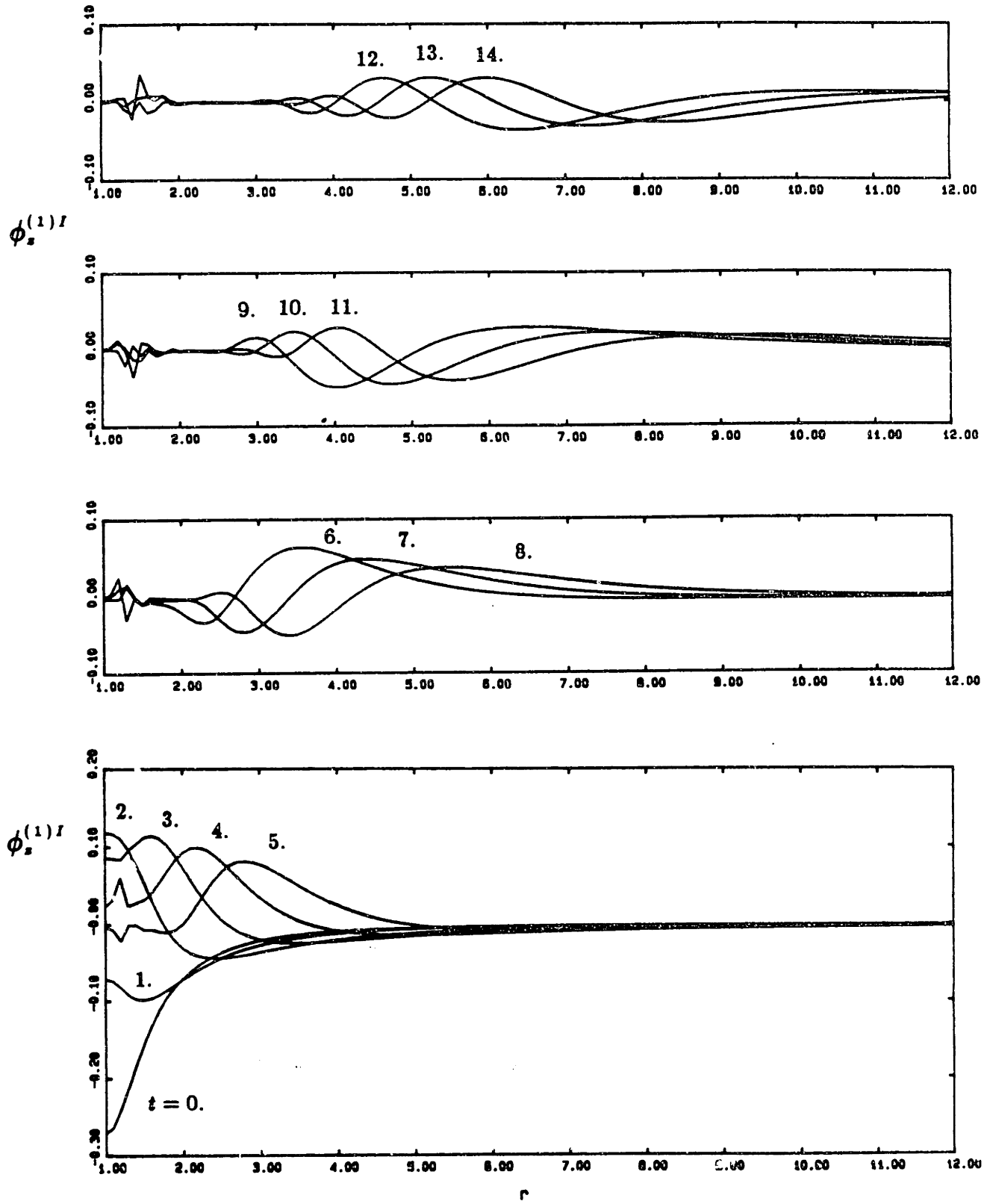

Figure 9-5. The heaving cylinder. $\phi_z^{(1)I}(\vec{r},t)$ on the free surface. $\Delta t = 0.1$, panelling: 24x36 (bottom & side x azimuthal). The region close to the body (Figure 9-3) has been interpolated through.

10. A SECOND APPROACH TO FREE-SURFACE QUANTITIES

OVERVIEW

Section 9 has raised doubts about the ability of the discretized Green formulation to evaluate the potential and its spatial and temporal derivatives on the free surface in proximity to the body. We would like to evaluate these same quantities by a method in which we can have greater confidence. Usually a closed-form solution is sought for this purpose, but in the case of the transient radiation problem there is none available. However we can make beneficial use of a formulation which is often employed for matching non-linear inner solutions to first-order outer solutions as in Lin, Newman, and Yue (1984). This matching takes place on a vertical, right-circular cylinder which encloses the non-linear portion of the solution and is of semi-infinite vertical extent. Exterior to the cylinder is a first-order potential which may be expressed in terms of the radial fluid velocity through the cylinder, and a Green function. For the present application, the interior potential is the first-order solution from (3.12).

In this section, we continue the analysis of the model problem of the heaving, right-circular cylinder. As is shown in Figure 10-1, the matching surface over which the radial fluid velocity must be evaluated is an infinitely deep continuation of the body itself. We can express the first-order, axisymmetric potential exterior to the infinite cylinder (of radius equal to 1) by:

$$\begin{aligned}\phi^{(1)}(r,z,t) = &\int_{-\infty}^{0} dz' \phi_r^{(1)}(1,z',t) D^{(0)}(r,z;1,z') \\ &+ \int_{0^+}^{t} d\tau \int_{-\infty}^{0} dz' \phi_r^{(1)}(1,z',t) D^{(F)}(r,z;1,z',t-\tau),\end{aligned} \tag{10.1}$$

where the Green function, $D = D^{(0)} + D^{(F)}$, is an axisymmetric function which satisfies the problem statement:

$$\nabla^2 D(r,z,t;r',z',\tau) = 0 \qquad (r,z,t) \neq (r',z',\tau), \quad \text{and } r > 1,\ z < 0, \tag{10.2}$$

$$D_r = \delta(z - z')\delta(t - \tau) \qquad r = 1, \quad z, z' < 0, \tag{10.3}$$

where δ signifies the Dirac function,

$$D_{tt} + D_z = 0 \qquad \text{on } z = 0, \tag{10.4}$$

$$D, \vec{\nabla} D, D_t \quad \text{are uniformly bounded as } \sqrt{r^2 + z^2} \to \infty, \quad \text{for } t \text{ finite}, \tag{10.5}$$

and,

$$D(r,z,t;r',z',\tau) = 0 \qquad t < \tau. \tag{10.6}$$

The derivation of $D(r,z,t;r',z',\tau)$ is straightforward and proceeds by separation of variables and Fourier integration as is familiar from the derivations of potentials for point singularities in Wehausen and Laitone (1960) Section 13. The results are that the Rankine portion of D is defined:

$$D^{(0)} = \frac{1}{\pi} \int_0^\infty dk\, \frac{1}{k} \mathcal{L}(k,r) \left[e^{-k|z-z'|} - e^{-k|z+z'|} \right]; \tag{10.7}$$

and the free-surface portion of D is defined :

$$D^{(F)} = \frac{2}{\pi} \int_0^\infty dk\, \frac{1}{\sqrt{k}} \sin\left(\sqrt{k}\,(t-\tau)\right) \mathcal{L}(k,r) e^{-k|z+z'|}; \tag{10.8}$$

in which $\mathcal{L}(k,r)$ is a rational function of ordinary Bessel functions:

$$\mathcal{L}(k,r) = \frac{J_0(kr)Y_1(k) - J_1(k)Y_0(kr)}{J_1^2(k) + Y_1^2(k)}. \tag{10.9}$$

Formulation (10.1) obviates the free-surface-body intersection problem discussed in Section 9 for a body which is wall sided at, and some distance below, the free surface. In the computation of $\phi_r^{(1)I}(1,z,t)$, the panel method is used to find the first-order potential on the body as has been described in previous sections, then Green's second identity, is used to find $\phi_r^{(1)}(1,z,t)$ on the infinite cylinder. In the latter computation there are no field points close to the free surface because $\phi_r^{(1)I}$ is prescribed on the part of the infinite cylinder which is actually the body. Subsequently, in the application of (10.1), although there may be field points on the free surface arbitrarily close to the body, for the *heave* mode

$$\phi_r^{(1)}(1,z,t) = 0 \qquad \text{on the } \textit{vertical} \text{ portion of } S_B\,, \tag{10.10}$$

so that the quadrature does not include the body surface. As long as the interest is in free-surface quantities, $|z \pm z'|$ does not approach zero, being never smaller than the extent of the wall-sidedness.

A further benefit of this formulation is that the behavior of the first-order potential and its derivatives is more apparent than it is in (9.6). In (10.1) we may observe two characteristics: (1) the non-zero limit of $|z \pm z'|$ ensures that very short waves are indeed damped exponentially with wave number, so that at large time, very close to the body, we can expect no large-amplitude, rapid oscillation of the free surface; and (2), the z-derivative of the first-order potential will have the amplitude of each wave-component increased by a factor of its wave number, but will still be similarly damped.

NUMERICAL IMPLEMENTATION

The implementation of (10.1) involves the first-order panel methods which have been discussed in various aspects over the previous sections. The first-order potential on the body, solved for by T$\bar{\text{I}}$MIT , is used to compute $\phi_r^{(1)}(1,z,t)$ on a portion of the infinite cylinder by a formulation similar to (9.6). $\phi_r^{(1)}(1,z,t)$ is required from the

corner of the body, to a truncation point at sufficient depth to allow accurate evaluation of free-surface quantities. Computational effort may be reduced by matching the computed velocity to that due to a dipole located at the origin. While not a numerically or computationally difficult task, the results will confirm that this has not proved to be necessary in this study. Accurate evaluation of $\phi^{(1)}(r,z,t)$ close to the submerged body corner cannot be expected in light of the results presented in Section 9 for the free-surface-body intersection. However, empirical evidence suggests that depth improves the situation, and more importantly depth allows an infinite-fluid analytical approximation to the locally two-dimensional, corner flow. Unlike the potential at the free-surface-body intersection, the flow at the submerged corner is singular. The strength of the singularity is a function of the included angle. That is, for included angle $\beta = \frac{\pi}{n}$, the two-dimensional potential may be written in *complex* form as (Newman, 1977):

$$F(Z) = Z^n, \tag{10.11}$$

with the result that close to the corner of this body (for which $n = 2/3$):

$$\phi_r^{(1)}(1,z,t) \propto \frac{1}{(z_0 - z)^{1/3}}, \tag{10.12}$$

where z_0 is the draft of the body (in this case $z_0 = 0.5$). This representation of the radial velocity may be matched to the computed radial velocity at some distance below the corner, and its contribution in (10.1) may be evaluated analytically or numerically. The location of the matching point is determined by obtaining the correct value of the flux through the infinite cylinder below the body at each time step within a specified tolerance. $\phi_r^{(1)}(1,z,t)$ is assumed constant over vertical segments of the infinite cylinder, and so is evaluated at a finite set of field points between the corner and the truncation point. These field points are the mid-points of equal length segments in a mapped space. The space s is related to the vertical axis z by:

$$z = z_0 - s^{2/3} \qquad (z_0 - z_T)^{3/2} < s < 0, \tag{10.13}$$

where z_T is the truncation point. This mapping for cube-root singularities is the analogue of cosine spacing for square-root singularities.

The Green function evaluation is done by Romberg quadrature in the wavenumber k, while the Bessel functions in $\mathcal{L}(k,r)$ are computed from ascending series and asymptotic representations (Abramowitz and Stegun, 1964). To compute $\phi_z^{(1)I}(r,0,t)$, which is the quantity presented in the results for this method, the partial derivative with respect to z of equation (10.1) must be taken. On the right-hand side of this formulation, only $D^{(0)}$ and $D^{(F)}$ are functions of z. The z-derivatives of $D^{(0)}$ and $D^{(F)}$ are evaluated in the same fashion as $D^{(0)}$ and $D^{(F)}$ themselves, as the convergence of these quadratures is still exponential in k.

The integration in z is performed analytically on each segment once $\phi_r^{(1)}$ is assumed to be peicewise constant. The discrete form of (10.1) to be solved for the potential on the free surface is:

$$\phi^{(1)}(r,0,t) = \frac{2}{\pi} {\sum_{m=0}^{M}}' \Delta t \sum_{j=1}^{N_C} \phi_{rj,m}^{(1)} \int_0^\infty dk \left[e^{kz_{2j}} - e^{kz_{1j}}\right] \frac{1}{k^{3/2}} \sin(\sqrt{k} t_{M-m}) \mathcal{L}(k,r)$$
$$M = 0, 1 \ldots M_T, \tag{10.14}$$

where the prime indicates that weights of one-half apply when $m = 0$ or $m = M$, N_C is the total number of segments on the truncated semi-infinite cylinder, and z_{2j} and z_{1j} are the end points of the j^{th} segment. Note that when $z = 0$ the Rankine portion of the Green function $D^{(0)}$ vanishes. After the partial derivative with respect to z is taken, the formulation for the z-derivative of the first-order impulsive potential which we will use to compare with results in Section 9 is:

$$\phi_z^{(1)I}(r,0,t) = \frac{-2}{\pi}\sum_{j=1}^{N_C}\phi_{rj,m}^{(1)I}\int_0^\infty dk\,\left[e^{kz_{2j}} - e^{kz_{1j}}\right]\frac{1}{k}\mathcal{L}(k,r)$$

$$+\frac{2}{\pi}\sum_{m=0}^{M}{}'\Delta t\sum_{j=1}^{N_C}\phi_{rj,m}^{(1)I}\int_0^\infty dk\,\left[e^{kz_{2j}} - e^{kz_{1j}}\right]\frac{1}{\sqrt{k}}\sin(\sqrt{k}t_{M-m})\mathcal{L}(k,r)$$

$$M = 0, 1 \ldots M_T\,. \tag{10.15}$$

RESULTS

Expression (10.15) has been evaluated using $\phi^{(1)I}(1,z,t)$ at 48 field points mapped as in (10.13) with $z_T = -6.0$. In establishing the matching point for the application of (10.12), a tolerance on the comparison of the flux through the infinite cylinder to that through the body was set at one-percent. This is an order of magnitude larger than the error which is introduced by ignoring the flux through the cylinder for $z_T > z > -\infty$.

Figure 10-2 confirms our conclusion that the behavior of $\phi_z^{(1)I}$ at the free-surface-body intersection is an artifact of the panel method and the constant strength representation of the solution. The values at the free-surface-body intersection confirm that the large-time limit is indeed zero. Of greater significance is the fact that the large-amplitude short waves seen in (9.4) are also due to the discrete form of the Green formulation. As discussed above, (10.1) does not predict this large-amplitude behavior. Rather, we see that the initial impulsive disturbance of the free surface, which contains all wave lengths, disperses with increasing time, and wave amplitude is attenuated exponentially with wave number. Away from the free-surface-body intersection the results agree well with those in Figure 9-4.

Figure 10-3 presents $\phi_z^{(1)I}$ over a greater extent of the free-surface. The agreement with Figure 9-5 confirms that the quadrature of Green's second identity used in Section 9 produces accurate results on the free surface in the region which is not local to the body. In the local region, that method is not reliable, but here, Figure 10-3 indicates that $\phi_z^{(1)I}$

is approaching zero after the initial disturbance bigins to disperse. Since $\phi_s^{(1)I}$ appears explicitly in the integrand of the unsteady second-order force formulation for $F^{(2)F}(t)$, (8.24), any poor behavior close to the body in other derivatives of the potential which constitute $\mathcal{H}^{(2)}(t)$, will not be important. This provides some optimism that accurate evaluation of the second-order unsteady force due to the inhomogeneity of the second-order free-surface condition is possible using the formulation in Section 8 with some refinement of the computational method.

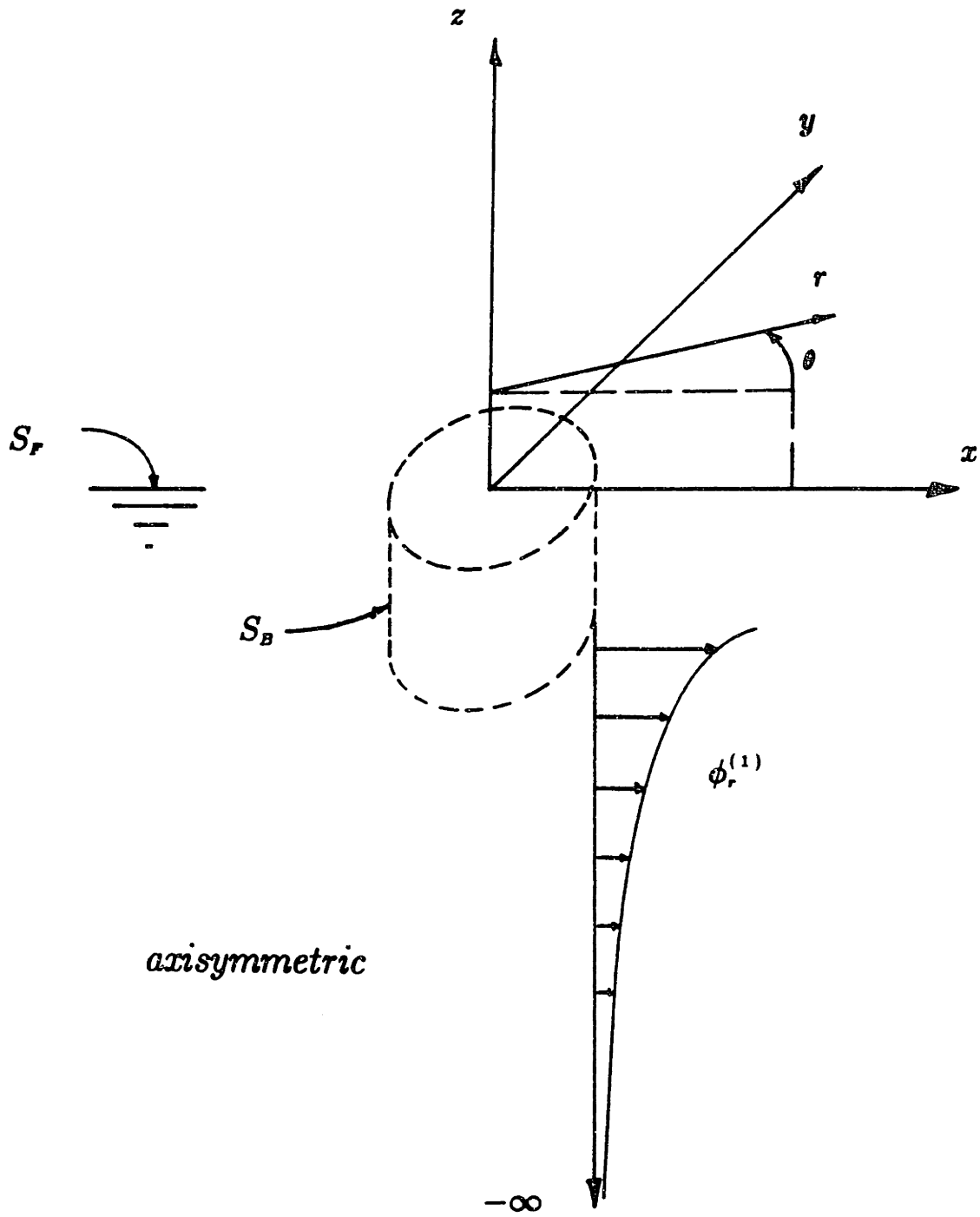

Figure 10-1. The coordinate system for the alternate method. Note that the semi-infinite cylinder, on which $\phi_r^{(1)}(1, z, t)$ is specified, is an extension of the body itself.

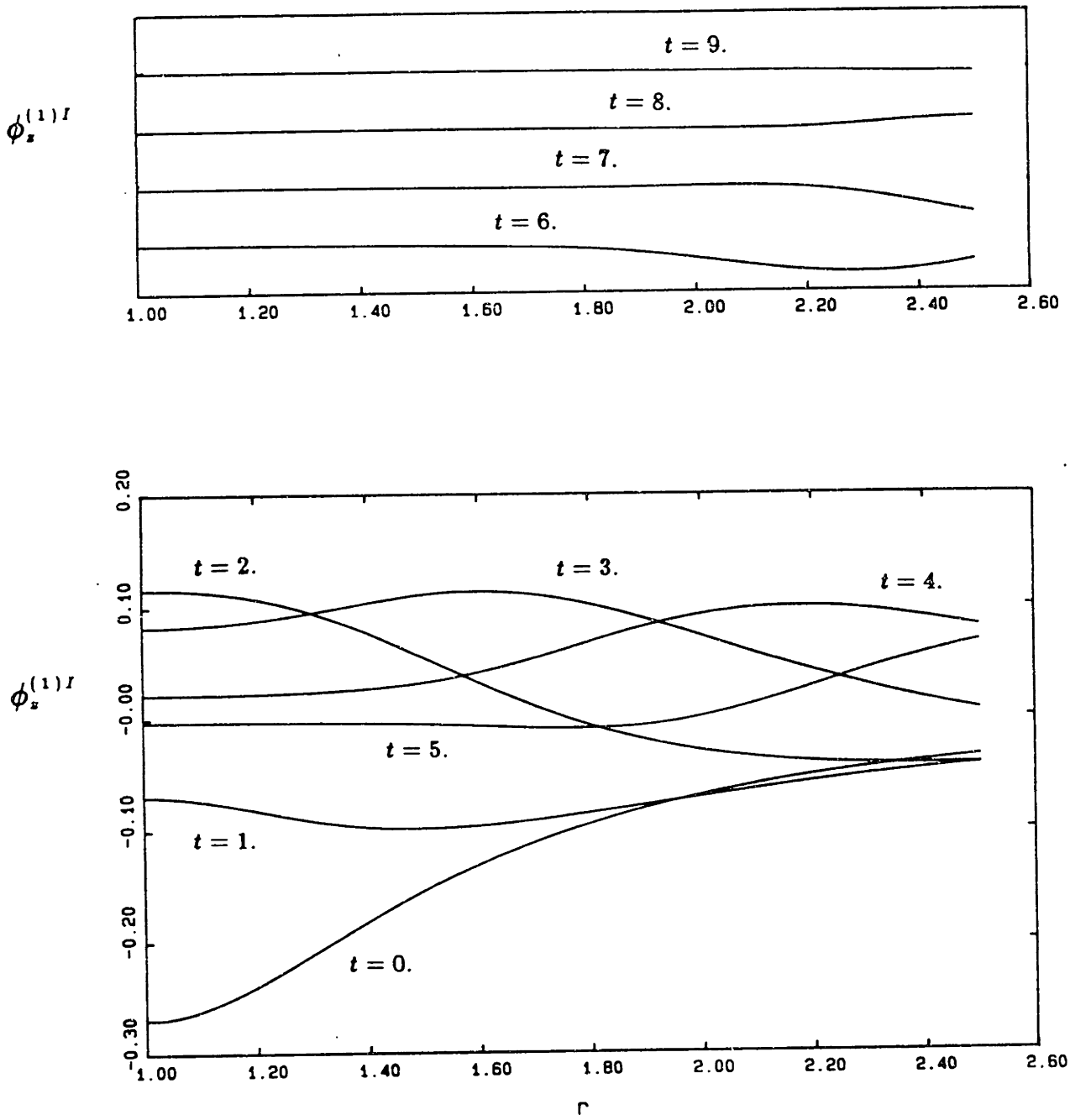

Figure 10-2. The heaving cylinder. $\phi_z^{(1)I}(\vec{r},t)$ on the free surface in the region close to the body. $\Delta t = 0.1$; panelling on the body: 24x36 (bottom & side x azimuthal); the infinite cylinder truncated at $z = -6.0$, discretized by 48 points. Compare with Figure 9-4.

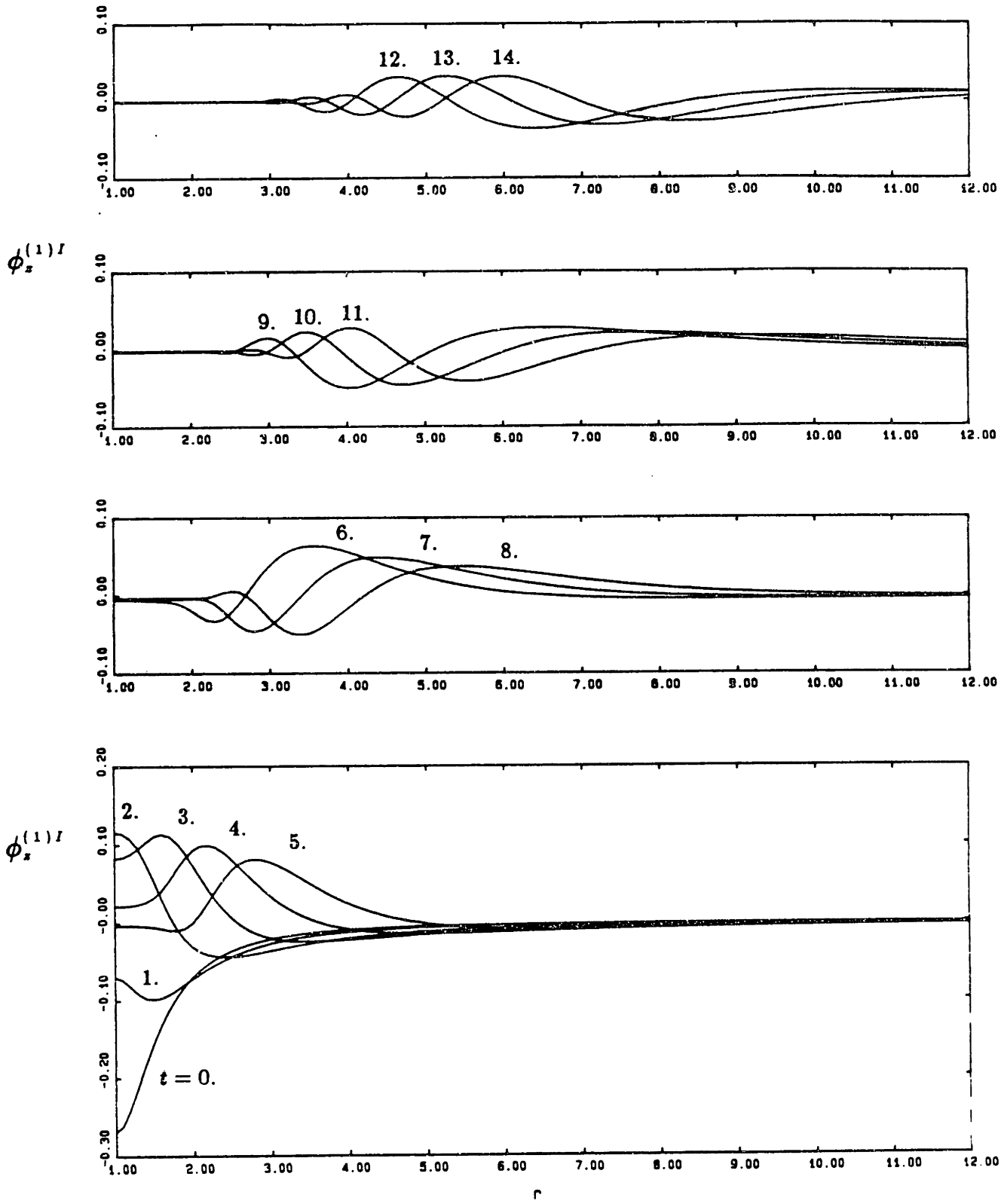

Figure 10-3. The heaving cylinder. $\phi_z^{(1)I}(\vec{r}, t)$ on the free surface. $\Delta t = 0.1$; panelling on the body: 24x36 (bottom & side x azimuthal); the infinite cylinder truncated at $z = -6.0$, discretized by 48 points. Compare with Figure 9-5.

11. CONCLUSIONS AND RECOMMENDATIONS

The first-order, three-dimensional, general-body, transient, radiation problem has been solved. Impulse response functions and the complimentary frequency-domain results (obtained by Fourier transform) have been presented for simple and complex bodies. In the sections of the Thesis which present these integrated results, the emphasis has been on analyzing and improving the accuracy and utility of the solution. The large-time asymptotic approximation to the impulse response function has been derived to arbitrary order and has been demonstrated to be important in the computation of accurate frequency-domain hydrodynamic coefficients for simple bodies, by implementation at $O(t^{-9})$.

In the process of deriving the asymptotic expansion for large time, the underlying analysis which takes place in the frequency domain has provided closed-form expressions for the first several terms of the added-mass and damping coefficients. Further analysis may provide more such expressions. Conversely, the method suggests that the high-frequency asymptotic representation of the frequency-domain hydrodynamic coefficients, may be derived by Fourier transformation of a small-time expansion of the impulse response function.

For complicated bodies, such as the TLP, the asymptotic representation is apparently not useful, as it is difficult to distinguish between the irregular-frequency effects and the physical resonances. However for these bodies, irregular-frequency effects are not pronounced. In addition to the fact that the impulse response function is required for simulations, there is a another substantial benefit to transient analysis of bodies with strong hydrodynamic resonances. The resonances cause the frequency-domain coefficient functions to be quite oscillatory and repeated frequency-domain analysis

to reveal these extrema can be computationally inefficient. However, a preliminary, low-accuracy, transient analysis and Fourier transform can reveal the nature of these functions and allow a more effective analysis in the frequency domain.

At second-order, the equation to be solved for the potential in the the general-body, three-dimensional, transient, radiation problem has been presented. In addition, compact expressions for the second-order, unsteady force due to this potential have been derived. Both of these problems require the quadrature of quadratic products of temporal and spatial derivatives of the first-order solution on the free surface. If this difficulty can be overcome in the force formulations, then the solution of the integral equation for the second-order potential can be solved with additional computational effort. It should be recognized that a similar derivation, with an assisting potential, leads to analogous force expressions for the second-order diffraction problem.

Computation of second-order quantities for the general body is, as yet, impeded by the inaccuracy of the first-order quantities on the free surface in proximity to the body. The evidence indicates that accurate field-point results are not possible from Green's second identity when the field point is close to the edge of a constant strength panel. Also, the potential solution-vector for points at the panel centroids may contain sufficient error close to the free surface to inaccurately specify the amplitude of short waves. The point made in Section 9, that field-point calculations are not a part of the panel method, is important because in the quadratures which constitute the right-hand sides of the second-order potential problem, the second-order force computation, and the Green formulation for the first-order potential or its derivatives at field points, there is no requirement that the representation of the potential on the body be only the piecewise constant panel-method solution. It is possible to augment the panel method result with analytical information, such as spatial derivative specification at the waterline, or by curve fitting the results over the entire body. These techniques may be the source of the improvement necessary in the quadratures involved in the second-order problems.

In the penultimate section of the Thesis, the computation of accurate free-surface quantities is demonstrated for the right-circular cylinder. These results are presented

for comparison to the results of Section 9 and they may be used as the benchmark for any general-body method which attempts to improve on the method presented here. Benchmark second-order forces may be computed from these results as well. The orientation of the Thesis has been toward the solution of the general body problem, hence the emphasis has been placed on investigating the discrete solution rather than on the generation of second-order force results for a particular body such as the right-circular cylinder.

Further work on the perturbation approach to the transient problem must improve the local accuracy of the first-order solution. It must be stressed that the intersection problem contains difficult physics as well as numerics. In this Thesis, the case of a heaving, wall-sided body has been discussed in detail, because the potential flow is not singular at the free-surface-body intersection. For other modes or other bodies, the flow is weakly singular at precisely this location of greatest numerical difficulty. The free-surface-body intersection problem is important not only in second-order analysis, but in the nonlinear problem as well. In a general body nonlinear problem, a useful method for closing the nonlinear domain is to match to a first-order outer solution. The intersection of the matching boundary and the free surface is no different from the free-surface-body intersection.

A careful analysis of the perturbation approach to the transient radiation problem has been undertaken. There have been successes in the accurate characterization of the integrated first-order quantities by both computational and analytical means. For the point-wise solution in the fluid field, required for accurate second-order computations, difficulties have been documented at the free-surface-body intersection. We leave to future investigations the numerical approaches which will allow the computation of accurate and efficient second-order and nonlinear solutions.

REFERENCES

Abramowitz, M. and Stegun, I. A. 1964 *Handbook of Mathematical Functions.* U. S. Government Printing Office, Washington D. C. or Dover Press, New York.

Adachi, H. and Ohmatsu, S. 1979 On the influence of irregular frequencies in the integral equation solutions to the thime-dependent free surface problems. *J. Soc. Nav. Arch. Japan* **146.**

Beck, R. F. and Liapis, S. 1987 Transient motions of floating bodies at zero speed. *J. Ship Research* **31**, 3, 164-176.

Breit, S. R., Newman, J. N., and Sclavounos, P. D. 1985 A new generation of panel programs for radiation-diffraction problems. *Proc. 3rd International Conf. on the Behaviour of Offshore Structures* (BOSS), Delft.

Cummins, W. E. 1962 The impulse response function and ship motions. *Schiffstechnik,***9**, 101-109.

Department of Ocean Engineering, MIT 1988 *WAMIT A radiation-diffraction panel program for wave-body interactions.* Department of Ocean Engineering, Massachusetts Institute of Technology, Cambridge.

Dommermuth, D. G. and Yue, D. K.-P., 1987 Numerical simulations of axisymmetric flows with a free surface. *J. Fluid Mech.,* **178** , 195-219.

Eatock Taylor, R. and Jefferys, E. R. 1986 Variability of hydrodynamic load predictions for a tension leg platform. *Ocean Engineering* **13** , 5, 449-490.

Faltinsen, O. and Løken, A. E. 1978 Drift forces and slowly varying horizontal forces on a ship in waves. *Proc. Symp. on App. Math. Dedicated to the Late Professor Dr. R. Timman* , University of Technology Delft.

Finkelstein, A. 1953 The initial value problem for transient water waves. Dissertation, NYU, New York, 1953.

Greenhow, M. 1986 High- and low-frequency asymptotic consequences of the Kramers-Kronig relations. *J. Eng. Math.* **20**, 293-306.

Hulme, A. 1982 The wave forces acting on a floating hemisphere undergoing forced periodic oscillations. *J. Fluid Mech* **121**, 443-463. 127-135.

Jefferys, E. R. 1987 Numerical problems of first-order diffraction theory. *Second International Workshop on Water Waves and Floating Bodies* Report No. AM-87-06, University of Bristol, Bristol, England.

John, F. 1950 On the motion of floating bodies II. *Comm. Pure and App. Math.* **3**, 45-101.

Kim, M.- H. 1988 PhD. Thesis in preparation. Massachusetts Institute of Technology, Cambridge, Massachusetts.

King, B. 1987 Time-domain analysis of wave exciting forces on ships and bodies. The Department of Naval Architecture and Marine Engineering Report No. 306, The University of Michigan, Ann Arbor, Michigan.

Korsmeyer, F. T., Lee, C.- H., Newman, J. N., and Sclavounos, P. D. 1988 The analysis of wave effects on tension leg platforms. *OMAE* Conference, Houston, Texas.

Korsmeyer, F. T. and Sclavounos, P. D. 1987 The long-time asymptotic expansion of the impulse response function for a floating body. Submitted for publication.

Lee, C.-H. and Sclavounos, P. D. 1987 Removing the irregular frequencies from boundary integral equations in wave body interactions. Submitted for publication.

Liapis, S. J. 1986 Time domain analysis of ship motions. The Department of Naval Architecture and Marine Engineering Report No. 302, The University of Michigan, Ann Arbor, Michigan.

Lighthill, M. J. 1958 *Fourier Analysis and Generalised Functions.* Cambridge University Press, Cambridge.

Lighthill, M. J. 1979 Waves and hydrodynamic loading. *Proc. 2nd International Conf. on the Behaviour of Offshore Structures,* London, 1-40.

Lin, W.-M., Newman, J. N., and Yue, D. K. 1984 Nonlinear forced motions of floating bodies. *The Fifteenth Symposium on Naval Hydrodynamics* , Hamburg.

Molin, B. 1979 Second-order diffraction loads upon three-dimensional bodies. *Applied Ocean Research,* **1**, No. 4, 197-202.

Newman, J. N. 1974 Second-order slowly varying forces on vessels in irregular waves. *Proc. Internat. Symp. on Dynamics of Marine Vehicles and Structures in waves.* Univ. Coll. London, 182-186.

Newman, J. N. 1977 *Marine Hydrodynamics.* The MIT Press, Cambridge, Massachusetts and London, England.

Newman, J. N. 1984 An expansion of the oscillatory source potential. *App. Ocean Res.* **6**, 116-117.

Newman, J. N. 1985a Transient axisymmetric motion of a floating cylinder. *J. Fluid Mech.* **157**, 17-33.

Newman, J. N. 1985b The evaluation of free-surface Green functions, Fourth International Conference on Numerical Ship Hydrodynamics, Washington D. C. 4-19.

Newman, J. N. 1986 Distributions of sources and normal dipoles over a quadralateral panel, *J. Eng. Maths.* **20** 113-126.

Ogilvie, T. F. 1964 Recent progress toward the understanding and prediction of ship motions. *The Fifth Symposium on Naval Hydrodynamics,* Bergen, 3-128.

Ogilvie, T. F. 1983 Second-order hydrodynamic effects on ocean platforms. *International Workshop on Ship and Platform motions,* Berkeley, California.

Olver, F. W. J. 1974 *Asymptotics and Special Functions.*Academic Press, New York.

Sclavounos, P. D. 1987 Radiation and diffraction of second-order surface waves by floating bodies. Submitted for publication.

Simon, M. J. and Hulme, A. 1985 The radiation and scattering of long waterwaves. *Symposium on Hydrodynamics of Ocean Wave-Energy Utilization of the International Union of Theoretical and Applied Mechanics.* 419-432.

Stoker, J. J. 1957 *Water Waves.* Interscience Publishers, Inc. New York.

Wang, P. F. 1987 The radiation condition and numerical aspects of second-order surface wave radiation and diffraction. PhD Thesis, Massachusetts of Technology, Cambridge, Massachusetts.

Wehausen, J. V. and Laitone, E. V. 1960 Surface waves. *Handbuch der Physik.* **9**, 446-778.

Wehausen, J. V. 1971 The motion of floating bodies. *Ann. Rev. Fluid Mech.* **3**, 237-268.

Yeung, R. W. 1982 The transient heaving motion of floating cylinders. *J. Eng. Math.*, **16**, *97-119.*

APPENDIX

The transient radiation problem which is defined in Section 2 may be expanded in powers of a small parameter to produce a series of linear problems at each order. The problems at first- and second-order are defined in Sections 3 and 7 respectively. We wish to derive an integral equation to replace the initial-boundary value problem at any order. This is done via Green's second identity making use of a Green function. In principle the problem can be reduced to an integral equation to be solved with contributions on the body surface alone, at any order. However in practice, this is feasible only at first order. So in the following, we use the first-order transient Green function to derive the Fredholm-Volterra integral equation which applies to the problem at every order. Use of this Green function has the benefit of removing terms involving the unknown potential from the free surface, although there is still an integral involving known quantities to be calculated on the free surface.

Let $\phi^{(n)}(\vec{x},t)$ be the potential at $O(\epsilon^n)$ which solves:

$$\nabla^2\phi^{(n)}(\vec{x},t) = 0 \qquad \text{in the fluid domain} \tag{A.1}$$

$$\phi_{tt}^{(n)} + \phi_z^{(n)} = \mathcal{H}^{(n)} \qquad \text{on } S_F \tag{A.2}$$

where $\mathcal{H}^{(n)}$ vanishes at $O(\epsilon)$, but at higher orders involves products of spatial and temporal derivatives of solutions at lower orders.

$$\vec{n}(\vec{x}) \cdot \vec{\nabla}\phi^{(n)} = \mathcal{B}^{(n)} \qquad \text{on } S_B, \quad t > 0 \tag{A.3}$$

where $\vec{n}$ is not a function of time, as it is defined as the unit-normal vector on the body in the initial position; and where $\mathcal{B}^{(n)}$ involves contributions from lower-order solutions, from the expansion of the body velocity, and from corrections to the normal due to the body motion around its initial position.

$$\vec{\nabla}\phi^{(n)} \to 0 \qquad \text{on } S_\infty \text{ for } t \text{ finite} \tag{A.4}$$

a discussion of this boundary condition is available in Stoker (1957). The free-surface boundary condition is second-order in time, so we expect that we must specify both $\phi^{(n)}(\vec{x},t)$ and $\phi_t^{(n)}(\vec{x},t)$ as initial conditions:

$$\phi^{(n)}(x,y,0,0^+) = 0, \tag{A.5}$$

and

$$\phi_t^{(n)}(x,y,0,0^+) = I^{(n)} \tag{A.6}$$

where condition (A.5) results from (2.7), and the right-hand side of (A.6), $I^{(n)}(0^+)$, involves lower-order solutions and may be derived at any particular order from (2.6) and (2.3).

We make use of the Green Function derived by Wehausen and Laitone (1960), which may be written:

$$G(\vec{x};\vec{\xi},t) = \frac{1}{R} - \frac{1}{R'} + 2\int_0^\infty dk\,[1-\cos(k^{\frac{1}{2}}t)]e^{-kY}J_0(kX), \tag{A.7}$$

where

$$\left.\begin{matrix} R' \\ R \end{matrix}\right\} = [(x-\xi)^2 + (y-\eta)^2 + (z \pm \varsigma)^2]^{1/2},$$

$$Y = -(z+\varsigma),$$

and

$$X^2 = (x-\xi)^2 + (y-\eta)^2 \,.$$

Stoker (1957) discusses this Green function in detail; here we note the spatial and temporal properties which figure in the ensuing derivation:

• $G(\vec{x};\vec{\xi},t)$ satisfies the Laplace equation, the first-order, homogeneous free-surface boundary condition and its gradient vanishes at S_∞,

• $G(\vec{x};\vec{\xi},t)$ is symmetric in both space and time; the specific temporal properties required in the derivation are:

$$G(\vec{x};\vec{\xi},0^+) = 0 \qquad \text{on } S_F \tag{A.8}$$

$$G_t(\vec{x};\vec{\xi},0^+) = 0 \qquad \text{on } S_F \tag{A.9}$$

In the following derivation we will omit spatial arguments for clarity. We use the functions $\phi_\tau^{(n)}(\vec{x},\tau)$ and $G(\vec{x};\vec{\xi};t-\tau)$ in Green's second identity to write:

$$\begin{aligned}\iint_{S_B} d\vec{\xi}\,[\phi_\tau^{(n)}(\tau)G_{n_\xi}(t-\tau) - \phi_{n_\xi\tau}^{(n)}(\tau)G(t-\tau)] \\ + \iint_{S_F} d\vec{\xi}\,[\phi_\tau^{(n)}(\tau)G_{n_\xi}(t-\tau) - \phi_{n_\xi\tau}^{(n)}(\tau)G(t-\tau)] \\ + 2\pi\phi_\tau^{(n)}(\tau) = 0,\end{aligned} \tag{A.10}$$

where the last term has arisen from the treatment of the spatial singularity as is well known in potential theory, and the volume integral and the surface integral on S_∞ have vanished because both $\phi^{(n)}(\vec{x},t)$ and $G(\vec{x};\vec{\xi},t)$ satisfy the Laplace equation and conditions at spatial infinity as in (A.4). We integrate (A.10) in time, τ, from $\tau = 0^+$ to $\tau = t$, where the 0^+ acknowledges the Heaviside property of the body boundary

condition which forces the fluid motion. After integration by parts of the term to be evaluated on S_B, we have:

$$\iint_{S_B} d\vec{\xi}\,\left[\phi^{(n)}(\tau)G_{n_\xi}(t-\tau)-\phi^{(n)}_{n_\xi}(\tau)G(t-\tau)\right]_{0^+}^{t}$$
$$-\int_{0^+}^{t} d\tau \iint_{S_B} d\vec{\xi}\,\left[\phi^{(n)}(\tau)G_{n_\xi\tau}(t-\tau)-\phi^{(n)}_{n_\xi}(\tau)G_\tau(t-\tau)\right]$$
$$+\int_{0^+}^{t} d\tau \iint_{S_F} d\vec{\xi}\,\left[\phi^{(n)}_\tau(\tau)G_{n_\xi}(t-\tau)-\phi^{(n)}_{n_\xi\tau}(\tau)G(t-\tau)\right]$$
$$+2\pi\int_{0^+}^{t} d\tau\,\phi^{(n)}_\tau(\tau)=0. \qquad (A.11)$$

We can use the free-surface boundary condition to make the free-surface time-integral exact, that is:

$$\int_{0^+}^{t} d\tau \iint_{S_F} d\vec{\xi}\,\left[\phi^{(n)}_\tau(\tau)G_{n_\xi}(t-\tau)-\phi^{(n)}_{n_\xi\tau}(\tau)G(t-\tau)\right]$$
$$=-\int_{0^+}^{t} d\tau \iint_{S_F} d\vec{\xi}\,\left[\phi^{(n)}_\tau(\tau)G_{\tau\tau}(t-\tau)-\phi^{(n)}_{\tau\tau\tau}(\tau)G(t-\tau)\right]$$
$$-\int_{0^+}^{t} d\tau \iint_{S_F} d\vec{\xi}\,\mathcal{H}^{(n)}_\tau(\tau)G(t-\tau). \qquad (A.12)$$

The first integral on the right-hand side is now exact, so we have:

$$\int_{0^+}^{t} d\tau \iint_{S_F} d\vec{\xi}\,\left[\phi^{(n)}_\tau(\tau)G_{n_\xi}(t-\tau)-\phi^{(n)}_{n_\xi\tau}(\tau)G(t-\tau)\right]$$
$$=\iint_{S_F} d\vec{\xi}\,\left[\phi^{(n)}_\tau(0^+)G_\tau(t)+\phi^{(n)}_{n_\xi}(0^+)G(t)\right]$$
$$-\int_{0^+}^{t} d\tau \iint_{S_F} d\vec{\xi}\,\mathcal{H}^{(n)}_\tau(\tau)G(t-\tau)-\iint_{S_F} d\vec{\xi}\,\mathcal{H}^{(n)}(0^+)G(t), \qquad (A.13)$$

where we have used the properties of $G(\vec{x};\vec{\xi},0)$, (A.8) and (A.9) to eliminate terms, and the free surface condition (A.2) to re-introduce $\phi^{(n)}_{n_\xi}(0^+)$ in the first right-hand

side integral. This latter step allows the elimination of terms to be evaluated at $t = 0^+$ on S_B in (A.11) as follows.

By Green's second identity we may write:

$$
\begin{aligned}
-\iint_{S_B} d\vec{\xi}\,[\phi^{(n)}(0^+)G_{n_\xi}(t) - \phi^{(n)}_{n_\xi}(0^+)G(t)] & \\
+ \iint_{S_F} d\vec{\xi}\,\phi^{(n)}_{n_\xi}(0^+)G(t) - 2\pi\phi^{(n)}(0^+) & \qquad (A.14)\\
= \iint_{S_F} d\vec{\xi}\,\phi^{(n)}(0^+)G_{n_\xi}(t), &
\end{aligned}
$$

and the right-hand side of this expression vanishes due to (A.5). All of the left-hand side terms of (A.14) are present in (A.11), once we have used the result on the right-hand side of (A.13), so they may be eliminated. This reduces (A.11) to:

$$
\begin{aligned}
\iint_{S_B} d\vec{\xi}\,[\phi^{(n)}(t)G_{n_\xi}(0) - \phi^{(n)}_{n_\xi}(t)G(0)] & \\
- \int_{0^+}^{t} d\tau \iint_{S_B} d\vec{\xi}\,[\phi^{(n)}(\tau)G_{n_\xi\tau}(t-\tau) - \phi^{(n)}_{n_\xi}(\tau)G_\tau(t-\tau)] & \\
+ \iint_{S_F} d\vec{\xi}\,[\phi^{(n)}_\tau(0^+)G_\tau(t) - \mathcal{H}^{(n)}(0^+)G(t)] & \\
- \int_{0^+}^{t} d\tau \iint_{S_F} d\vec{\xi}\,\mathcal{H}^{(n)}_\tau(\tau)G(t-\tau) & \\
+ 2\pi\phi^{(n)}(t) = 0. & \qquad (A.15)
\end{aligned}
$$

From a numerical point of view, it is convenient to perform another integration by parts to remove the partial derivative with respect to time, τ, from $\mathcal{H}^{(n)}_\tau(\tau)$ as this function already contains gradients and temporal derivatives of lower order solutions which are difficult to evaluate. Finally, we may write:

$$2\pi\phi^{(n)}(\vec{x},t) + \iint_{S_B} d\vec{\xi}\,\phi^{(n)}(\vec{x},t)G^{(0)}_{n_\xi}(\vec{x};\vec{\xi}) + \int_{0^+}^{t} d\tau \iint_{S_B} d\vec{\xi}\,\phi^{(n)}(\vec{\xi},\tau)G^{(F)}_{n_\xi t}(\vec{x};\vec{\xi},t-\tau)$$
$$= \int_{0^+}^{t} d\tau \iint_{S_B} d\vec{\xi}\,B^{(n)}(\vec{\xi},\tau)G^{(F)}_{t}(\vec{x};\vec{\xi},t-\tau) + \iint_{S_B} d\vec{\xi}\,B^{(n)}(\vec{\xi},t)G^{(0)}(\vec{x};\vec{\xi})$$
$$+ \int_{0^+}^{t} d\tau \iint_{S_F} d\vec{\xi}\,\mathcal{H}^{(n)}(\vec{\xi},\tau)G^{(F)}_{t}(\vec{x};\vec{\xi},t-\tau) + \iint_{S_F} d\vec{\xi}\,I^{(n)}(0^+)G^{(F)}_{t}(\vec{x};\vec{\xi},t), \tag{A.16}$$

where we have used the convenient decompostion of $G(\vec{x};\vec{\xi},t)$ into its time independent Rankine part, designated $G^{(0)}$, and its time dependent wave part, designed $G^{(F)}$, that is:

$$G(\vec{x};\vec{\xi},t) = G^{(0)}(\vec{x};\vec{\xi}) + G^{(F)}(\vec{x};\vec{\xi},t) \tag{A.17}$$

with

$$G^{(0)}(\vec{x};\vec{\xi}) = \frac{1}{R} - \frac{1}{R'}, \tag{A.18}$$

$$G^{(F)}(\vec{x};\vec{\xi},t) = 2\int_0^\infty dk\,[1-\cos(k^{\frac{1}{2}}t)]e^{-kY}\,J_0(kX). \tag{A.19}$$

This completes the derivation of the Fredholm-Volterra formulation for the radiation problem at any order. The specialization of (A.16) to a particular order is made by substitution of the proper right-hand sides from the boundary and initial conditions for $B^{(n)}(\vec{x},t)$, $\mathcal{H}^{(n)}(\vec{x},t)$, and $I^{(n)}(0^+)$.